

# Structural Dynamics and Synaptic Development in the Visual System

by

Serkan Oray

BS Biomedical Engineering, University of Southern California  
MS Biomedical Engineering, University of Southern California

Submitted to the Department of Brain and Cognitive Sciences in  
Partial Fulfillment of the Requirements for the Degree of

Doctor of Philosophy

at the

Massachusetts Institute of Technology

June, 2004

© Massachusetts Institute of Technology 2004, All rights reserved

Signature of Author: \_\_\_\_\_

Department of Brain and Cognitive Sciences  
May 14, 2004

Certified by: \_\_\_\_\_

Mriganka Sur  
Sherman Fairchild Professor of Neuroscience  
Head, Department of Brain and Cognitive Sciences

Accepted by: \_\_\_\_\_

Earl Miller  
Professor of Neuroscience  
Chairman, Department Graduate Committee

## **Abstract**

This thesis takes as its subject three model systems which exhibit interesting properties in the developing nervous system. The first study details the developmental properties of dendritic spines, the principle sites of excitatory synaptic contacts, during a period of synaptogenesis in the developing mouse cortex. The second study extends these findings and examines the properties of dendritic spines during a period of heightened visual cortical plasticity and describes how manipulations of visual input alter these dendritic structures. The third and final study examines the distribution of glutamate receptors, which are key components of excitatory synaptic contacts, during a period of stereotyped anatomical plasticity in the developing ferret lateral geniculate nucleus. Each of these studies focus specifically on the interactions between neuronal structure and function, principally at the level of synaptic contacts. The conclusions of this thesis are that structure and function are intimately related and that altering one has important consequences for the other.

## Acknowledgments

First and foremost, I would like to thank my thesis advisor, Mriganka Sur. Mriganka's guidance has contributed immeasurably to my thesis work and to my development as a scientist. I began my graduate training with a very broad set of interests and Mriganka gave me the freedom to explore these ideas and encouraged me to slowly focus on those areas which interested me the most. As I sharpened my thinking, Mriganka was constantly available to help me develop my ideas and push my experiments forward. Mriganka is an exceptional scientist and teacher and it has been my privilege to pursue my graduate studies under his mentorship.

I would also like to thank the other members of my thesis committee: Mark Bear, Yasunori Hayashi, Takao Hensch, and Guosong Liu as well as Elly Nedivi, who served on my oral qualifying committee. Their comments and input have been very valuable and have considerably improved this thesis.

Additionally, I would like to thank the many exceptional members of the Sur laboratory. When I first joined the laboratory, it was my great fortune to collaborate with Carsten Hohnke; he took me under his wing and taught me everything he could about the LGN and electrophysiology. After Carsten's departure, I had the opportunity to work closely with Cathy Leamey, who's exuberance, dedication, and academic

curiosity were truly inspirational. I would also like to thank Ania Majewska, who opened my eyes to the world of two-photon microscopy and dendritic spines. Ania brought to the lab cutting edge tools and a keen scientific mind, and it has been an honor to collaborate with her on multiple parts of this thesis. Lastly, I'd like to thank the many other past and present members of the Sur laboratory, in particular my fellow graduate students James Schummers, Brandon Farley, Charlene Ellsworth, and Sam Hornig. The members of the Sur laboratory have enriched my life with their intellect and camaraderie and it has been a pleasure to work with them throughout my graduate career.

I would like to acknowledge my parents, Teresa Oray and Erdoğan Oray, and my brother Ayhan Oray, for their unequivocal support and their constant encouragement of my academic aspirations. I would also like to give my heartfelt thanks to Amy Dierberger who's seen me at my best and at my worst over the last four years and has supported me through it all. Lastly, I'd like to thank my two furry ladies, Sophie and Nixie, who have constantly reminded me that eating and sleeping are good and that belly-rubs are even better. Thank you.

## Collaborations

Parts of this thesis were carried out in collaboration with other members of the Sur Laboratory and all data is reproduced here with their permission. The *in vivo* spine motility experiments described in chapter 3 and shown in Figure 3-1 were conducted by Ania Majewska. The gene chip data discussed in chapter 3 and shown in Figure 3-4 are a small part of a larger data set that was collected by Cathy Leamey, Alvin Lyckman, and Daniela Tropea. Likewise, the tPA *in situ* hybridization experiments were carried out in collaboration with Alvin Lyckman and Sam Horng, and the tPA immunostaining experiments were primarily conducted by Jennifer Shieh.

## Table of Contents

<b>ABSTRACT.....</b>	<b>2</b>
<b>ACKNOWLEDGMENTS .....</b>	<b>3</b>
<b>TABLE OF CONTENTS.....</b>	<b>6</b>
<b>CHAPTER 1: INTRODUCTION.....</b>	<b>7</b>
<b>CHAPTER 2: EFFECTS OF SYNAPTIC ACTIVITY ON DENDRITIC SPINE MOTILITY OF DEVELOPING CORTICAL LAYER V PYRAMIDAL NEURONS .....</b>	<b>12</b>
<b>CHAPTER 3: DENDRITIC SPINE DYNAMICS ARE REGULATED BY MONOCULAR DEPRIVATION AND EXTRACELLULAR MATRIX DEGRADATION .....</b>	<b>49</b>
<b>CHAPTER 4: SHORT AND LONG-TERM REGULATION OF AMPA AND NMDA RECEPTORS IN THE DEVELOPING FERRET LGN .....</b>	<b>73</b>
<b>CHAPTER 5: SUMMARY AND CONCLUSIONS.....</b>	<b>107</b>
<b>REFERENCES.....</b>	<b>112</b>

# CHAPTER 1

## Introduction

One of the most daunting and interesting questions confronting modern neuroscience is how the human brain, composed of approximately  $10^{11}$  neurons and making on the order of  $10^{15}$  synaptic connections, develops from a few embryonic cells into a precisely organized system. Neurons throughout the brain perform specialized functions which are, in part, determined by their morphological properties and their patterns of input and output connections. Amazingly, neurons and networks of neurons are also plastic and can alter their functional properties as well as their structural characteristics, both through the period of brain development, as well as later in adult life. Examining the interaction between structure and function at the level of brain regions, principally in terms of patterns of connectivity within and between different brain areas, has significantly advanced the field of neuroscience. New techniques, which allow visualization of subcellular structures, including the sites of dendritic and axonal contacts, promise to further advance this understanding and potentially reconcile structure and function at unprecedented resolution at the level of individual synapses.

## **Outline of the thesis**

This thesis is composed of three studies which consider the issue of structure and function at subcellular scales and attempt to eventually merge these observations with what is known about structure and function at the level of networks and brain regions. Chapter two begins with a description of dendritic spines, the fundamental unit of both excitatory synapses and dendritic structure in the central nervous system. Even though the functional properties of spines are not completely understood, they are distinguished by their readily-observable, dynamic morphologies, and for their ability to compartmentalize post-synaptic signals. This chapter focuses on characterizing the developmental regulation and activity-dependence of spine dynamics in a set of transgenically labeled neurons in the mouse cortex with two-photon microscopy (Figure 1-1). Two-photon microscopy is also combined with fluorescent immunohistochemistry and confocal microscopy to examine the relationship between spine dynamics and the expression of glutamatergic receptors on individual spines.

In chapter three, the work on spine dynamics is advanced to specifically explore the structural consequences of functional changes in the primary visual cortex. The mammalian primary visual cortex is especially susceptible to changes in visual input during a well-defined critical period, in which closing one eye leads to a loss of responsiveness of neurons to the deprived eye and a shift in response towards the open

eye. Following prolonged monocular deprivation, this functional alteration is accompanied by a change in the structure of thalamocortical axon arbors in layer IV. The steps that intervene between the functional and anatomical changes are poorly understood and this chapter examines the rapid structural changes at the level of dendritic spines that occur following brief monocular deprivation. The chapter concludes with experimental and mechanistic evidence suggesting that degradation of the extracellular matrix may be involved in this structural plasticity and proposes a simple model to account for the observations.

Chapter four returns to the issue of glutamate receptors in developing systems, and explores the consequences of region-wide anatomical reorganization in the ferret lateral geniculate nucleus (LGN) on the expression patterns of glutamate receptors at retinogeniculate inputs. In the ferret LGN, retinal axons segregate into eye specific regions (laminae) during the first two postnatal weeks and subsequently into ON/OFF sublaminae during the third and fourth postnatal weeks. Although others have shown that the AMPA and NMDA subtypes of glutamate receptors maintain stable functional properties during the period of ON/OFF sublamination, this chapter explores the spatial and temporal distributions of AMPA and NMDA receptors, particularly with respect to their overlapping co-expression. Additionally, pharmacological manipulations are performed on acute slices taken during the period of ON/OFF sublamination to

determine the effects of activity blockade and enhancement, which are known to have important anatomical consequences, on the subsequent expression profiles of AMPA and NMDA receptors. The work detailed in this chapter concludes the experimental aspect of this thesis. Finally, chapter five summarizes the work presented in chapters two through four and presents overall conclusions.

The data presented in chapters two through four were initially written for individual publication and, as such, each chapter includes relevant literature reviews and extensive citations. Since the topics covered in the three chapters are inter-related, some parts of the reviews and citations may overlap, though explicit textual redundancy has been avoided.

## **Publications**

The work detailed in this thesis has led to five abstracts at the Society for Neuroscience meetings (1999-2003) as well as three journal articles, one of which has been published and the other two which are in the process of submission. Only the published article is explicitly referenced in this thesis.

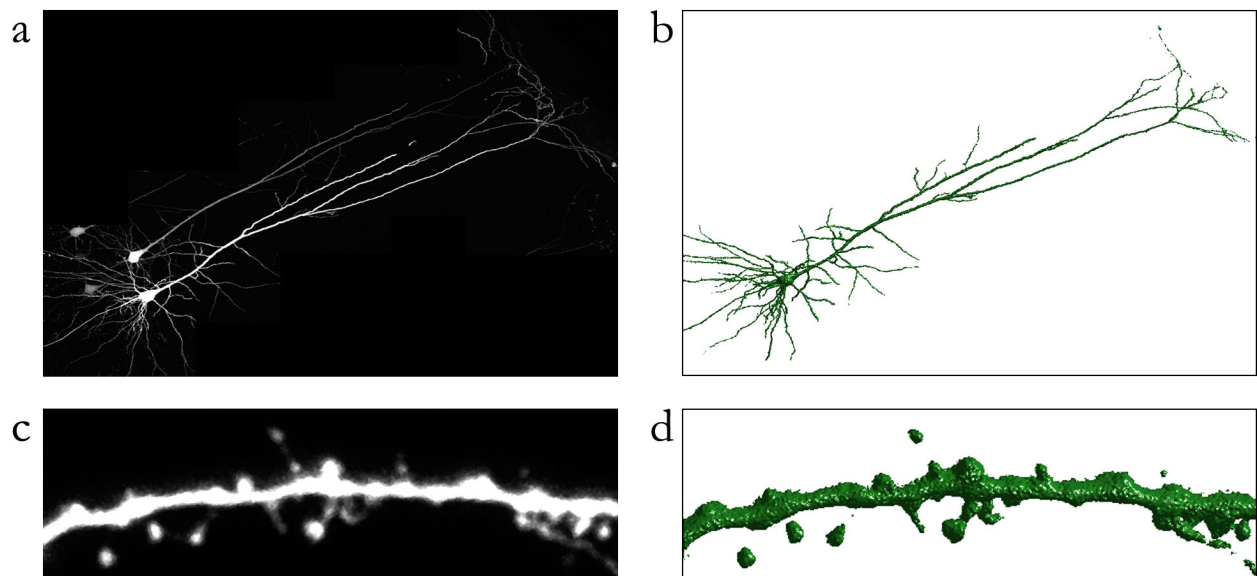


**Figure 1-1.** The morphology of layer V pyramidal neurons. **a**, A projection of a volume of images (z-stack) showing several layer V pyramidal neurons which express green fluorescent protein (GFP). These neurons have their cell bodies in cortical layer V, and extend long apical dendrites approximately 500-700  $\mu\text{m}$  toward the cortical surface (upper right). **b**, A three-dimensional surface reconstruction of the neuron shown in **a**. **c**, Apical dendritic spines, on the order of 1-2  $\mu\text{m}$  in length on a different neuron. **d**, A three dimensional surface reconstruction of the spines shown in **c**.

## CHAPTER 2

# Effects of synaptic activity on dendritic spine motility of developing cortical layer V pyramidal neurons

### INTRODUCTION

Most excitatory synapses in the mammalian cortex terminate on dendritic spines<sup>1,2</sup>. Spines are structural specializations which are morphologically diverse and are likely to be involved in calcium compartmentalization and regulation<sup>3-5</sup>. Interestingly, spines also exhibit dynamic changes in size and shape which have been documented *in vitro*<sup>6-10</sup> and *in vivo*<sup>11,12</sup>. It is likely that dynamic rearrangements of the post-synaptic apparatus have functional consequences<sup>13</sup>. Spine dynamics might also reflect recent synaptic activity as manipulations of activity through AMPA and NMDA receptors as well as of general neuronal excitability have altered spine motility in dissociated culture<sup>8,9</sup>. However, the same effects were not observed in slice culture<sup>6</sup>. Defining the relationship, if any, between synaptic activation and spine dynamics in a system where more network circuitry is preserved is critical for understanding the link between spine structure and function.

In cortex, AMPA and NMDA receptor subunits are developmentally regulated such that NR1 expression decreases<sup>14</sup>, NR2B is replaced by NR2A subunits<sup>15-17</sup>, and GluR2 expression, which reduces calcium permeability, increases<sup>18</sup> as development proceeds. Additionally, immature synapses are thought to exist in a “silent” configuration composed primarily of NMDA receptors<sup>19-22</sup> which later gain AMPA receptors. These developmental changes in glutamatergic receptors suggest a situation where young, motile spines express an immature complement of receptor subunits which are then altered and replaced as the synapse matures. However, since calcium transients in spines appear to stabilize their motility<sup>8,9</sup>, these same immature receptors, known to contribute to elevated post-synaptic calcium, might also contribute to spine stabilization.

To determine whether synaptic activity regulates cortical spine dynamics and whether spine dynamics are related to glutamate receptor expression, we used two-photon microscopy in acute slices to examine the apical dendrites of cortical layer V neurons during a period when synaptogenesis is occurring throughout cortex. We find that spine motility is developmentally regulated and, in agreement with previous slice studies<sup>6</sup>, is unaffected by manipulating the general excitatory state of the network with bath application of tetrodotoxin (TTX) or membrane depolarization with KCl. Bath application of AMPA or NMDA, however, induced a reduction in spine motility,

showing that synaptic transmission is linked to morphological dynamics. Further, we performed immunolabeling for GluR1, GluR2, NR1, and NR2B subunits on slices previously imaged for motility. We found no correlation between receptor subunit expression and spine motility. These data show that spine motility in cortical spines is regulated by glutamatergic transmission, yet whole-spine expression of glutamate receptor subunits cannot explain the variability in spine motility.

## **METHODS**

### **Slice preparation and pharmacology**

Slices were prepared from postnatal day 9 (p9) to p20 transgenic mice expressing green fluorescent protein (GFP; transgenic line M) in a subset of their cortical neurons, predominantly in layer V<sup>23</sup>. All experiments were performed under protocols approved by MIT's Institutional Animal Care and Use Committee and conformed to NIH guidelines. Mice were deeply anesthetized with sodium pentobarbital (35 mg/kg, i.p.; Henry Schein Inc., Indianapolis, IN) and the brain was removed and transferred to a Vibratome (model 1000; Ted Pella Inc., Redding, Ca) containing a cold (4°C) solution containing (in mM): NaH<sub>2</sub>PO<sub>4</sub> (1), NaHCO<sub>3</sub> (25), KCl (3), MgSO<sub>4</sub> (2), dextrose(10), sucrose (252), CaCl<sub>2</sub> (2.5), and kynurenic acid (5). Slices were cut in the coronal plane at a thickness of 300 μm while in this solution and then transferred to a holding chamber containing room temperature artificial cerebrospinal fluid (ACSF) containing (in mM):

NaH<sub>2</sub>PO<sub>4</sub> (1), NaHCO<sub>3</sub> (25), KCl (3), MgSO<sub>4</sub> (2), dextrose(10), NaCl (126), and CaCl<sub>2</sub> (2.5). Slices were allowed to equilibrate for 1 hour at room temperature and were then transferred to a submersion chamber and continuously perfused with ACSF. Multiple slices from each animal were typically examined on each recording day. Some slices were additionally treated with 1  $\mu$ M tetrodotoxin (TTX; Sigma, St. Louis, MO), 10-60 mM KCl (Sigma), 2  $\mu$ M (S)- $\alpha$ -Amino-3-hydroxy-5-methylisoxazole-4-propionic acid (AMPA; Sigma), 50  $\mu$ M N-Methyl-D-aspartic acid, (NMDA; Sigma) or 1-2  $\mu$ g/mL Cytochalasin-D (Sigma) in ACSF while in the submersion chamber.

### **Two-photon imaging**

Images were collected on a custom-built two-photon laser-scanning microscope<sup>24</sup> consisting of a Fluoview confocal scanhead (Olympus, Melville, NY) and a Ti:S laser (Tsunami, Spectra-physics, Menlo Park, CA) pumped by a 10 W solid state source (Millenia, Spectra-physics). The Ti:S laser provided 100 fsec pulses at 80 MHz at a wavelength of 920 nm and fluorescence was detected with a photomultiplier tube (HC125-02, Hamamatsu, Japan) in whole field detection mode. Layer V pyramidal neurons expressing GFP were first identified under low power (10x air lens, 0.25 NA, Olympus) and individual dendrites were then identified at higher power (60x water immersion lens, 0.9 NA, IR2, Olympus) with full-field epifluorescence illumination. The 60x lens was used for subsequent identification of spiny dendrites under digital zoom

(5-8x) using two-photon imaging. Stacks with images spaced 1  $\mu\text{m}$  apart in the z-dimension were acquired every 2 or 3 minutes using Fluoview (Olympus) software over a period of 1-1.5 hours with a digital resolution of 800 by 600 or 1024 by 1024 pixels. In experiments involving bath application of pharmacological agents, z-stacks were acquired for a control period of 45 minutes, followed by a wash-in period of 10-15 minutes where no images were collected, and a second z-stack acquisition period of 45 minutes.

### **Immunostaining**

After two-photon imaging, slices were fixed in 4% paraformaldehyde and then transferred to 30% sucrose for cryoprotection. The 300  $\mu\text{m}$  slices were then frozen and resectioned in a cryostat (Reichert-Jung, now Leica, Frigocut 2800) at 40  $\mu\text{m}$ . Floating sections were blocked and permeabilized with 0.5% Triton X-100 for 30 min in normal sera, incubated with primary antibodies for 48 hr at 4°C, and subsequently incubated with secondary antibodies for 2 hr at room temperature. Sections were then mounted in buffer, coverslipped, and sealed. The following antibodies were used: mouse anti-NMDA receptor subunit 1 (NR1) (1:250, 2  $\mu\text{g}/\text{mL}$ ; PharMingen, San Diego, CA), rabbit anti-NMDA receptor subunit 2B (NR2B) (1:500, 2  $\mu\text{g}/\text{mL}$ ; Upstate Biotechnology, Lake Placid, NY), rabbit anti-glutamate receptor subunit 1 (GluR1) (1:67, 2.2  $\mu\text{g}/\text{mL}$ ; Upstate Biotechnology), mouse anti-glutamate receptor subunit 2 (GluR2) (1:500, 2  $\mu\text{g}/\text{mL}$ ;

Chemicon, Temecula, CA), goat anti-mouse Alexa 568 (1:200, 10  $\mu\text{g}/\text{mL}$ ; Molecular Probes, Eugene, OR), and goat anti-rabbit Cy5 (1:200, 7.5  $\mu\text{g}/\text{mL}$ ; Chemicon, Temecula, CA).

### **Confocal microscopy**

Immunostained sections were examined with full-field epifluorescence illumination in order to identify the neurons which had previously been imaged with two-photon microscopy. Confocal scanning microscopy was performed on a Bio-Rad (Hercules, CA) MRC-1024ES confocal system mounted on a Zeiss (Oberkochen, Germany) Axioplan microscope. All images were collected with a Zeiss Plan-Neofluar 40x oil-immersion objective with numerical aperture 1.4. Fluorescence images were obtained with a krypton-argon laser with standard lines at 488 nm (GFP), 568 nm (Alexa568), and 647 nm (Cy5) with standard filters. Z-stacks encompassing the same volumetric region that had previously been imaged with two-photon microscopy were gathered with a digital resolution of 1024 by 1024 pixels with digital zoom (6-10x) at 1  $\mu\text{m}$  increments. In order to maintain image registration and minimize bleedthrough, the three fluorescence images from the GFP and two secondary antibodies were collected sequentially with each increment of the focal plane.

## Two-photon image analysis

Images collected with the two-photon microscope were exported to MATLAB (MathWorks Inc., Natick, MA) and processed using custom-written algorithms. The four dimensional data sets  $(x,y,z,t)$  were reduced to three dimensions  $(x,y,t)$  by calculating two dimensional maximum projections of each image stack. This method of analysis underestimates spine dynamics since movements in the  $z$ -direction are not analyzed, but has the advantage of improving image contrast. The image projections were then median-filtered to reduce shot noise, and aligned to the first time point using a cross-correlation analysis. Individual spines were characterized with 3 measurements: the length of the spine as a function of time (measured from dendrite to spine tip), the diameter of the spine neck (approximate), and the diameter of the spine head (measured at its widest point). Spine motility was defined as the mean change in spine length per unit time ( $\mu\text{m}/\text{min}$ ). This measurement, in combination with the cross-correlation compensation for image drift, has the advantage of being insensitive to small variations in image alignment. Spine morphologies (stubby, mushroom, or thin) and filopodia were automatically defined using the measured head diameter, neck diameter and length for the first and last time points of every experiment, based on standard criteria<sup>25</sup>. Values are reported as mean  $\pm$  standard error. Significance values

for correlations were calculated from a linear regression analysis and the comparison of control and drug conditions were performed using a parametric paired t-test statistic.

### **Confocal image analysis**

Images collected with the confocal microscope were also exported to MATLAB. The three fluorescent image stacks, corresponding to the GFP-labeled structure of the dendrite and the fluorescence from the two secondary antibodies, were in perfect register and alignment; therefore it was possible to use the GFP signal to demarcate the  $x,y$ , and  $z$  boundaries of each individual spine and to then look at only these regions in the volumetric immunostaining stacks. The immunostaining intensity for each subunit was then calculated by integrating over all of the pixels within the volume which defined a single spine. Since the expression of receptor subunits should be enriched in spines as compared to dendrites, it was possible to normalize the immunostaining intensity at each spine with the intensity in an adjacent region of dendrite in order to account for local variations in staining intensity and in order to pool relative expression values across multiple dendrites and neurons. As with the spine motility analysis, relative expression values are reported as mean  $\pm$  standard error and significance values were calculated with linear regression analysis.

## RESULTS

### Spine motility as a function of age

We examined the motility of dendritic protrusions on GFP-expressing cortical layer V pyramidal neurons using two-photon microscopy in an acute slice preparation (Figure 2-1). Neurons from a variety of cortical regions with dendritic arborizations in multiple laminar compartments were imaged between the first and third postnatal weeks, a period of significant synaptogenesis across the cortex and within the individual layers of the rodent cortex<sup>26-28</sup>. As such, our results represent general properties of cortical layer V pyramidal neurons. The motility of individual protrusions was quantified over a period of 1 to 1.5 hours by measuring the mean change in protrusion length as a function of time (see Methods). This was found to be the most consistent and simple metric to use for large numbers of spines and has been used successfully in previous studies<sup>11,12</sup>. During the imaging period, it was very rare to see spines appear and disappear. It is likely that spine turnover occurs over longer periods on the order of days and such changes might be difficult to capture in our acute slice preparation. Additionally, protrusions were automatically categorized into one of four morphological classes: stubby, mushroom, or thin spines, and filopodia (Figure 2-2). The variability in the distribution of spine motilities (excluding filopodia) on cortical layer V pyramids in acute slices was substantially reduced (Figure 2-3a), and mean

motility significantly decreased with age (Figure 2-3b;  $r^2=0.695$ ,  $p<0.001$ ,  $n=2392$  spines from 69 cells in 36 animals) as assessed by first order best fit linear regression. This trend was consistent for each of the three types of spines (Figure 2-3c; thin,  $r^2=0.586$ ,  $p<0.005$ ,  $n=342$ ; mushroom,  $r^2=0.644$ ,  $p<0.005$ ,  $n=1412$ ; and stubby,  $r^2=0.721$ ,  $p<0.001$ ,  $n=638$ ), but not for filopodia ( $r^2=0.215$ ,  $p>0.1$ ,  $n=220$ ) which exhibited high motility at all ages examined. These findings extend previous reports *in vivo* in the somatosensory system<sup>11</sup>, and are consistent with observations of spine motility in dissociated culture<sup>9</sup> and slice culture<sup>6</sup>.

### **Spine morphology as a function of age**

In addition to characterizing spine motility over this two week period, we also considered developmental changes in spine morphology. It is generally considered that filopodia are an immature morphological protrusion and that mature spines tend towards mushroom and stubby shapes<sup>29,30</sup>. Consistent with this idea, we observed an increase in the relative number of mushroom spines over this two week period ( $r^2=0.569$ ,  $p<0.005$ ), rising from approximately 40% to 60% of the population. At the same time, the relative number of filopodia decreased significantly ( $r^2=0.485$ ,  $p<0.05$ ) falling from approximately 20% to less than 5% of the population. The relative number of thin and stubby spines remained constant over this period. These data suggest that

filopodia are present in large numbers in young dendrites and are replaced by spines at older ages, dominated principally by mushroom spines.

Additionally, we considered the frequency with which spines changed their morphological classifications over the course of our experiments, and whether these frequencies were altered over the two week developmental period. It has previously been reported that the majority of spines maintain stable morphologies, though a relatively large number, 40-50%, shift their morphologies or become undetectable<sup>31</sup>. We compared the morphologies of individual spines at the beginning and end of our experiments and observed that 29% of spines changed their morphologies over the course of 45 to 60 minutes (Figure 2-4). Interestingly, 63% of thin spines were morphologically unstable, shifting their classification to either mushroom (47%) or thin (16%) spines by the end of the experiments. In contrast, 76% of mushroom and 79% of stubby spines retained their classifications throughout the experimental period. These results suggests that thin spines, which make up a small fraction (14%) of the total spine population, are particularly prone to morphological fluctuation. In this light, thin spines might be akin to proto-spines<sup>29</sup> and occupy an intermediary step between immature filopodia and more stable mushroom or stubby spines in this system. Also, there was no apparent age-dependence of the overall rate of morphological changes or on any of the individual types of morphological switching, suggesting that similar

mechanisms may underly the dynamic changes in morphology throughout this developmental period.

### **Dependence of spine motility on actin dynamics**

Dendritic spines are enriched in actin<sup>32</sup> and their motility can be attributed to the polymerization and depolymerization of filamentous actin<sup>33</sup>. Blockade of actin polymerization at the barbed end with Cytochalasin-D<sup>6,7,34</sup> or sequestering monomeric actin with Latrunculin A<sup>7,9</sup> have been shown to inhibit spine motility. To confirm that the motility of spines on layer V pyramidal neurons was also actin-dependent, we imaged protrusions (both spines and filopodia) in acute cortical slices before and after application of 1-2  $\mu\text{g}/\text{mL}$  Cytochalasin-D (Figure 2-5a). The motility of young (p10) protrusions was significantly reduced by 43% (control  $0.044 \pm 0.0021 \mu\text{m}/\text{min}$ , Cytochalasin  $0.025 \pm 0.0009 \mu\text{m}/\text{min}$ ,  $n=37$ ,  $p<0.0001$ ). These data suggest that Cytochalasin-D reduces protrusion motility to approximately  $0.025 \mu\text{m}/\text{min}$  at this age, irrespective of the initial level of motility. We repeated this analysis after measuring the motility of old (p18) protrusions before and after Cytochalasin-D treatment, and found that average motility was reduced by 41.6% (control  $0.032 \pm 0.0031 \mu\text{m}/\text{min}$ , Cytochalasin  $0.0187 \pm 0.0016 \mu\text{m}/\text{min}$ ,  $n=27$ ,  $p<0.0005$ ). This suggests that at this later age, Cytochalasin-D reduces protrusion motility to approximately  $0.020 \mu\text{m}/\text{min}$ . These results were significant at both ages whether filopodia were or were not included in the

analysis. Protrusion motility of 0.025  $\mu\text{m}/\text{min}$  at p10 and 0.020  $\mu\text{m}/\text{min}$  at p18 probably represents the average minimum motility when actin polymerization is blocked at filamentous actin barbed ends at these ages.

### **Dependence of spine motility on activity**

There are varying reports concerning the activity-dependence of spine motility. Increased extracellular KCl, which increases a neuron's excitability, has been shown to either inhibit motility<sup>8</sup> or have no effect<sup>6</sup>. Specifically, in dissociated hippocampal cultures, increasing extracellular potassium to 6 mM was sufficient to inhibit spine motility<sup>8</sup>, while other have been unable to see any effect in cultured slices in the range of 6-60 mM<sup>6</sup>. We assessed the effects of increasing extracellular potassium concentration on protrusion motility in young slices (p13) by raising the bath KCl concentration from 3 mM to 10 or 60 mM (Figure 2-5b). In both cases, there was no effect of increased KCl on protrusion motility (control  $0.046 \pm 0.0037 \mu\text{m}/\text{min}$ , 10 mM KCl  $0.044 \pm 0.0018 \mu\text{m}/\text{min}$ ,  $n=31$ ,  $p>0.5$ ; control  $0.046 \pm 0.0038 \mu\text{m}/\text{min}$ , 60 mM KCl  $0.044 \pm 0.0034 \mu\text{m}/\text{min}$ ,  $n=29$ ,  $p>0.5$ ). The results were identical when filopodia were excluded from the analysis. This result confirms the previous results in cultured slice<sup>6</sup> and suggests that there may be important differences in the efficacy of KCl on spine motility between slices and dissociated cultures.

Tetrodotoxin (TTX), a toxin which blocks sodium channels involved in action potential generation, has also been shown to be involved with in motility. In dissociated hippocampal culture, TTX has been shown to increase actin turnover<sup>34</sup> and to increase spine motility<sup>9</sup>. We used 1  $\mu$ M TTX to determine the effects of action potential blockade on protrusion motility in our acute slice preparation at p14 (Figure 2-5c). In two experiments, we saw no effect of TTX on protrusion motility (experiment 1, control  $0.046 \pm 0.0030$   $\mu$ m/min, TTX  $0.045 \pm 0.0026$   $\mu$ m/min,  $n=27$ ,  $p>0.7$ ; experiment 2, control  $0.035 \pm 0.0018$   $\mu$ m/min, TTX  $0.032 \pm 0.0013$   $\mu$ m/min,  $n=53$ ,  $p>0.2$ ). As in the previous experiments, removing filopodia from the analysis gave the same result. As with the KCl treatment, there appears to be no effect of manipulating cell excitability on spine motility in our acute slice preparation.

### **Dependence of spine motility on glutamatergic activity**

Since spines contain the post-synaptic elements of a synapse, their dynamics may influence synaptic efficacy and may in turn be influenced by synaptic transmission. In hippocampal cultures, spine dynamics were inhibited by glutamatergic receptors while antagonists of the NMDA receptor had no effect on spine motility<sup>8</sup>. Alternately, in cultured slices, glutamate, NMDA, or CNQX, an antagonist of AMPA and kainate receptors, were found to have no effect on spine motility<sup>6</sup>. To investigate the effects of glutamatergic receptor activation on protrusion motility in our slice preparation, we

bathed slices in either 2  $\mu\text{M}$  AMPA (Figure 2-5d) or 50  $\mu\text{M}$  NMDA in zero magnesium ACSF (Figure 2-5e). In the youngest protrusions (p9), 2  $\mu\text{M}$  AMPA significantly reduced protrusion motility by 29.6% (control  $0.068 \pm 0.0075 \mu\text{m}/\text{min}$ , AMPA  $0.048 \pm 0.0050 \mu\text{m}/\text{min}$ ,  $n=23$ ,  $p<0.05$ ). This effect was mediated by a strong reduction in the motility of filopodia as the difference disappeared after removing the filopodia from analysis (control  $0.063 \pm 0.0084 \mu\text{m}/\text{min}$ , AMPA  $0.046 \pm 0.0065 \mu\text{m}/\text{min}$ ,  $n=16$ ,  $p>0.2$ ), though the general trend remained. At older ages, 2  $\mu\text{M}$  AMPA also reduced protrusion motility by either 23.9% at p13 (control  $0.034 \pm 0.0022 \mu\text{m}/\text{min}$ , AMPA  $0.026 \pm 0.0013 \mu\text{m}/\text{min}$ ,  $n=23$ ,  $p<0.05$ ) or 13.2% at p14 (control  $0.034 \pm 0.0019 \mu\text{m}/\text{min}$ , AMPA  $0.030 \pm 0.0014 \mu\text{m}/\text{min}$ ,  $n=45$ ,  $p<0.5$ ). The results at p13 and p14 were nearly identical when filopodia were removed from analysis. Spine motility was also reduced by bath application of NMDA in the absence of external magnesium at p11 (control  $0.044 \pm 0.0047 \mu\text{m}/\text{min}$ , NMDA  $0.031 \pm 0.0025 \mu\text{m}/\text{min}$ ,  $n=20$ ,  $p<0.005$ ) and in two separate experiments at p13 (experiment 1 control  $0.028 \pm 0.0014 \mu\text{m}/\text{min}$ , NMDA  $0.025 \pm 0.0011 \mu\text{m}/\text{min}$ ,  $n=35$ ,  $p<0.05$ ; experiment 2 control  $0.037 \pm 0.0030 \mu\text{m}/\text{min}$ , NMDA  $0.027 \pm 0.0019 \mu\text{m}/\text{min}$ ,  $n=34$ ,  $p<0.005$ ). These results were also identical whether or not filopodia were removed from analysis. For all three experiments with NMDA application, spine motility was briefly recorded while perfusing ACSF containing zero magnesium without NMDA over the slices. Spine motility in this condition was not significantly different from spine

motility in control ACSF in all three experiments ( $p > 0.4$  in each experiment). These results, interestingly, confirm results in dissociated cultured neurons that protrusion motility is reduced by glutamatergic activity<sup>8</sup>.

### **Glutamate receptor expression and protrusion motility**

Since glutamatergic receptor expression is developmentally regulated in the cortex<sup>14-18</sup> and since glutamatergic activation appears to be important for regulating dendritic protrusion motility, we were interested in examining whether glutamate receptor expression might correlate with spine motility. Based on the observation that AMPA and NMDA receptor subunits are developmentally regulated, young, motile spines might express an “immature” set of receptor subunits and correlate positively with high levels of NR1 and NR2B, low levels of GluR2, and a low GluR1 to NR1 ratio, while older, more stable spines would have the inverse of these relationships. Alternately, since glutamatergic activation appears to stabilize spines and since post-synaptic calcium transients have been implicated in regulating spine motility in culture<sup>8,9</sup>, receptor subunits which facilitate calcium influx, such as NR1, NR2B, and the absence of GluR2, could contribute to protrusion stabilization and be negatively correlated with motility.

In order to correlate the expression of AMPA and NMDA receptors with protrusion motility, we fixed slices post-imaging and then double immunostained for

pairwise combinations of NR1, NR2B, GluR1, or GluR2 receptor subunits. In low power images, these subunits were very highly expressed in the hippocampus and were expressed to a lesser degree in the cortex<sup>35</sup>. Using the characteristic dendritic arbors of the GFP-expressing neurons, we were able to identify, after immunostaining, the same spines which had previously been imaged with the two-photon microscope. The region of these spines was then re-imaged with high resolution confocal microscopy in order to assess the expression of the various receptor subunits. Numerical analysis was performed by first identifying the structure of the spine based on the structural GFP signal and then integrating the immunostaining signal over the entire volume of the spine. Figure 2-6 shows a typical experiment in which spines were first imaged with two-photon microscopy (Figure 2-6a,b) and then immunostained for GluR2 and GluR1 subunits (Figure 2-6c,d,e). In this experiment, there was no correlation between GluR1 staining intensity or GluR2 staining intensity with protrusion motility (GluR1,  $r^2=0.045$ ,  $p>0.3$ ; GluR2,  $r^2=0.042$ ,  $p>0.3$ ,  $n=25$  from one cell). This lack of correlation was consistent across the entire population of protrusions which were examined (Figure 2-6f,g; GluR1,  $r^2=0.0058$ ,  $n=168$ ,  $p>0.3$ , 6 cells; GluR2,  $r^2=0.0019$ ,  $n=80$ ,  $p>0.5$ , 3 cells). Similarly, Figure 2-7 shows a typical dendritic region which was imaged with two-photon microscopy (Figure 2-7a,b) and subsequently immunostained for NR1 and NR2B subunits (Figure 5C,D,E). We found no correlation between NR1 staining intensity or NR2B intensity

with spine motility (NR1,  $r^2=0.017$ ,  $p>0.4$ ; NR2B,  $r^2=0.039$ ,  $p>0.2$ ,  $n=41$  from one cell). As with the AMPA receptor subunits, the entire population of protrusions showed no correlation between NMDA receptor subunits and protrusion motility (Figure 5F,G; NR1,  $r^2=0.013$ ,  $n=223$ ,  $p>0.05$ , 11 cells; NR2B,  $r^2<0.001$ ,  $n=99$ ,  $p>0.9$ , 4 cells). These results suggest that AMPA and NMDA receptor expression is extremely variable on a spine to spine basis, and that this variability does not correlate with the observed motility of individual spines.

### **Glutamate receptor co-expression and protrusion motility**

Since there was no obvious correlation between absolute receptor expression and protrusion motility, we wondered whether the important factor for motility might be the relative expression of different subunits with respect to one another. In general, due to nonlinearities in the immunostaining process, it is not possible to quantify the absolute number of receptors as a function of staining intensities, though it is possible to measure their relative abundance qualitatively. In order to directly assess the effects of the coexpression of the various receptor subunits in our data set on spine motility, we examined the NR2B to NR1, GluR2 to GluR1, and NR1 to GluR1 ratios in relation to spine motility. None of these three ratios correlated with protrusion motility (NR2B/NR1,  $r^2=0.008$ ,  $n=99$ ,  $p>0.3$ ; GluR2/GluR1,  $r^2<0.006$ ,  $n=80$ ,  $p>0.4$ ; NR1/GluR1,  $r^2<0.001$ ,  $n=88$ ,  $p>0.8$ ), indicating that the relative expression of receptor subunits, at

least in the pool of receptors available in a spine, is not an important factor in regulating motility.

Additionally, we were interested in examining how well the components of AMPA and NMDA receptors correlated with the other subunits of the receptors. In fact, the correlation between NR1 and GluR1 expression in individual spines was very strong ( $r^2=0.0762$ ,  $n=88$ ,  $p<0.01$ ), suggesting that, although there is a lot of variability, the relative expression level of these two receptor subunits was linked. The correlated expression of the NR1 and NR2B receptor subunits was also significant ( $r^2=0.0409$ ,  $n=99$ ,  $p<0.05$ ), indicating that high levels of NR1 expression tended to also have high levels of NR2B expression. Interestingly, the expression of GluR1 and GluR2 receptor subunits was not significantly correlated ( $r^2=0.018$ ,  $n=80$ ,  $p>0.2$ ), implying that GluR2 expression is not dependent on GluR1 expression. This supports the hypothesis that the presence of GluR1 and GluR2 receptor subunits are independently regulated at the level of the dendritic spine<sup>36-38</sup>. Further, the lack of correlation between GluR2 and GluR1 expression serves as a negative control, indicating that there is no major systematic bias of detecting correlated expression.

### **Glutamate receptor expression and spine morphology**

Since spine motility and glutamatergic receptor expression do not appear to be correlated, we asked whether simpler metrics, such as the size or morphology of a spine

could be predictive of its receptor expression profile. There was no correlation between receptor expression and spine size (NR1  $r^2=0.0143$ ,  $n=216$ ,  $p>0.05$ ; NR2B  $r^2=0.0036$ ,  $n=92$ ,  $p>0.5$ ; GluR1  $r^2=0.0049$ ,  $n=161$ ,  $p>0.3$ ; GluR2  $r^2=0.0033$ ,  $n=74$ ,  $p>0.05$ ), contrary to some previous reports<sup>39</sup>. However, there was a significant difference in both GluR1 and NR2B expression across spine morphologies (Figure 2-8). Thin spines and filopodia had a lower expression of GluR1 than mushroom spines (thin vs. mushroom,  $p<0.05$ , filopodia vs. mushroom  $p<0.05$ ) and filopodia had a higher expression of NR2B than thin ( $p<0.05$ ), mushroom ( $p<0.01$ ), or stubby spines ( $p<0.001$ ). These results confirm a previous report that there are few AMPA receptors in filopodia or thin spines in comparison to high receptor expression in mushroom spines<sup>40</sup>. Since filopodia are very motile, we additionally examined whether the most motile spines might have similar NR2B and GluR1 profiles to filopodia. After selecting the 20 most motile spines (not including filopodia), we found that the most motile spines were not significantly different from mushroom spines for GluR1 expression ( $p>0.3$ ), nor were they different from any class of spine for NR2B expression (thin spines,  $p>0.9$ ; mushroom spines,  $p>0.5$ ; stubby spines,  $p>0.2$ ). Filopodia make up a small percentage (4.9%) of the data sets shown in Figures 4 and 5, so it is not surprising that their high motility and strong correlation with GluR1 and NR2B expression do not influence the correlations within the larger data set of all protrusions. Taken, together, these results support the idea that

filopodia may be immature protrusions which express relatively high levels of the “young” NMDA receptor subunit NR2B, and lack the AMPA receptor subunit GluR1, which is thought to convert “silent” into functional synapses. Also, since thin spines have lower GluR1 expression, they may represent an intermediate state between filopodia and more stable spines, where AMPA receptors are entering, or being removed from, spines. These results highlight that, although spine morphology may be important for determining functional maturity at synapses, it cannot explain all of the variation in glutamatergic receptor expression in the thin, mushroom and stubby spine morphologies.

## **DISCUSSION**

In order to assess whether synaptic activation influenced the structural dynamics of dendritic spines, we have examined spine motility on apical dendrites of layer V pyramidal neurons in an acute slice preparation. Our results help to resolve an important debate regarding the importance of synaptic activity on dendritic structural dynamics by demonstrating, in a preparation with significant intact circuitry, a reduction in spine motility by glutamatergic activation of AMPA or NMDA receptors. This effect had previously been shown in dissociated culture<sup>8</sup>, but was not observed in cultured slice preparations<sup>6</sup>. The stabilizing effect of synaptic activation on spines is in contrast to generalized depolarization with KCl or blockade of action potentials with

TTX which had no effect on spine dynamics. These results also suggest an apparent disparity between experiments in dissociated culture systems<sup>8,9</sup> which find a strong effect of KCl and TTX on spine motility, and those in cultured slice which find no effect. It is unclear why this should be so, though the difference could lie in the sparse connectivity of low-density cultures as opposed to the tissue-specific structure of connections present in slice preparations, or in the use of GFP-actin (as used in the culture experiments) to visualize spines rather than the spines themselves. These results argue strongly for the hypothesis that glutamatergic activity provides a regulatory mechanism for spine motility in intact systems and that this relationship is likely to be preserved *in vivo*.

Other experiments have also explored the importance of synaptic activity for regulating dendritic spines. Notably, AMPA receptor activation via spontaneous glutamate release appears to be necessary for maintaining spine morphology and density in hippocampal slice cultures over a period of days<sup>41</sup>. Interestingly, this study also found no effect of action potential blockade via TTX application in altering spine density or morphology profiles, suggesting that the maintenance is specific to AMPA receptor activation. This spine maintenance may be similar to spine dynamics, as both are likely to be integrative processes where spines with inadequate or overabundant activation over long periods may alter their morphological and dynamic properties in

response to their specific history of activation. Also, studies of synaptic activation by focal stimulation in hippocampal slice cultures have shown that filopodial outgrowth can occur within 30 minutes of potentiation<sup>42</sup> or lead to the emergence of new spines over the course of several hours<sup>43</sup>. In these studies, it is not clear that spine motility and protrusion outgrowth are synonymous, as one can imagine a scenario where a local potentiating signal induces the outgrowth of a spine and then serves to stabilize the spine once it has appeared. However, the implication of these experiments is that synaptic activation is important for both the formation of new spines and presumably new synapses, as well as for altering spine morphology and structural dynamics.

One potentially important experimental paradigm which may resolve the role of spine motility in intact systems is the analysis of spines *in vivo*. In some areas of the cortex, spines and synapses are constantly being created and removed over long time scales<sup>44</sup> in the intact animal, though there is still some controversy regarding this point<sup>45</sup>. Also, in one initial experiment, spine motility was dramatically reduced in the somatosensory barrel cortex following whisker trimming<sup>11</sup>. This reduction in spine motility, at first, seems counterintuitive, given that reduced activity tends to increase spine motility in dissociated cultures<sup>9,34</sup>. Recent work in our laboratory suggests that the difference between the *in vitro* and *in vivo* work might also be an effect specific to the somatosensory system, as visual deprivation experiments results in increased spine

motility *in vivo* during the critical period<sup>12</sup>. Further experiments are needed to determine whether the relationship between activity-dependent mechanisms that regulate spine movement might also shape the formation and loss of synaptic connections.

### **Developmental effects on spine motility**

In the mouse cortex, synaptogenesis occurs at an accelerated rate for the first two postnatal weeks, but is ongoing until approximately p32<sup>26</sup> and has been shown to occur concurrently across the cortex and throughout the cortical layers<sup>27,28,46,47</sup>. During this period of elevated synaptogenesis in cortex, we find that spine motility on layer V pyramidal neurons throughout the cortex is actin-dependent and decreases for all spine types except filopodia, which remain highly motile but become less frequent in number as development progresses. These findings significantly extend a previous report of spine motility *in vivo* in layer II pyramidal cells in the somatosensory system<sup>11</sup>, and suggest that the decrease in spine motility is a common property of all morphological classes of spines (but not filopodia) as well as a general property of developing, spiny pyramidal neurons. These findings also corroborate results from cerebellar, cortical, and hippocampal slice cultures<sup>6</sup> and dissociated cell culture experiments<sup>9</sup> which found a decrease in spine motility with days *in vitro*.

### **Glutamate receptor subunit expression and spine motility**

Having observed a strong influence of synaptic glutamate receptor activation on spine motility, we further examined the expression of glutamate receptor subunits on individual spines. Initially, we expected that spine motility would be either correlated with the developmental expression of AMPA and NMDA receptors, or with the ability to flux calcium ions which could then stabilize the cytoskeletal network. However, in our population of spines, the relative expression patterns of NR1, NR2B, GluR1, GluR2, or the ratios of the glutamatergic subunits did not correlate with the motilities of individual spines.

Since spine motility decreases with age, it is tempting to assume that the variations in motility at any point in development reflect the relative ages of individual spines, such that “young” spines are more motile and “old” spines are less motile. However, in cortex, the developmentally regulated change in the relative expression of glutamatergic receptor subunits<sup>14-18</sup> is superimposed on the reduction in spine dynamics. Our data suggests that these two processes are essentially independent and the subunit expression is insufficient for predicting spine motility. Further, subunits which might enhance the flux of calcium and potentially stabilize the cytoskeleton, such as the NR2B subunit, are present in abundance at young ages when spines are most motile and, in our data, on filopodia, suggesting that calcium cannot be the only

determinant of a spine's dynamic profile. Rather, it seems likely that multiple, possibly homeostatic, developmental events shape both a spine's ability to respond to an influx of calcium as well as the complement of receptor subunits which determine its ability to respond to synaptic stimulation.

Finally, there is the consideration of whether immunostaining provides sufficient resolution to accurately detect receptor expression in individual spines and whether this has any bearing on the functional distribution of subunits in the synapse. Certainly, immunostaining for receptors in a section<sup>48</sup> is more complicated than in culture<sup>22</sup> and reflects both membranous and cytoplasmic receptor expression. However, there is some evidence that the cytoplasmic receptor expression is proportional to expression at synapses<sup>49-52</sup>. Further, in experiments where exogenous AMPA receptor subunits were overexpressed in hippocampal neurons, once the subunits were driven into spines by mechanisms involving their cytoplasmic tails, their expression at synapses was detectable with electrophysiological recordings<sup>22,37,53</sup>. These findings suggest that assaying endogenous receptor subunit expression in individual spines might be sufficient to estimate the amount of functional subunits incorporated at the synapse. Taken together, our findings suggest that spine dynamics are intimately related to glutamatergic synaptic activity, but that the expression pattern of glutamatergic

receptor subunits appears to be insufficient to explain spine motility either from a developmental or cytoskeletal stabilization perspective.

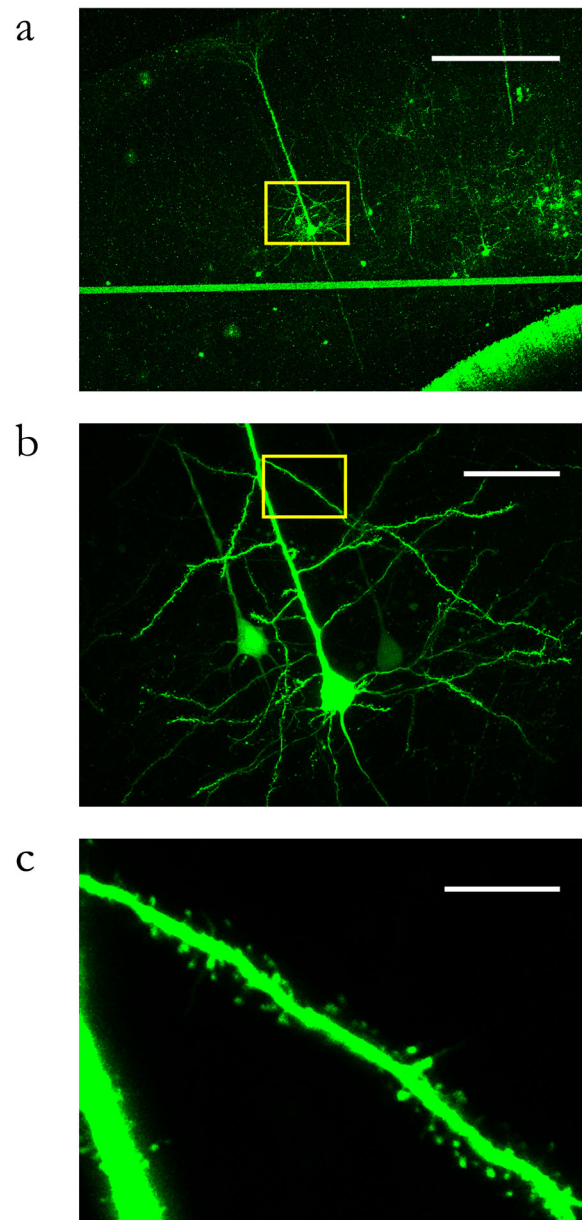


**Figure 2-1.** Acute slices from mice expressing GFP in a subset of their layer V pyramidal neurons were imaged with two-photon microscopy at successively higher magnifications. **a**, Multiple neurons express GFP in a 10x field of view (scale bar, 400  $\mu\text{m}$ ). The long horizontal line is auto-fluorescence from a piece of nylon used to immobilize the slice. **b**, At 60x, it is easy to distinguish features of single cells including primary and secondary dendritic branches off the apical dendrite (scale bar, 50  $\mu\text{m}$ ). **c**, By using the zoom feature of the laser scanning system, individual spines can be identified and tracked over time (scale bar, 10  $\mu\text{m}$ ).

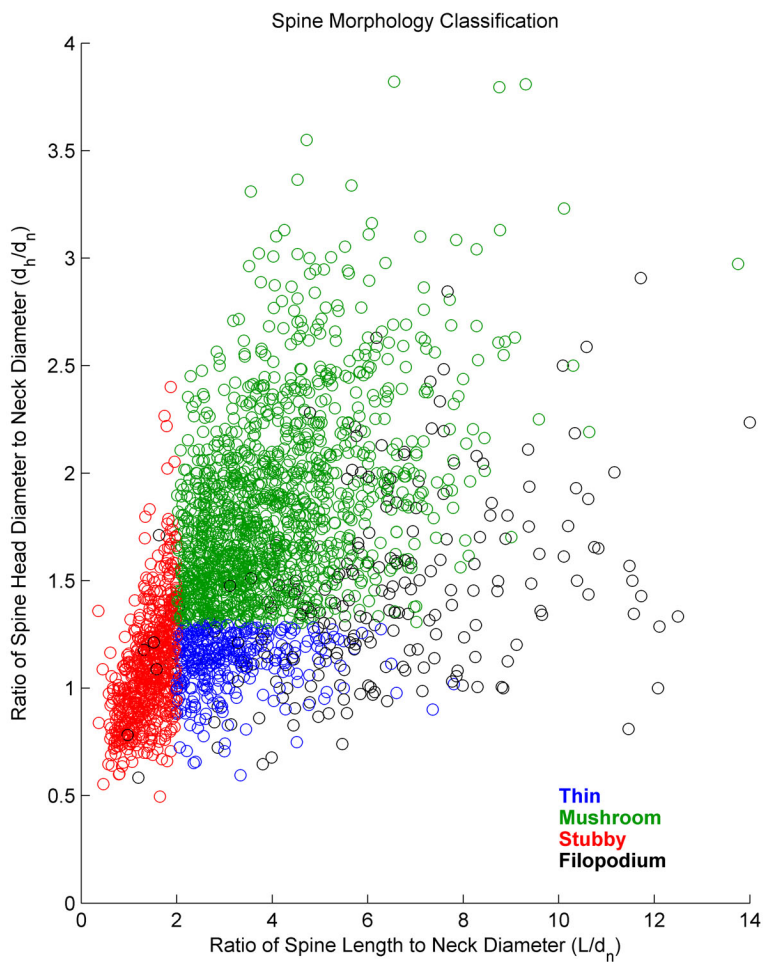


**Figure 2-2.** Dendritic protrusion morphologies are classified based on proportions of neck and head diameter and spine length. The morphological properties of 2612 dendritic protrusions (2392 spines, 220 filopodia) are shown. Thin spines (blue), mushroom spines (green), and stubby spines (red) were automatically classified based on morphological parameters, while filopodia were classified by eye based on their length and dynamic properties.

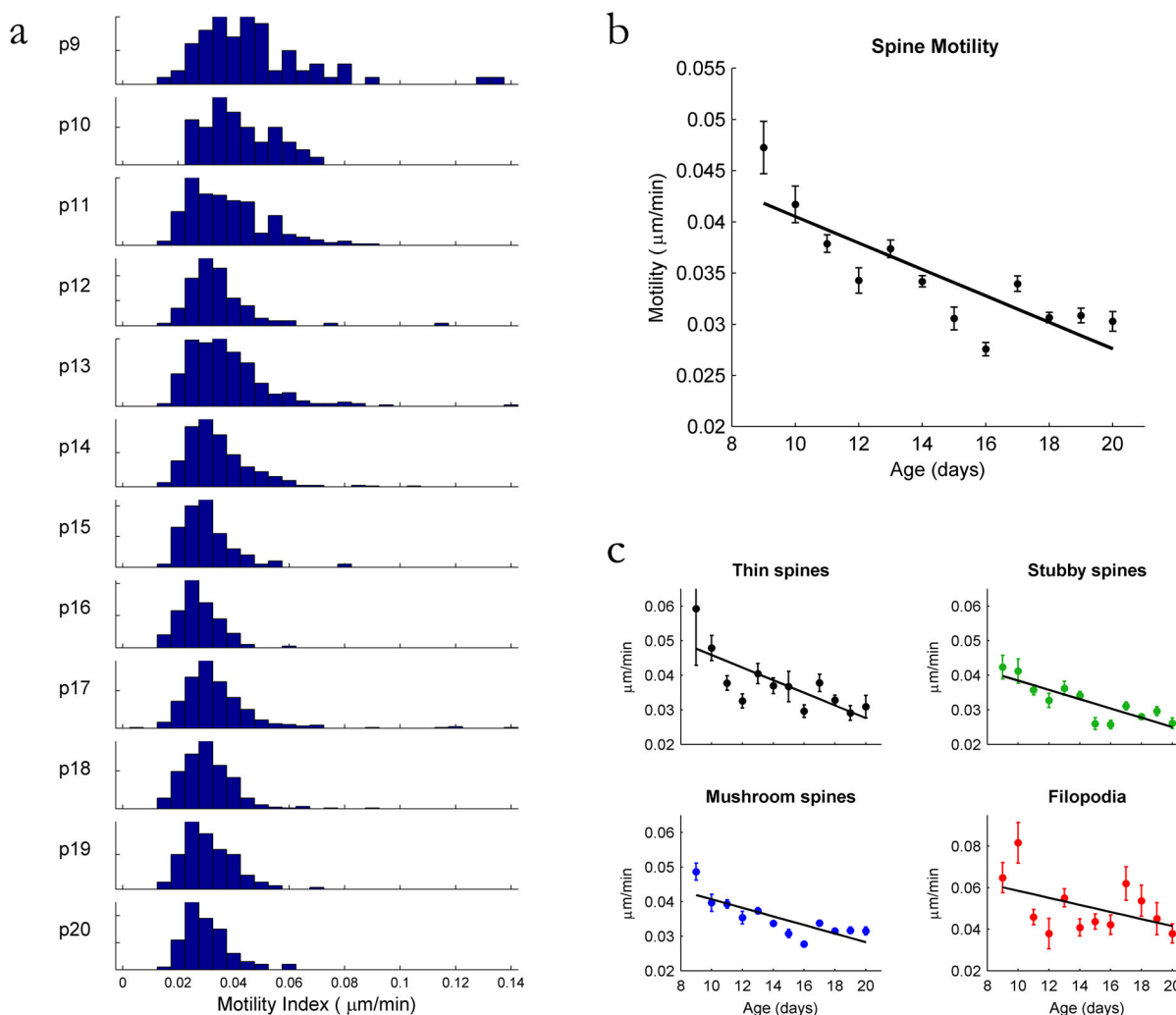


**Figure 2-3.** Spine motility (measured in  $\mu\text{m}/\text{min}$ ) declines as a function of age. **a**, The distribution of motility from all spines measured from p9 to p20 shows a decline in both the variability and mean in spine motility. **b**, Mean spine motility for all dendritic spines (thin, mushroom, and stubby) decreases significantly over development. **c**, The decrease in motility is shown for each type of spine as well as filopodia. Motility decreases significantly for each spine classification, while filopodia maintain a high level of motility throughout the developmental period.

	To Thin	To Mushroom	To Stubby	Total
Thin	126 (37%)	161 (47%)	54 (16%)	342
Mushroom	193 (14%)	1075 (76%)	144 (10%)	1412
Stubby	43 (7%)	89 (14%)	504 (79%)	638

**Figure 2-4.** Dendritic spines change morphological classifications over a single experimental session. Rows designate starting morphology while columns indicate final morphology. Spines listed along the diagonal did not change their classification (thin to thin, mushroom to mushroom, stubby to stubby). The majority of mushroom and stubby spines remained stable over the experimental period, while most thin spines were converted into mushroom spines. The final column lists the total number of thin, mushroom, and stubby spines in this data set. (These totals include 1 stubby and 2 thin spines from which reliable morphological measurements could not be made at the end of the experimental session.) Since filopodia were defined by their dynamic properties, they were assumed to remain filopodia for the entirety of the experiment and are not listed here.

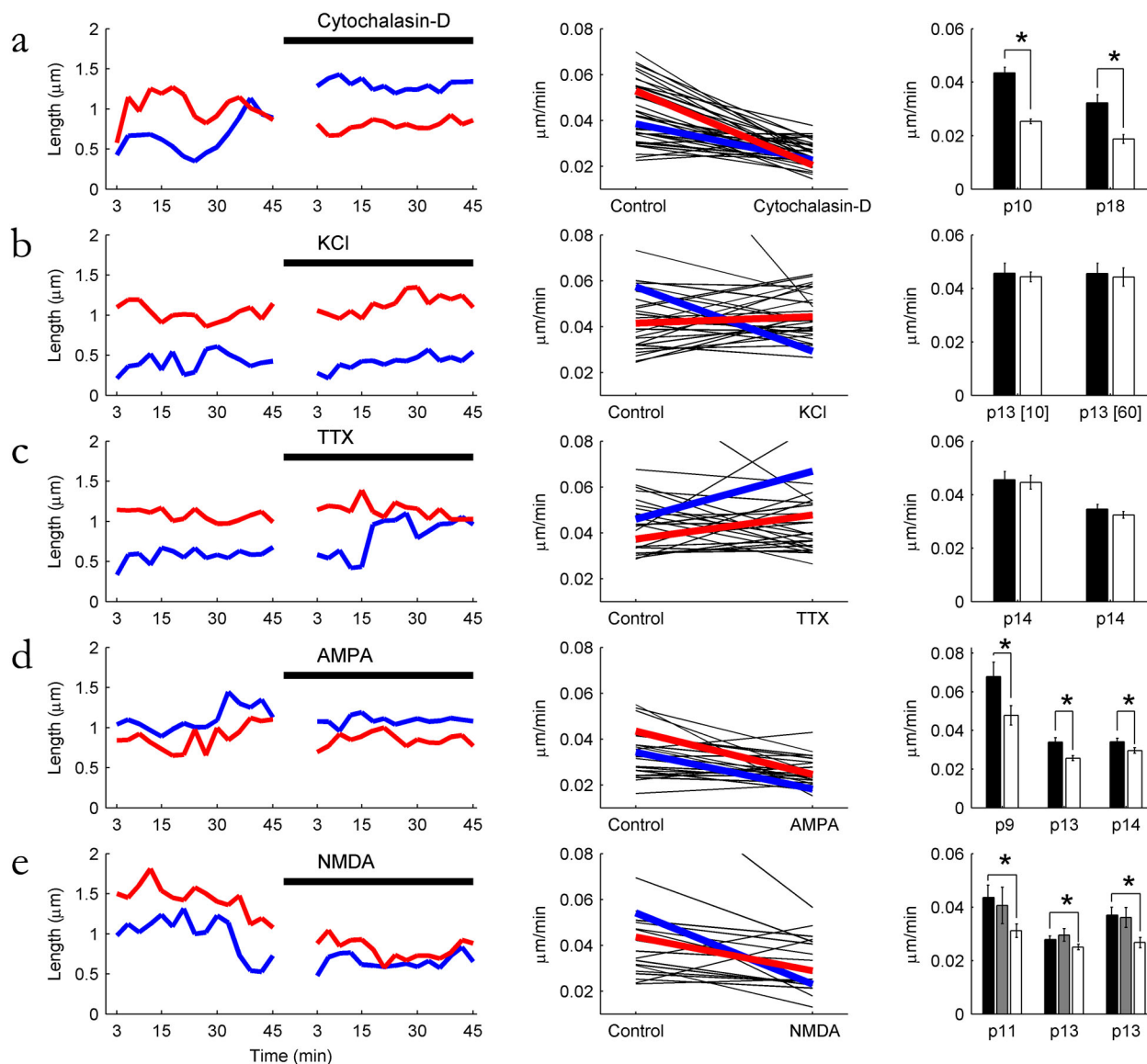


**Figure 2-5.** Protrusion motility is reduced by glutamatergic activation and blockade of actin polymerization. **a**, Cytochalasin-D significantly reduces spine motility in two example spines (left panel), as well as other spines in a single experiment (middle panel). Two experiments in “young” (p10) and “old” (p18) animals are summarized in the right panel. **b**, Depolarization with KCl at p13 has no effect on spine motility. **c**, Action-potential blockade with TTX also has no effect in two separate experiments at p14. **d**, AMPA significantly reduces spine motility at p9, p13, and p14. **e**, NMDA significantly reduces spine motility at p11 and in two separate experiments at p13. Grey bars in the rightmost panel indicate spine motility in ACSF containing zero magnesium; spine motility is not significantly different from normal ACSF.

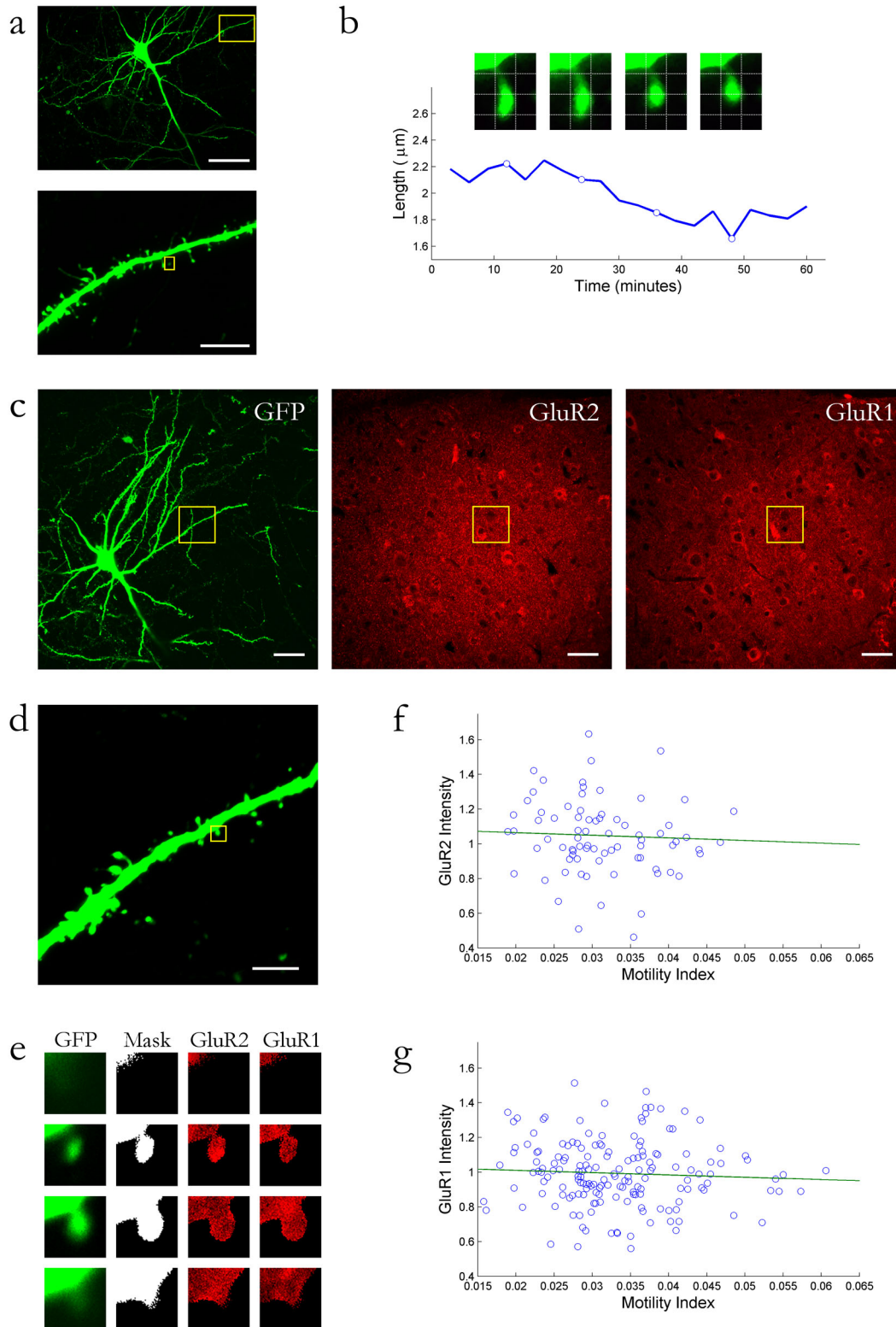


Figure 2-6

**Figure 2-6.** AMPA receptor expression is insufficient to explain spine motility. **a**, The top panel shows a maximal z-projection of a neuron imaged with two-photon microscopy (scale bar, 50  $\mu\text{m}$ ). The lower panel shows the boxed region in the top panel at higher magnification (scale bar, 10  $\mu\text{m}$ ). **b**, The length of the spine boxed in the lower panel of **a** is measured over time. The inset images show the spine at each of the timepoints indicated by circles in the plot. **c**, The same neuron from **a** is re-imaged under confocal microscopy after it has undergone immunostaining for AMPA receptor subunits GluR2 and GluR1. The left panel shows a maximal z-projection of the neuron, while the middle and right panels show single z-planes of the immunostaining for GluR2 and GluR1 (scale bars, 50  $\mu\text{m}$ ). **d**, The same region from the bottom panel of **a** and the boxed region of **c** is shown at higher magnification. The scale bar represents 10  $\mu\text{m}$  in the focal plane. **e**, An individual spine which is boxed in **d** is shown at four z-levels, each spaced 1  $\mu\text{m}$  apart. The left column shows the structural GFP fluorescence and the second column shows a thresholded version of the GFP image which acts as a mask to locate the spine in the immunostaining image. The third and fourth columns show the GluR2 and GluR1 immunostaining for this particular spine. **f**, The population data for all spines indicate that there is no correlation between GluR2 immunostaining intensity and spine motility or **g**, between GluR1 immunostaining intensity and spine motility.

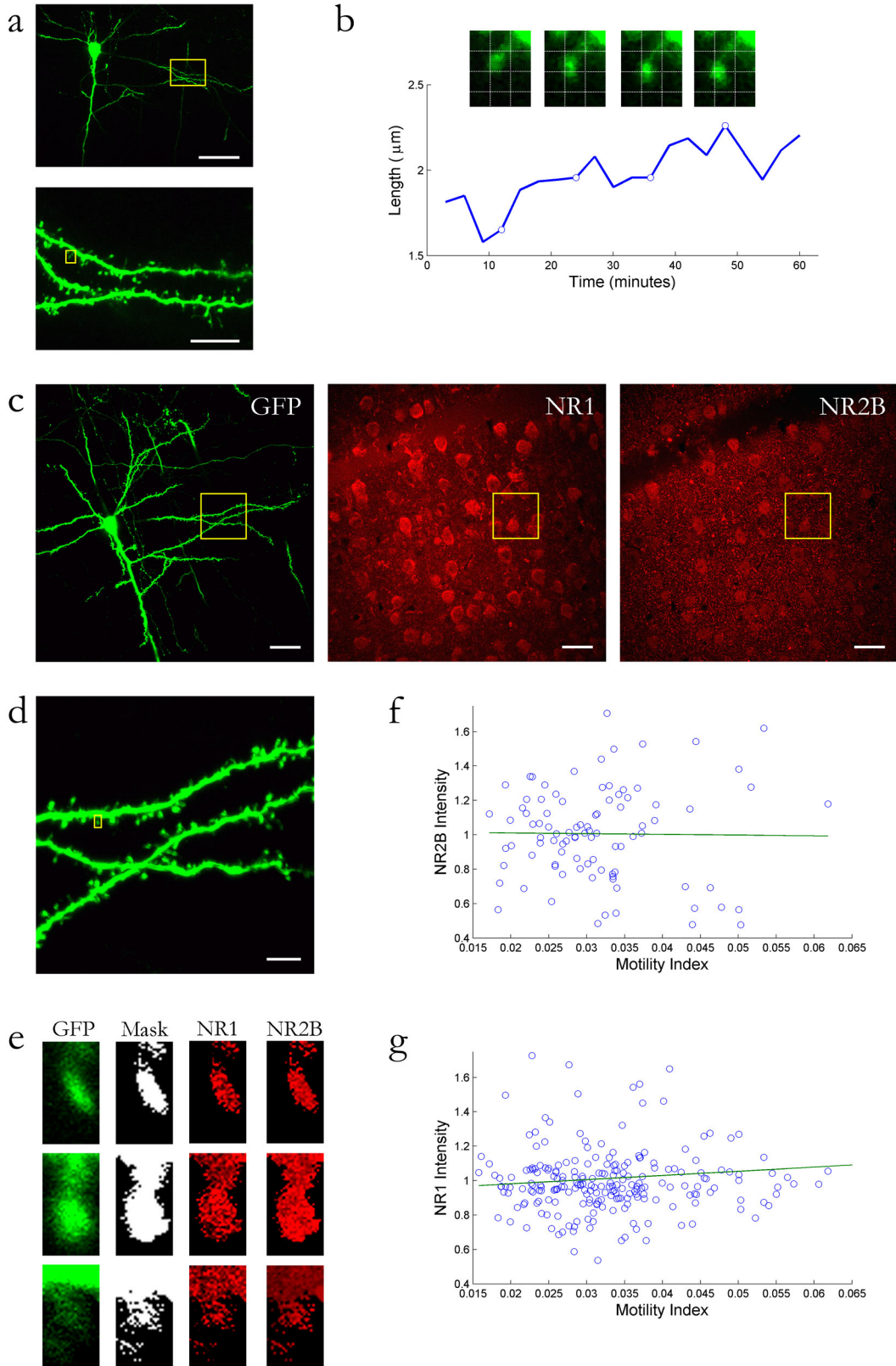
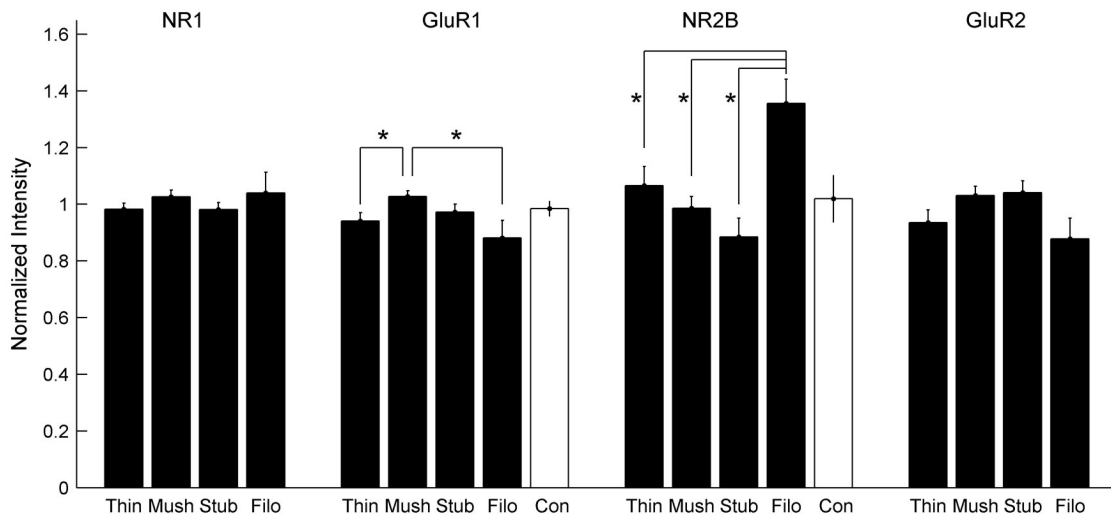


Figure 2-7

**Figure 2-7.** NMDA receptor expression is insufficient to explain spine motility. All conventions are as described for Figure 2-6. **a,b**, A dendritic section imaged under two-photon microscopy **c,d,e**, is re-imaged after immunostaining for NMDA receptor subunits NR1 and NR2B (scale bars as in Figure 2-6). **f**, The population data for all spines indicate that there is no correlation between NR1 immunostaining intensity and spine motility or **g**, between NR2B immunostaining intensity and spine motility.



**Figure 2-8.** Normalized receptor expression is dependent on spine morphology. Thin spines and filopodia have less GluR1 expression than mushroom spines, and filopodia have more NR2B expression than the other spine classifications. Additionally, the 20 most motile spines (white bars for GluR1 and NR2B), not including filopodia, do not exhibit the same expression patterns as filopodia. Comparisons indicated by an asterisk are significant at  $p < 0.05$ .

## CHAPTER 3

# Dendritic spine dynamics are regulated by monocular deprivation and extracellular matrix degradation

### INTRODUCTION

Ocular dominance plasticity occurs in the visual cortex during a well-defined critical period, first observed in cats<sup>54-56</sup> and recently described in mice<sup>57</sup>, and has served as a model for experience-dependent plasticity throughout the central nervous system. In mice, the critical period for ocular dominance plasticity in V1 occurs just as the processes of excitatory and inhibitory synaptogenesis are coming to a close<sup>26,46</sup>, and is likely to be controlled by the functional maturation of inhibitory connections<sup>58-61</sup>. Monocular deprivation, for even one to two days, at the peak of the critical period, shifts the responses of cells towards the open eye<sup>55,56,62-64</sup>. This rapid change in the functional properties of cortical neurons is accompanied by long term depression (LTD) of synapses in the deprived cortex<sup>65-67</sup>. In contrast, the reduction of cortical area driven by the closed eye and concomitant expansion of the open eye, as examined by the extent and complexity of thalamocortical axonal arbors, proceeds on the timescale of weeks to months<sup>68-70</sup>. This indicates that following monocular deprivation, processes at the level

of synapses may guide large-scale reorganization of anatomical connectivity. Further, recent work has found that both changes in functional properties and anatomical connectivity may occur more rapidly in the horizontal connections of the superficial and deep cortical layers before being relayed to layer IV<sup>64,71</sup>, suggesting that there might be a top-down reorganization following ocular dominance plasticity. However, the mechanisms that intervene between the rapid loss of physiological responses driven by the deprived eye and the anatomical reorganization of dendritic and axonal arborizations remain unknown.

One possible locus of both functional and anatomical change is at the level of dendritic spines which are structural specializations that contain the post-synaptic elements of excitatory synapses<sup>4</sup>. Spines receive the majority of excitatory input in the mammalian CNS<sup>1,2</sup> and are known to be important for compartmentalizing synaptic signals<sup>72-79</sup>. Additionally, spines are motile structures<sup>6,7</sup> whose dynamics are likely to play a role in their functional properties<sup>13</sup>. These dynamics may be further regulated by glutamatergic activity<sup>8</sup> although this finding is still controversial<sup>6</sup> (*see previous chapter*). Spine dynamics decrease over development<sup>11</sup> and, by the critical period for ocular dominance plasticity in mice, spines have achieved a relatively stable state<sup>12</sup>. Binocular deprivation, by reducing visual cortical activity over long periods of time, increases

spine motility<sup>12</sup>. This increase in dynamics may reflect a process by which spines are destabilized and actively try to increase their synaptic drive.

Here we examine rapid structural changes at the level of synapses by imaging dendritic spines following brief monocular deprivation. Our findings provide clear evidence that brief monocular deprivation initiates a rapid upregulation in structural dynamics and that this effect is initially restricted to the superficial and deep layers of cortex. We also find that spine motility is elevated by proteolysis of the extracellular matrix (ECM) with the tPA/plasmin cascade, which has previously been implicated in ocular dominance plasticity<sup>80,81</sup>. Further, monocular deprivation occludes a subsequent effect of ECM degradation in a lamina-specific manner, strongly suggesting that this mechanism may be active *in vivo* to permit structural remodeling during experience-dependent plasticity in the visual system.

## **METHODS**

### **Monocular deprivation**

Mice (C57/Bl6) expressing GFP (strain GFP-M) or YFP (strain YFP-H) in a subset of their cortical neurons (principally layer V pyramidal neurons)<sup>23</sup> were anesthetized at postnatal days 26 or 40 and maintained in deep anesthesia using isoflurane. Monocular deprivation was performed by scoring the eyelids and then sealing them shut with tissue adhesive (Vetbond, 3M, St. Paul, MN). Mice were checked over the next 2-3 days

to ensure that the eye remained closed. A total of 18 mice were used in the *in vivo* experiments (6 control, 4 deprived at p28; 4 control, 4 deprived at p42) and 24 mice were used in the slice experiments (15 control, 9 deprived).

### **Two-photon imaging**

Mice were prepared for *in vivo* imaging and imaged as described previously<sup>12</sup>. Briefly, primary visual cortex was identified using stereotaxic coordinates and either a small craniotomy was drilled in this area, or the skull was thinned without making a craniotomy. Imaging was performed with a custom-made two-photon microscope consisting of a Ti:S laser (Tsunami, Spectra-physics, Menlo Park, CA) pumped by a 10W solid state source (Millennia, Spectra-physics) coupled to a modified Fluoview confocal scanhead (Olympus, Melville, NY). Superficial dendrites were initially identified with wide-field epi-fluorescence illumination, and were subsequently imaged using a 60x, 0.9 numerical aperture lens with digital zoom (5-10x). Volumetric z-stacks were typically collected with a 800x600 acquisition window with 0.5-1  $\mu\text{m}$  z-steps every five minutes over two hours. In some animals, at the end of the imaging session, injections of cholera toxin subunit B (CTB, List Biologic, Campbell, CA) coupled to Alexa Fluor 594 (Molecular Probes, Eugene, OR) were made adjacent to imaged areas in order to facilitate identification of imaged cells after fixation. Mice were transcardially perfused

and fixed with paraformaldehyde and coronal sections were cut to verify the location of imaged cells in V1.

### **Slice preparation and enzyme application**

Acute slices were prepared from p28-29 mice after deep anesthesia with sodium pentobarbital (35mg/kg, i.p.; Henry Schein Inc., Indianapolis, IN). The brain was removed and sectioned in cold (4°C) solution containing (in mM):  $\text{NaH}_2\text{PO}_4$  (1),  $\text{NaHCO}_3$  (25), KCl (3),  $\text{MgSO}_4$  (2), dextrose(10), sucrose (252),  $\text{CaCl}_2$  (2.5), and kynurenic acid (5) in a coronal plane with a thickness of 300  $\mu\text{m}$ . After sectioning, slices were transferred to a holding chamber containing room temperature artificial cerebrospinal fluid (ACSF) containing (in mM):  $\text{NaH}_2\text{PO}_4$  (1),  $\text{NaHCO}_3$  (25), KCl (3),  $\text{MgSO}_4$  (2), dextrose(10), NaCl (126), and  $\text{CaCl}_2$  (2.5). Slices were allowed to equilibrate for 1 hour before transferring to the microscopy submersion chamber which was continuously perfused with warm (35°C) ACSF. For enzymatic reactions, slices were either perfused with 0.5  $\mu\text{g}/\text{mL}$  tPA (American Diagnostica, Stamford, CT) for 45 minutes or were removed from the submersion chamber and incubated with 0.2 U/mL plasmin (Sigma, St. Louis, MO) in a small volume of ACSF for 45 minutes before being returned to the microscopy submersion chamber. Images were collected with two-photon microscopy every 6 minutes for 1.5 hours before and 1.5 hours after enzyme treatment.

## Image Analysis

Z-stack images were exported to MATLAB (MathWorks, Natick, MA) and processed using custom algorithms. Spine motility was analyzed on two-dimensional projections in ImageJ (NIH, Bethesda, MD), where motility was defined as the average change in spine length per unit time<sup>11,12</sup>. Spine turnover was rarely observed in single imaging sessions. All values are presented as mean  $\pm$  standard error of the mean and all statistical analyses were performed using either a parametric t-test statistic for populations of monocularly deprived and control spines, or a parametric paired t-test statistic for enzymatic treatments.

## tPA Visualization

Gene expression analysis was conducted at four time points (P0, P14, P27, and P60) in control and one time point (p27) with long monocular deprivation (2 weeks) in primary visual cortex using the Affymetrix U74v2abc series of chips<sup>82-85</sup>. tPA mRNA expression was further assessed in cortical tissue using *in situ* hybridization<sup>85</sup> in 50  $\mu$ m paraformaldehyde-fixed sections as previously described<sup>86</sup>. tPA protein was examined in fixed sections from control and monocularly deprived P28 mice with a monoclonal antibody against human tPA (PAM-3, American Diagnostica)<sup>87,88</sup>. Primary antibody binding was visualized with a secondary antibody conjugate to horseradish peroxidase (HRP) that catalyzed the deposition of Alexa Fluor 568 tyramide (TSA, Molecular

Probes). Enzyme activity was also assessed in 10  $\mu\text{m}$  fresh frozen sections taken from P28 control and monocularly deprived animals with the EnzCheck Gelatinase/Collagenase Assay Kit (Molecular Probes)<sup>89</sup>. All reactions were visualized with a Zeiss (Oberkochen, Germany) AxioCam MRm camera attached to a Zeiss Axioskop 2 microscope and controlled by Zeiss Axiovision software.

## RESULTS

### MD alters spine dynamics *in vivo*

In order to examine whether monocular deprivation rapidly alters dendritic structure in a manner consistent with physiological changes, we visualized the dynamic structural properties of synapses by imaging dendritic spines *in vivo*. Spines from the apical arbor of layer V pyramidal neurons were imaged using two-photon microscopy (Figure 3-1) at the height of the critical period (p28-29)<sup>57</sup> either with or without short-term monocular deprivation (two to three days, starting on p26). Spine motility in the binocular region of V1, contralateral to the deprived eye, was 35% higher than motility in control, non-deprived animals (Figure 3-1e, n=147 control, 221 deprived,  $p < 0.0001$ ). This indicates that sensory deprivation in a fully innervated, yet plastic cortex was able to initiate a rapid sequence of events leading to increased structural dynamics at the level of individual spines. Such an increase in spine dynamics may reflect structural destabilization of a population of spines whose function is affected by visual

deprivation. This, in turn, could precede a change in spine density<sup>90</sup>. Interestingly, the upregulation of spine motility is restricted to the critical period as monocular deprivation at later ages (p42) had a modest effect of reducing spine motility (Figure 3-1e, n=112 control, 153 deprived,  $p<0.005$ ), suggesting that in older animals, deprivation may selectively stabilize spines. This may reflect alternate processes that regulate ocular dominance plasticity in the adult cortex<sup>91</sup>.

### **MD alters spine dynamics *in vitro***

*In vivo* imaging with two-photon microscopy has the advantage of visualizing small structures in the living animal, though the signal to noise ratio becomes limiting as one images deeper into the tissue. To examine spines situated throughout the cortical layers, we took coronal slices from visual cortex from deprived and non-deprived animals (Figure 3-2a). Spine motility in this preparation also decreases as development proceeds (*see previous chapter*), and reaches a stable level by the critical period. As with *in vivo* imaging, the motility of spines contralateral to the deprived eye was elevated (9%, n=503 control, 581 deprived,  $p<0.0001$ ) following brief monocular deprivation as compared to non-deprived cortex (Figure 3-2d). This change was not accompanied by a change either in average spine length, neck diameter, or head diameter (Figure 3-2e). This suggests that an analysis of spine morphology in a fixed preparation could

overlook an early indicator of potential structural remodeling which is only observed by examining the dynamic properties of spines.

Motivated by the finding that electrophysiological changes in supra- and infragranular layers precede those in layer IV<sup>64</sup>, we further divided our data set into multiple regions. These were defined as either proximal, middle, and distal based on their distance from the cell soma (Figure 3-3c) or deep, middle, and superficial based on their distance from the cortical surface (Figure 3-3d). With both of these analyses, the population of spines closest to the cortical surface, which are closest in laminar location to the population visualized *in vivo*, increased their motility ~20% following deprivation as compared to non-deprived spines (distal, n=297 control, 231 deprived,  $p < 0.0001$ ; superficial n=260 control, 207 deprived,  $p < 0.0001$ ). Furthermore, an inspection of spines in other parts of the arbor reveals clear laminar differences in spine motility. Those spines located in the middle of the dendritic arbor, in layer IV, showed no increase in spine motility following deprivation (mid in Figure 3-3c, n=42 control, 237 deprived,  $p > 0.5$ ; mid in Figure 3-3d, n=64 control, 180 deprived,  $p > 0.5$ ), while those spines in the deep, infragranular region (proximal, n=164 control, 113 deprived,  $p < 0.001$ ; deep, 179 control, 194 deprived,  $p < 0.005$ ), showed an elevation of motility following deprivation. These results indicate that the distribution of synaptic contacts across the apical dendritic arbor are not homogenous, and that spines on a single neuron, separated only

by several hundred micrometers, can experience differential environments for structural plasticity. Further, since the altered dynamics are present in the superficial and deep layers, it is likely that functional changes in horizontal connections in these layers induce the rapid post-synaptic increase in structural dynamics.

### **ECM degradation by tPA and plasmin**

One way in which structural plasticity might be differentially regulated is by localized remodeling of the extracellular matrix<sup>92</sup>. The extracellular matrix is composed of a multitude of molecules which directly interact with cell surface proteins and provide structural support<sup>93</sup>. Tissue type plasminogen activator (tPA), which acts by cleaving extracellular plasminogen and converting it to enzymatically active plasmin, has been implicated in structural remodeling in peripheral nerve regeneration<sup>94</sup>, synaptic remodeling in LTP<sup>95</sup>, as well as fibrinolytic activity around sensory neuron growth cones<sup>96</sup>. tPA transcription<sup>97</sup> and secretion<sup>98</sup> occur in an activity-dependent manner and through BDNF exposure<sup>99</sup>, and although protein levels do not appear to change during ocular dominance plasticity<sup>80</sup>, enzyme activity is significantly increased with monocular deprivation<sup>81</sup>. These findings indicate that tPA is likely to play an important role in inducing tissue remodeling during the period of ocular dominance plasticity.

Although it is known that tPA mRNA responds rapidly to seizure, kindling, and tetanus<sup>97</sup>, it is not known how basal tPA mRNA levels are affected by a decrease in activity or long term depression. As part of a larger effort to discover genes involved in critical period plasticity<sup>85</sup>, we examined the developmental profile of tPA mRNA (Figure 3-4a). Gene chip analysis did not detect an increase in tPA mRNA following long monocular deprivation (Figure 3-4a), but importantly, it also did not detect a decrease in tPA mRNA. This suggests that either tPA mRNA has returned to basal, control levels after long deprivation (2 weeks) or that basal mRNA is not sensitive to reduced activity or long term depression and responds only to large increases in activity. Initial experiments suggest that it may be possible to detect tPA mRNA *by in situ* hybridization (Figure 3-4b), although staining in preliminary attempts was inconsistent and diffuse as compared to staining in cell-dense regions<sup>87,97,100</sup>. These results suggest that monocular deprivation may not alter tPA mRNA, though this does not preclude an effect of the molecule at the protein or enzymatic level.

To further address these questions, we examined tPA protein expression and gelatinase enzyme activity in the visual cortex following brief (2 day) monocular deprivation (Figure 3-4). Immunostaining for tPA protein confirmed that protein expression is not altered by ocular dominance plasticity (Figure 3-4c)<sup>80</sup>. Previous studies have quantified tPA enzyme activity in homogenized tissue<sup>81</sup>, extracts from cultured

neurons<sup>98,99</sup>, and in tissue sections using *in situ* zymography<sup>87,101</sup>. However, none of these methods possess the spatial resolution to detect laminar differences in enzyme activity. Instead, we examined gelatinase/collagenase activity as a proxy for tPA or plasmin with a new fluorescent technique<sup>89</sup>. Although this method provided excellent spatial resolution (Figure 3-4d), it lacked tPA or plasmin specificity, as a large class of extracellular matrix enzymes, including the MMP family<sup>89,102</sup>, possess gelatinase or collagenase activity. Given previous reports concerning stable protein expression during ocular dominance plasticity<sup>80</sup>, and our own results suggesting stable levels of mRNA, it appears that tPA enzyme activity must be tightly regulated in both space and time in order to have its observed effects<sup>80,81</sup>.

### **tPA and plasmin alters spine dynamics**

Since tPA may be important in both ocular dominance plasticity and tissue remodeling, we more closely examined its enzymatic effects on spine motility. Spines from p28 animals were imaged in visual cortex slices before and after a 45 minute period of enzyme application. Treatment with either exogenous plasmin or exogenous tPA (without exogenous plasminogen) significantly increased spine motility (Figure 3-5a, plasmin, 21% increase, n=191, p<0.0001; Figure 3-5b, tPA, 17% increase, n=94, p<0.0001). There was no apparent laminar specificity to this effect, as spines situated through all layers of the cortex were equally affected by tPA and plasmin. These results

indicate that proteolysis through the tPA/plasmin pathway can either induce structural plasticity or provide a permissive environment in which spine dynamics can be altered. Since plasminogen knockout animals have impaired ocular dominance plasticity<sup>90</sup>, it is likely that tPA acts through plasmin to degrade the extracellular matrix, and that this may be one of the first steps in translating functional changes at the level of synapses into structural rearrangements.

### **MD occludes subsequent effects of ECM degradation in a laminar fashion**

During ocular dominance plasticity, tPA exerts a critical role, as tPA knockout animals fail to enter a critical period<sup>81</sup>. To determine whether tPA/plasmin might be involved in the structural plasticity of dendritic spines during the critical period, we examined whether monocular deprivation would occlude a subsequent effect of exogenous tPA/plasmin. If a selective, local secretion of tPA is responsible for the laminar upregulation of spine motility, then those spines in the middle parts of the apical arbor, corresponding to layer IV, would be predicted to receive the least endogenous tPA, while extragranular spines should receive the most endogenous tPA. Consistent with this hypothesis, those regions where spine motility is upregulated by monocular deprivation (e.g. superficial layers) were unaffected by additional plasmin application (Figure 3-6a, n=88, p>0.5), suggesting that monocular deprivation occluded a further increase in spine dynamics via proteolysis of the extracellular matrix.

However, in middle regions where spine motility is unchanged following deprivation, spine motility was significantly increased by enzymatic treatment with plasmin (Figure 3-6b, n=60, p<0.0001). These results strongly suggest that the tPA/plasmin proteolytic cascade is active *in vivo* following brief monocular deprivation in the infra- and supragranular layers and provides a permissive extracellular environment in which spines are free to move, potentially as a prelude to changing their synaptic connectivity.

## DISCUSSION

Remodeling of the primary visual cortex during the critical period for ocular dominance plasticity is thought to progress from functional alterations in the response properties of single neurons<sup>55,57,64</sup> to large anatomical shifts in axonal arborizations<sup>68-70</sup>. This idea is based solely on the relative timing of functional and anatomical events and further pre-supposes that the thalamocortical projection to layer IV is the principal indicator of altered connectivity following ocular dominance plasticity. However, recent evidence suggests that both functional<sup>64</sup> and anatomical<sup>71</sup> changes in extragranular layers may precede, and subsequently inform, the altered connectivity in layer IV. Consistent with this hypothesis, we find that the dynamic properties of dendritic spines are substantially altered in laminar regions outside layer IV following two to three days of monocular deprivation during the peak of the critical period. Spines imaged both *in vivo* and *in vitro* showed elevated dynamics during this period, potentially reflecting a

series of events that destabilized both synapses and spine structure. Longer periods of deprivation, greater than three days, may be required to alter the properties of spines in the middle region of the cortex, and to alter the pattern of thalamocortical connectivity<sup>69</sup>.

Processes such as long term synaptic depression, which can account for the rapid functional changes following monocular deprivation<sup>67</sup>, may also induce the translation from synaptic and functional modification to increased structural dynamics. Spines are likely to be influenced by persistent changes in synaptic efficacy as prolonged activation can induce the formation of new protrusions<sup>42,43</sup> and accumulation of actin within dendritic spines<sup>103</sup>. Further, spines are stabilized by synaptic input<sup>8,41</sup> and significant loss of synaptic drive or long-lasting alteration of synaptic strength<sup>95</sup> could lead to increased structural dynamics<sup>12</sup>. Monocular deprivation is likely to destabilize spines which are initially part of the neural circuitry driven by inputs from the deprived eye, as synapses attempt to maintain homeostatic levels of activity by re-optimizing their connection to pre-synaptic partners or as a prelude to eventual synaptic loss and spine withdrawal (Figure 3-7). With monocular deprivation, significant spine loss occurs within four days<sup>90</sup>, suggesting that synapses which had initially served the deprived eye are likely to have either been lost or have altered their connections within this short period of time.

The mechanism by which structural dynamics are controlled at the level of spines remains unknown. However, as spines are enriched in actin<sup>32</sup> and spine dynamics are regulated by the rate of actin polymerization<sup>7,34</sup>, potential mechanisms for altering spine dynamics should modify the network of filamentous actin. Molecules that might directly fill this role are the Rho family of small GTPases<sup>5,104</sup> which can both promote and reduce spine number while altering spine morphology. However, as much as intracellular cues may be important for altering the properties of actin dynamics, properties of the extracellular space may also exert an influence on the structure of spines, either by binding to proteins expressed at the post-synaptic membrane or by forming physical barriers. Degradation of supportive molecules like fibrin, fibronectin, tenascin, and laminin by enzymes such as plasmin<sup>102</sup> may provide the physical flexibility required to alter existing neural structures. Indeed, we find that proteolysis of proteins in the extracellular matrix by tPA or plasmin can mimic the effect of ocular dominance plasticity by upregulating spine motility. Further, this effect is occluded by prior monocular deprivation as a function of the laminar location of the spines. tPA release into the extracellular space has previously been demonstrated in culture following depolarization<sup>98</sup> or exposure to BDNF<sup>99</sup>, implying that the tPA enzyme can be rapidly regulated and respond to activity-dependent signals. The tPA/plasmin cascade, which is known to be involved in ocular dominance plasticity<sup>80,81</sup>, may then act on the

extracellular matrix to provide a flexible and permissive environment for structural plasticity during the critical period (Figure 3-7). In this role, tPA/plasmin lies downstream of the initial induction of plasticity and serves as an effector of structural rearrangement to reshape the connectivity of the primary visual cortex.

We have identified, for the first time, rapid structural plasticity at the level of individual synaptic connections following monocular deprivation. This plasticity occurs in a lamina-specific manner, proceeding in step with functional changes which are known to occur rapidly in the horizontal connections present in the superficial and deep layers of visual cortex. We now show that one component of this structural plasticity is likely to be mediated by enzymes such as tPA and plasmin by local degradation of the extracellular matrix and generation of a flexible and permissive environment for structural rearrangement.

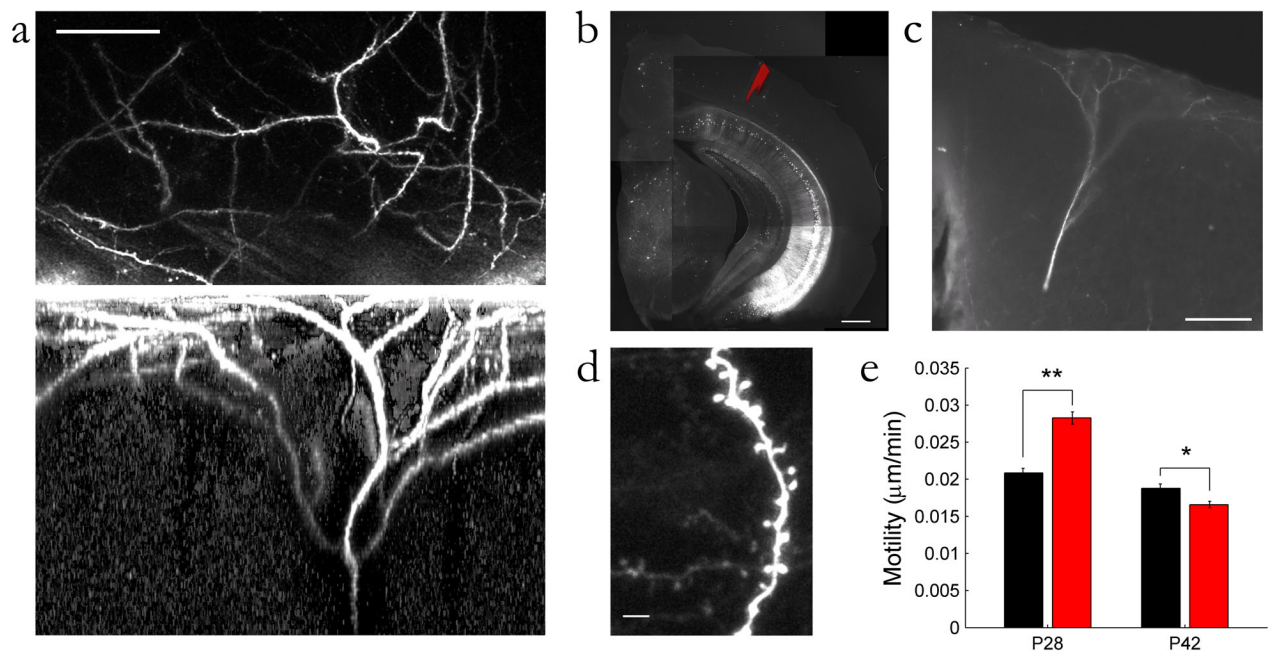


**Figure 3-1.** Spine motility is elevated *in vivo* contralateral to the deprived eye following short monocular deprivation during the critical period. **a**, Apical dendritic arbors from mice expressing GFP in a subset of their layer V pyramidal neurons are visualized with two-photon microscopy. The top panel shows a collapsed z-stack of the arbor from a top-down view and the lower panel shows a side-view of the same arbor after a volumetric projection in the x-z axis. Scale bar, 50µm in the x and y axes, 100µm in the z axis. **b**, The location of *in vivo* imaging is marked with an injection of Alexa Fluor 594 which is then used to verify that the imaged neuron was in the binocular region of V1. Scale bar, 500µm. **c**, The same neuron as in **b** at higher magnification showing the classic apical arbor of a layer V pyramidal neuron. Scale bar, 100µm. **d**, A sample image (the first image of a time series) indicates that spines are readily identifiable *in vivo* with sufficient signal to noise that they can be tracked reliably over several hours. Scale bar, 5µm. **e**, Spine motility is significantly elevated following brief deprivation during the critical period. Black bars, spines from non-deprived cortex, red bars, spines from cortex contralateral to the deprived eye. Double asterisk,  $p < 0.0001$ , single asterisk,  $p < 0.005$ .

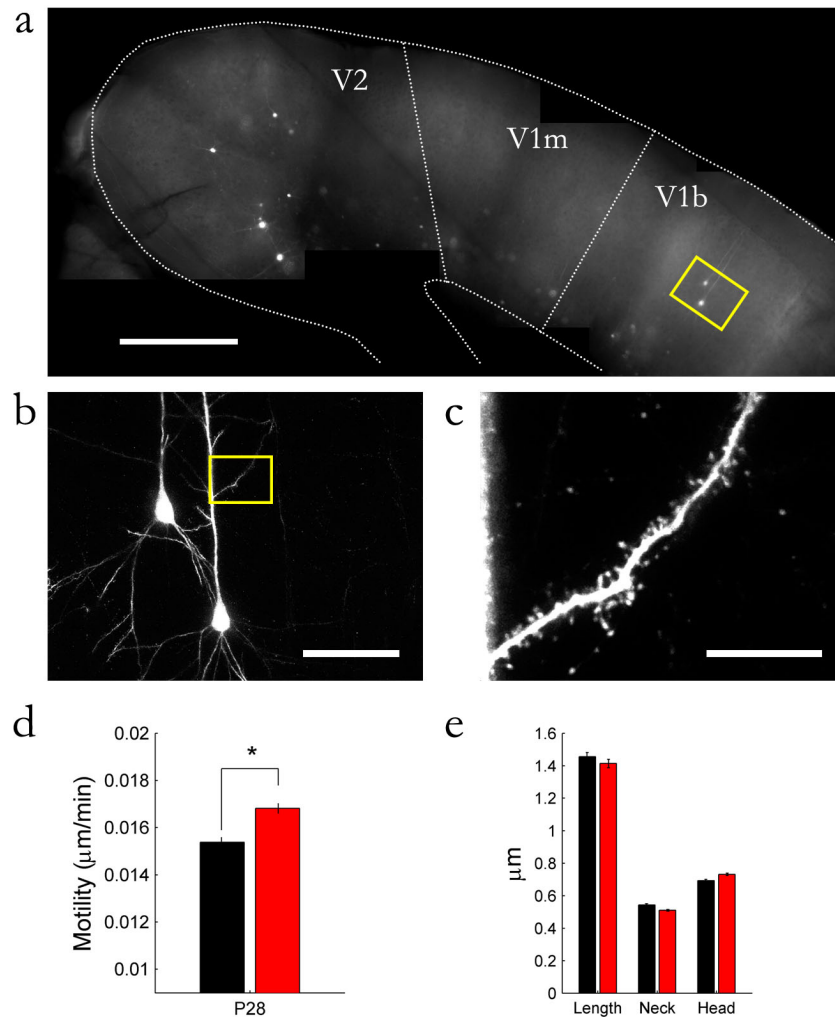


**Figure 3-2.** Spine motility is elevated in acute slice following short monocular deprivation. **a**, GFP expressing neurons are identified in the binocular portion of V1. Scale bar, 500µm. **b**, The two neurons shown boxed in **a** are imaged at 60x with two-photon microscopy. Scale bar, 50µm. **c**, A population of spines, proximal to the cell body, from the region shown in **b** are imaged every 6 minutes for 90 minutes. Scale bar, 10µm. **d**, Spine motility is elevated following deprivation during the critical period in acute slice. **e**, There is no apparent change in average spine length, neck diameter, or head diameter. Black bars, spines from non-deprived cortex, red bars, spines from cortex contralateral to the deprived eye. Asterisk,  $p < 0.0001$ .

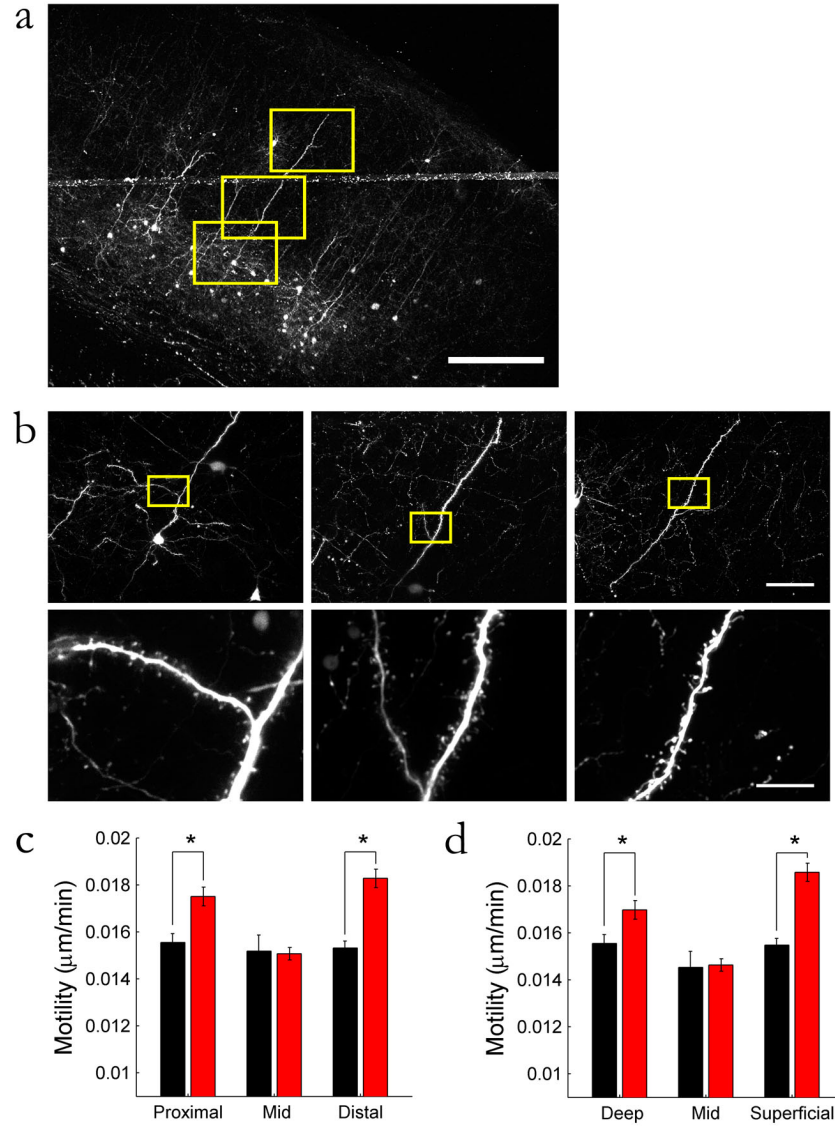


**Figure 3-3.** The upregulation of spine motility after monocular deprivation follows a laminar pattern. **a**, A large population of cells expressing GFP can be seen at 10x magnification, many of them extending long apical dendritic arbors. Scale bar, 300 $\mu$ m. **b**, The three boxed regions shown in **a** at 60x magnification, progressing from regions close to the cell body (left panel), midway up the apical arbor (middle panel) and distal from the cell body (right panel). Below each 60x image is a high magnification image of the population of spines from the boxed region in the upper panels. Scale bars, 50 $\mu$ m top panels, 10 $\mu$ m for lower panels. **c**, If spines are grouped based on their distance from the cell body, a clear laminar pattern to the elevation of spine motility is observed. **d**, Similarly, if spines are grouped based on their distance from the cortical surface, the same laminar pattern is evident. Black bars, spines from non-deprived cortex, red bars, spines from cortex contralateral to the deprived eye. Asterisk,  $p < 0.005$ .

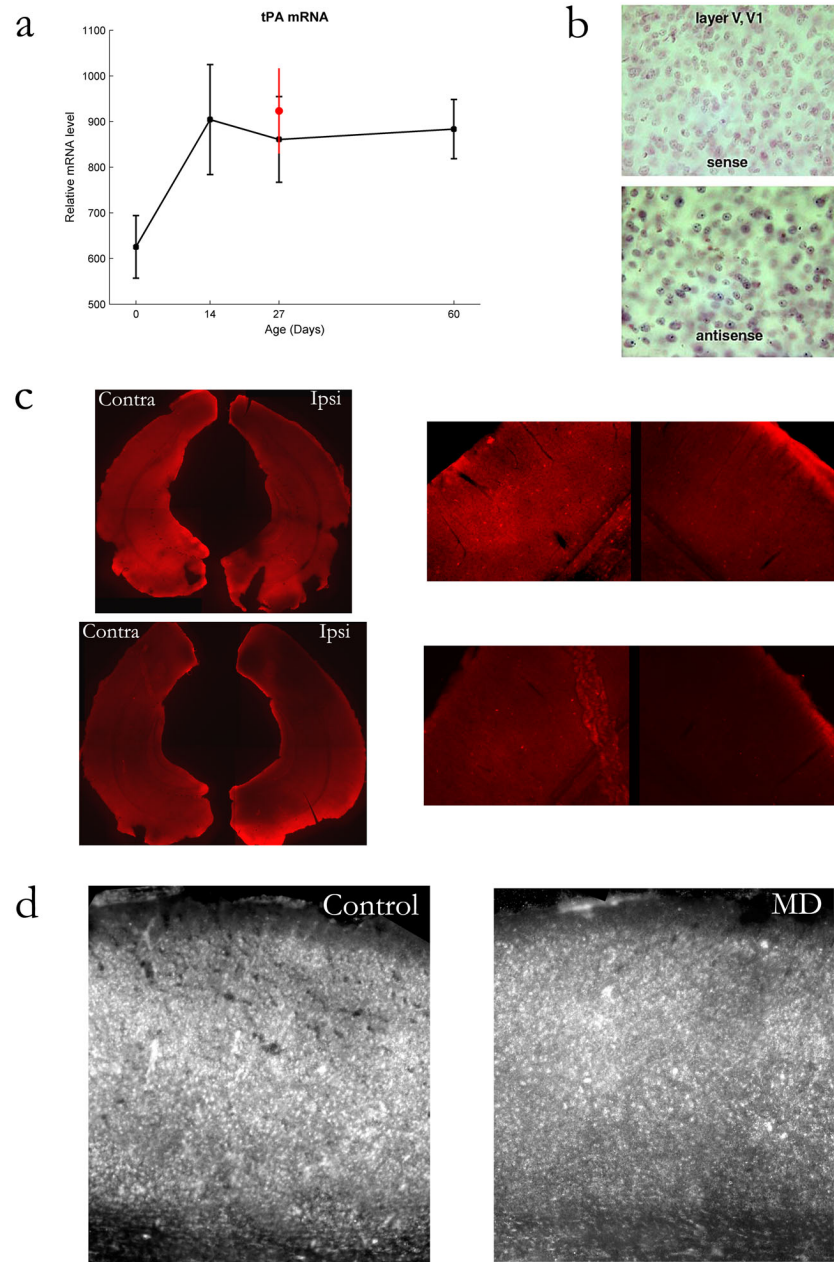


**Figure 3-4.** tPA Expression during the critical period. **a**, tPA mRNA levels in control animals (in black) increase in the first two postnatal weeks and remain stable into adulthood. tPA mRNA after long monocular deprivation (in red) is not significantly different from control. **b**, tPA *in situ* hybridization in control tissue, counterstained with neutral red, labels a subset of nuclei. **c**, tPA protein levels are variable, though no consistent effects are seen contralateral or ipsilateral to monocular deprivation in two animals. Magnified views of visual cortex are shown on the right. **d**, High resolution, *in situ* fluorescent gelatinase/collagenase activity is non-specific for tPA and does not show a consistent difference between control and monocularly deprived cortex.

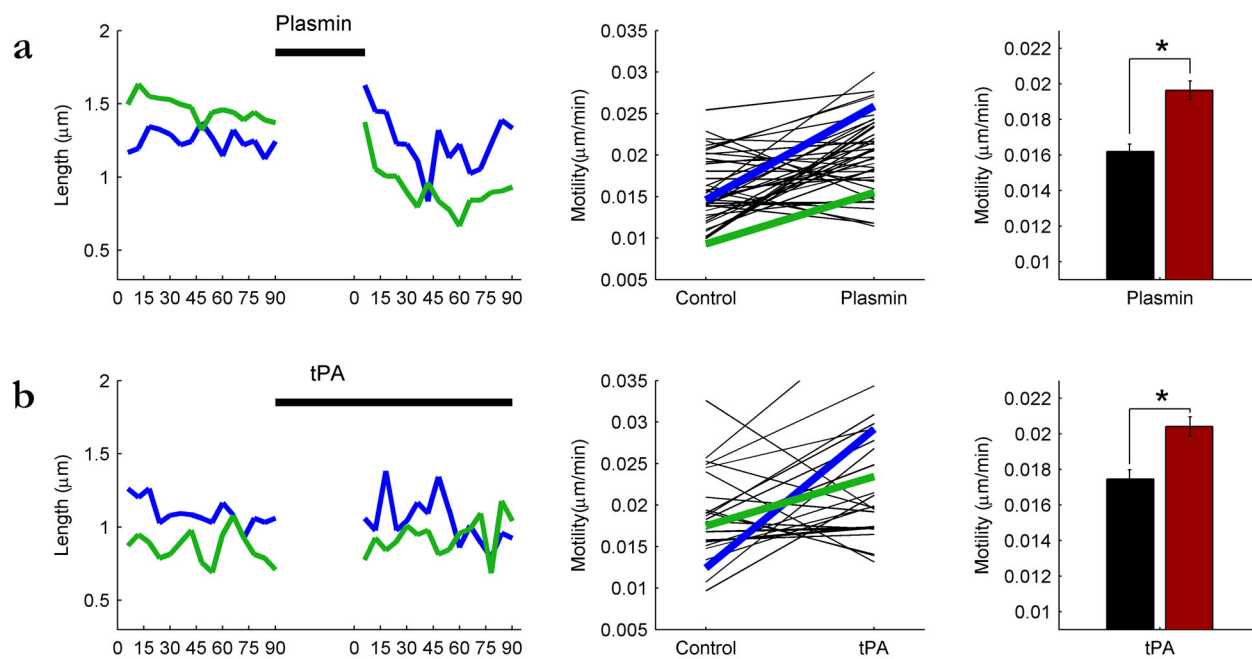


**Figure 3-5.** Spine motility is upregulated by degradation of the extracellular matrix. For each experimental condition, the blue and green traces in the left panels describe the change in length over time for two example spines before and after enzymatic degradation. Likewise, the middle panels show the motility index of a population of spines from a single experiment, including the spines from the left panel. The final column of panels shows the pooled effect of enzymatic degradation from all experiments. **a**, Spine motility is significantly elevated after proteolytic degradation with plasmin. **b**, Similarly, spine motility is significantly elevated after application of tPA with no exogenous plasminogen. Black bars, spines from non-deprived cortex, dark red bars, spines from non-deprived cortex following enzyme degradation. Asterisk,  $p < 0.0001$ .

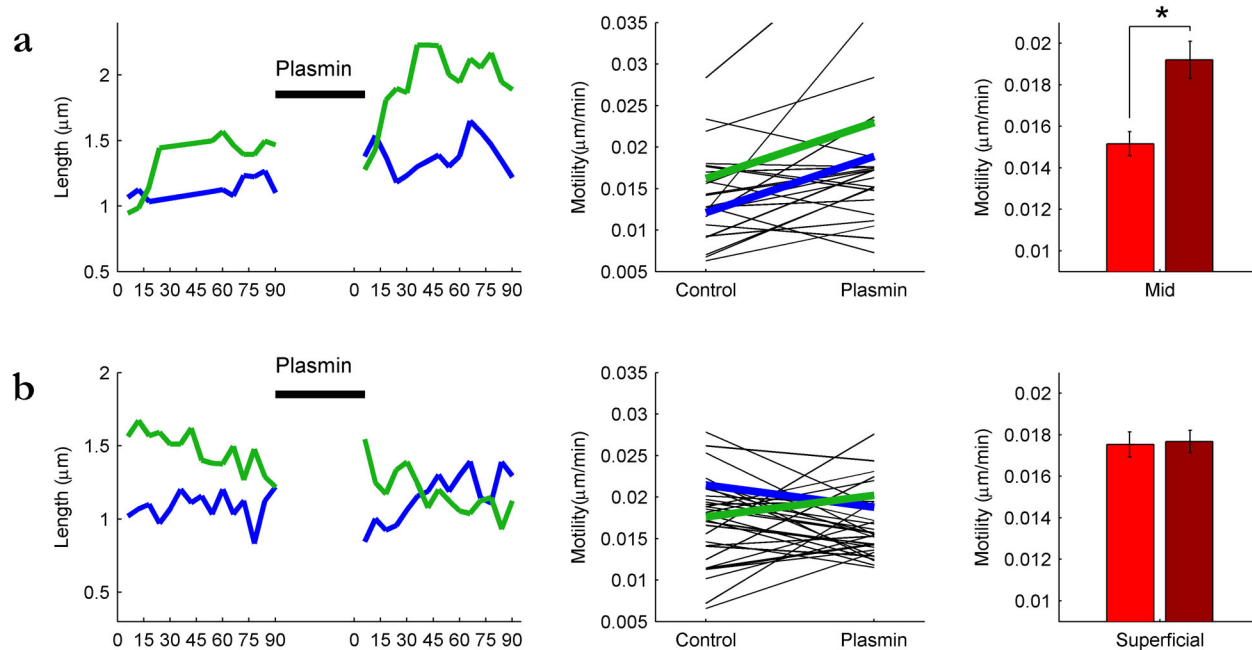


**Figure 3-6.** Monocular deprivation occludes extracellular matrix degradation in a laminar fashion. The change in length of example spines, motility before and after extracellular matrix degradation, and pooled population results are as in Figure 5. **a**, After monocular deprivation, plasmin significantly upregulates spine motility in the middle of the dendritic arbor. **b**, However, in the superficial part of the dendritic arbor, where spine motility is already upregulated by monocular deprivation, further upregulation by plasmin is occluded. Red bars, spines from cortex contralateral to the deprived eye, dark red bars, spines from cortex contralateral to the deprived eye following enzyme application. Asterisk,  $p < 0.0001$ .

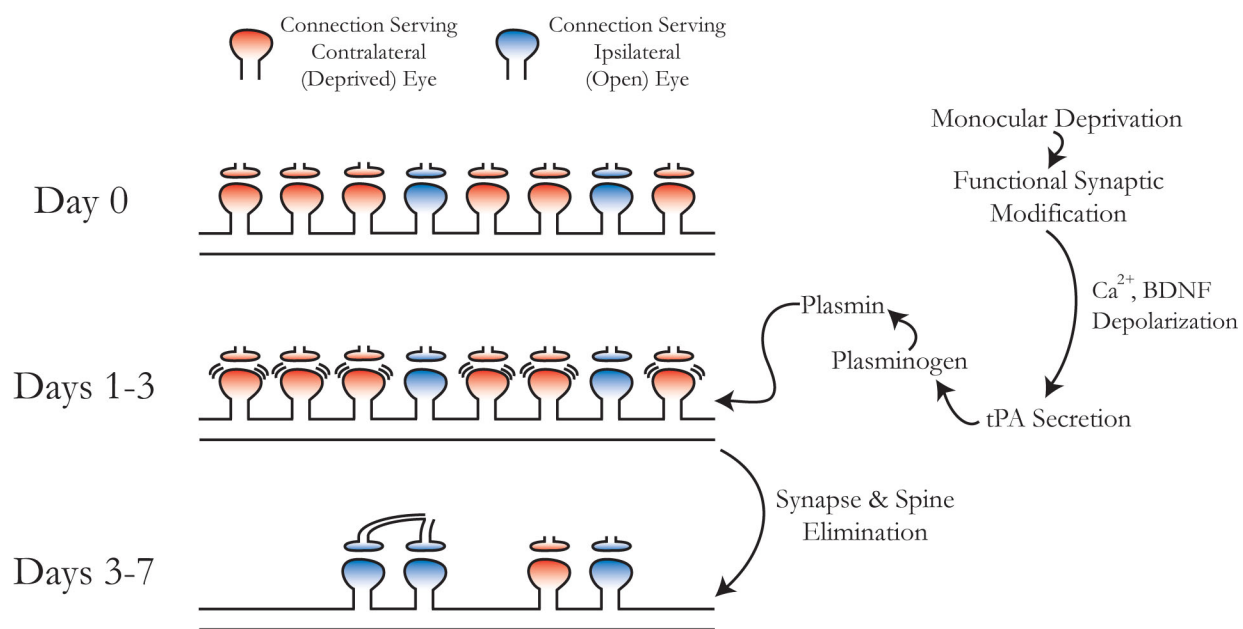


**Figure 3-7.** The proposed time course of functional and structural changes following monocular deprivation and key elements of extracellular matrix remodeling. Monocular deprivation during the critical period induces tPA secretion and the conversion of extracellular plasminogen into plasmin. Plasmin then acts on a number of molecules in the extracellular matrix, allowing increased structural dynamics (schematically depicted with wavy lines around spines). This increase in structural dynamics then facilitates a change in synaptic connectivity, such that spines receiving input from the deprived eye (shown in red) are either lost or converted, while those spines receiving input from the open eye (shown in blue) are maintained.

## CHAPTER 4

### Short and long-term regulation of AMPA and NMDA receptors in the developing ferret LGN

#### INTRODUCTION

The mammalian visual system is characterized by a very precise and orderly pattern of connections which are formed early in development and modified by afferent activity<sup>105-107</sup>. In the lateral geniculate nucleus (LGN) of the developing ferret, retinal axons segregate into eye specific laminae during the first two postnatal weeks and subsequently into ON/OFF sublaminae during the third and fourth postnatal weeks<sup>108,109</sup> while the LGN itself increases four fold in area (Figure 4-1). The spontaneous firing properties of retinal ganglion cells prior to eye-opening are likely to play an important role in the initial development of eye-specific layers<sup>110-114</sup>. Further, action potential blockade in the retina during the third postnatal week disrupts the formation of sublaminae<sup>115</sup>, as does blockade of the NMDA receptor<sup>108,109</sup>. This intriguing result suggests that processes such as long term potentiation (LTP) which rely on activation of NMDA receptors<sup>116,117</sup>, may play a role in sculpting the synaptic connectivity between the retina and the LGN. Indeed, LTP has been observed at the retinogeniculate

synapse<sup>118</sup>. By selectively enhancing retinal input at synapses that receive strong presynaptic input and generate postsynaptic action potentials, LTP may provide a mechanism which maintains and strengthens particular synapses and connections. This in turn could potentially guide structural rearrangements at the level of synapses as well as pruning within dendritic and axonal arbors, eventually resulting in anatomical rearrangements such as eye-specific lamination and sub-lamination in the LGN.

One of the dominant ideas, both in synaptic development and activity-dependent synaptic plasticity, is that synaptic efficacy can be regulated by the relative contribution of AMPA and NMDA receptor subunits at single synapses. First described as the silent synapse hypothesis<sup>19-21</sup>, this idea suggests that immature synapses contain mostly NMDA receptors which are difficult to activate at resting membrane potentials due to magnesium blockade. These silent synapses can be converted into fully functional synapses by the addition of AMPA receptors. Extensive work has extended this theory to describe AMPA receptor insertion and removal, NMDA receptor trafficking, and the effects of long term depression (LTD) and LTP on AMPA receptor phosphorylation and subsequent synaptic turnover<sup>20,22,36-38,53,119-122</sup>. Several alternative views have also been put forward, including the suggestion that presynaptic factors, such as the dynamics of glutamate release, may also determine postsynaptic currents based on glutamate binding and receptor desensitization rates<sup>123,124</sup>. A second idea has

been recently suggested that silent synapses may be an artifact of rapid AMPA receptor desensitization<sup>125</sup>, while a third has pointed out the properties of activity-dependent synaptic scaling, whereby changes in AMPA and NMDA receptor currents are coordinated in response to chronic activity blockade or enhancement<sup>126</sup>. The majority of research on silent synapses has been performed in the hippocampus and its exact relationship to developmental processes in other systems remains unclear. However, recent work provides strong evidence that the phosphorylation and internalization of AMPA receptors during LTD may be the principle molecular mechanism involved in rapid functional changes during ocular dominance plasticity in the visual cortex<sup>67</sup>. This work provides an initial demonstration that the well-characterized post-synaptic processes that are implicated in silent synapses may also be involved in regulating plasticity in other parts of the developing visual system.

During the extensive anatomical growth and reorganization of the LGN over the first four postnatal weeks, the properties of AMPA and NMDA receptors appear to be fairly stable. NMDA receptors play a strong role in retinogeniculate transmission through the first six postnatal weeks, though their efficacy begins to diminish around P21 with the maturation of inhibitory circuits<sup>127</sup>. Similarly, spontaneous and evoked excitatory postsynaptic currents (EPSCs) for both AMPA and NMDA receptors are stable between the second and fourth postnatal weeks<sup>48,128</sup>. Interestingly, silent

retinogeniculate synapses have been described in this developmental period, although the relative proportion of silent synapses is the same before and after ON/OFF sublamination<sup>48</sup>. To further investigate the anatomical correlates of these functional findings, AMPA and NMDA receptors have been examined in the ferret LGN with fluorescent immunohistochemistry. AMPA and NMDA colocalization was assessed before (P14), during (P21), and after (P28) ON/OFF sublamination, and the relative effect of activity on receptor expression during this period (P14-21) was tested with pharmacological methods. The results indicate that sublamination proceeds with a stable AMPA/NMDA contribution and that brief activity blockade can alter the AMPA to NMDA ratio.

## **METHODS**

### **Eye injections**

All experiments were performed under protocols approved by MIT's Institutional Animal Care and Use Committee and conformed to NIH guidelines. Animals were treated subcutaneously with atropine (0.1 mg/ kg in 9% saline) and then deeply anesthetized with isoflurane (2%) in a nitrous oxide (60%) and oxygen (40%) mixture. A small surgical blade was used to separate the eyelids to expose the conjunctiva on the lateral side of the eye. A 50  $\mu$ L Hamilton microsyringe was then used to inject 10  $\mu$ L of the anterograde tracer cholera toxin subunit B (CTB; 1% H<sub>2</sub>O; List

Biologic, Campbell, CA) into the eye. After eye injection, the eyelids were allowed to reclose, and an antibiotic ophthalmic ointment was applied. A 2 day survival period was allowed for axonal transport of the CTB to the LGN.

### **Immunofluorescence**

Postnatal day 14 (p14) to p28 ferrets were deeply anesthetized with sodium pentobarbital (35 mg/kg, i.p.; Henry Schein Inc., Indianapolis, IN) and perfused transcardially with isotonic saline, followed by 4% paraformaldehyde. The brain was removed, post-fixed for 24 hours, transferred to 30% sucrose for 24 hours, and then sectioned horizontally at 50  $\mu\text{m}$  with a cryostat (Reichert-Jung, now Leica, Frigocut 2800). Sections were blocked and permeabilized with 0.5% Triton X-100 for 30 minutes in normal sera, incubated with primary antibodies for 48 hours at 4°C, and subsequently incubated with secondary antibodies for 2 hours at room temperature. Sections were then mounted in buffer, coverslipped, and sealed. The following antibodies were used: mouse anti-NMDA receptor subunit 1 (NR1; 1:250; PharMingen, San Diego, CA)<sup>14</sup>, rabbit anti-glutamate receptor subunit 1 (GluR1; 1:1000; Upstate Biotechnology, Lake Placid, NY)<sup>129</sup>, rabbit anti-glutamate receptor subunit 4 (GluR4; 1:100; Chemicon, Temecula, CA)<sup>130,131</sup>, goat anti-CTB (1:1000; List Biologic)<sup>132</sup>, mouse anti-synaptophysin (1:10; Boehringer Mannheim, Indianapolis, IN)<sup>133</sup>, horse anti-mouse FITC (1:200; Vector Laboratories, Burlingame, CA), goat anti-rabbit Texas Red (1:200;

Vector), donkey anti-rabbit Texas Red (1:200, Jackson ImmunoResearch, West Grove, PA), and donkey anti-goat Cy5 (1:200, Chemicon). The specificity of the secondary antibodies was confirmed by omitting the primary antibodies; in all such control experiments, no fluorescence was observed.

### **Slice preparation and pharmacology**

Thalamic slices were prepared from p14 or p21 ferrets after deep anesthesia with sodium pentobarbitol. A block of tissue including the thalamus was removed from the head and dissected in a cold solution (4°C) containing (in mM): NaH<sub>2</sub>PO<sub>4</sub> (1), NaHCO<sub>3</sub> (25), KCl (3), MgSO<sub>4</sub> (2), dextrose(10), sucrose (252), CaCl<sub>2</sub> (2.5), and kynurenic acid (5). Slices were cut horizontally at 400 μm on a Vibratome (model 1000; Ted Pella Inc., Redding, CA) while in this solution and then transferred to a holding chamber containing room temperature artificial cerebrospinal fluid (ACSF) containing (in mM): NaH<sub>2</sub>PO<sub>4</sub> (1), NaHCO<sub>3</sub> (25), KCl (3), MgSO<sub>4</sub> (2), dextrose(10), NaCl (126), and CaCl<sub>2</sub> (2.5). Slices were allowed to equilibrate for 1 hour and were then bathed in one of five solutions: 30 μM N-Methyl-D-aspartic acid (NMDA; Sigma, St. Louis, MO) for 5 minutes, 100 μM D(-)-2-Amino-5-phosphonopentanoic acid (D-AP5; Sigma) for 30 minutes, 1 μM tetrodotoxin (TTX; Sigma) for 30 minutes, 20 μM Bicuculline Methiodine (BMI; Sigma) for 30 minutes, or a time-matched control solution of ACSF. Multiple slices from each animal were used such that each animal provided its own control and

several treatment slices. After pharmacological treatment, tissue was fixed in 4% paraformaldehyde and then transferred to 30% sucrose for cryoprotection. The 400  $\mu\text{m}$  slices were then frozen and resectioned to a thickness of 50  $\mu\text{m}$  on a cryostat. These sections were then processed for glutamate receptor immunofluorescence in the same manner as the whole brain sections described above.

### **Confocal microscopy**

Confocal scanning microscopy was performed on a Bio-Rad (Hercules, CA) MRC-1024ES confocal system mounted on a Zeiss (Oberkochen, Germany) Axioplan microscope. All images were collected with a Zeiss Plan-Neofluar 100x oil-immersion objective with numerical aperture 1.3. Fluorescence images were obtained with a krypton-argon laser with standard lines at 488 nm (FITC), 568 nm (Texas Red), and 647 nm (Cy5) with standard filters. The theoretical analog focal resolution limit (using the full width half maximum criterion) for our confocal apparatus at these wavelengths was 0.16  $\mu\text{m}$ , 0.19  $\mu\text{m}$ , and 0.21  $\mu\text{m}$  respectively<sup>134</sup>. Images were gathered sequentially with a digital resolution of 512 by 512 or 1024 by 1024 pixels and a digital zoom of 1 or 1.5x. At the lowest image resolution (100x objective, 512 by 512 image, 1x zoom), each pixel corresponded to 0.21  $\mu\text{m}$  in the focal plane, closely matching the analog resolution of the confocal system, while at the highest resolution (100x objective, 1024 by 1024 image, 1.5x zoom), each pixel corresponded to 0.07  $\mu\text{m}$  in the focal plane, providing three times

digital oversampling of the spatial signal. Electron microscopy studies in the A and A1 laminae of the cat LGN<sup>135,136</sup> suggest that the distance between the closest excitatory glutamatergic synapses of retinal or cortical origin is on the order of 1  $\mu\text{m}$  indicating that a pixel resolution of 0.07-0.21  $\mu\text{m}$  is adequate to resolve adjacent excitatory synapses. Similarly, the resolution in the z-dimension is limited by numerical aperture and wavelength (the analog z-resolution with excitation at 488 nm, is 0.42  $\mu\text{m}$ , and gets poorer at longer wavelengths) and is further controlled by the size of the confocal pinhole aperture. For these images, resolution in the z-axis was approximately 0.50  $\mu\text{m}$ . Images in the separate fluorescent channels were collected sequentially and were generated by Kalman filtering five frames at a single focal plane. All images were taken from the A or A1 layers of the LGN.

### **Image analysis**

In order to assess glutamate receptor colocalization at different points in development (P14, P21, and P28), AMPA and NMDA receptor subunits were visualized in the same field of view with one channel (red) of an image corresponding to the AMPA signal and a second channel (green) corresponding to the NMDA signal. In these experiments, acquisition parameters were optimized for each channel of each individual image in order to accurately represent the entire dynamic range of the immunofluorescence signals. In double-labeling experiments, each image channel was

analyzed independently to identify the highest intensity signal in the green and red channels by a percentile thresholding procedure. Colocalization of the two fluorescent signals was quantified as the number of pixels that had high intensity values in both the green and red channels. Black and white colocalization images were generated to show the spatial distribution of colocalization with each black pixel representing a colocalization event. In triple-labeling experiments, a third channel (blue) was acquired for each image, corresponding to the CTB labeling of retinogeniculate terminals. This channel was thresholded to identify the labeled terminals and then used to restrict the region of analysis for AMPA (red) and NMDA (green) signals to those sites which were apposed to retinogeniculate input. This was accomplished by using a custom, spherical filter which discarded from analysis all pixels that were more than 0.4  $\mu\text{m}$  distant from the edge of high intensity terminal labeling. These restricted images were then analyzed for colocalization of the red and green channels in the same manner described above. The clustering of colocalized pixels was assessed by sliding a window across the colocalization image and calculating the distance of a random data point from its nearest neighbor and comparing it with the distance between a random non-data point and its nearest data point. The clustering index was generated by taking the median of the ratio of these two numbers after multiple iterations<sup>137</sup>.

In order to assess relative changes in the expression of glutamate receptor subunits following drug treatments, AMPA and NMDA receptor subunits were again visualized in the same field of view. In these experiments, acquisition parameters were first optimized for control sections for each animal and were then maintained for all subsequent images. In this way, differences in fluorescence intensity across different images represented relative differences in AMPA and NMDA receptor subunit expression and was quantified as a percentage of control fluorescence. Triple-labeling experiments were also performed as described above to localize AMPA and NMDA signals apposed to retinogeniculate terminals. The intensity of fluorescence was analyzed at these restricted locations and was also quantified as a percentage of control. All image and statistical analysis was performed in MATLAB (MathWorks, Natick, MA) using custom algorithms. The Mann-Whitney U statistic was used to test for significance with experimental groups of two conditions, while a Kruskal-Wallis nonparametric ANOVA and Dunn's non-parametric multiple comparison statistic were used with experimental groups of three treatment conditions. In experiments involving pharmacological manipulations, Dunnett's test, which allows for multiple comparisons to a control group was used instead of Dunn's test to assess the effect of each drug. Scale bars in all immunofluorescence images represent 25  $\mu\text{m}$  in the focal plane and all values are presented as mean  $\pm$  standard error of the mean. A total of 18 ferrets were

used in the developmental colocalization experiments and 14 ferrets were used in the drug treatment slice experiments.

## RESULTS

### Developmental colocalization of AMPA and NMDA receptor subunits

To examine the expression of glutamatergic receptors during the period of ON/OFF sublamination, AMPA and NMDA receptor subunits were visualized in the A and A1 layers of the developing ferret LGN. If AMPA receptors are progressively inserted at NMDA-only synapses during this period of anatomical rearrangement and refinement, it should be possible to observe an increase in the colocalization of AMPA and NMDA receptors as development proceeds. Both NR1, the obligatory NMDA receptor subunit, and GluR1, an abundant AMPA receptor subunit were reliably detected from P14 through P28 (Figure 4-2). There was significant overlap of the label for both subunits, and their colocalization was constant throughout the period of sublamination (P14, n=15 images from 2 animals; P21, n=22 images from 4 animals; P28, n=14 images from 3 animals;  $p > 0.05$ ; Figure 4-2b,c). One drawback of this immunostaining technique is that it does not differentiate between intracellular and extracellular subunit expression<sup>49</sup>. If AMPA and NMDA receptor subunits are produced at locations near one another such as in the soma or endoplasmic reticulum, there is the possibility that colocalization will be dominated by the level of somatic receptor

expression. In particular, any increase in colocalization at synapses may be masked by a decrease in receptor subunit translation, and hence, a decrease in the level of somatic colocalization. If this were the case, one would also expect to see a decrease in the clustering of colocalized pixels, corresponding to the decrease in expression at the soma. To address this issue, a cluster analysis (see Methods) was performed on the images of GluR1 and NR1 colocalization. The clustering of GluR1 and NR1 is similar before and after ON/OFF sublamination ( $p > 0.05$ ), although it increases significantly from P14 to P21 ( $p < 0.05$ ; Figure 4-2d). These results indicate that, although there may be a transient increase in somatic receptor production at P21, this effect is not present at P14 and P28 and therefore not likely to mask an increase in colocalization between these two age points.

Unlike NMDA receptors, AMPA receptors do not include an obligatory subunit. Consequently, to determine whether the observed pattern of colocalization was in some way unique to the GluR1 subunit, double-labeling experiments were repeated with antibodies to the GluR4 subunit (Figure 4-3a). The development of GluR4-NR1 colocalization during ON/OFF sublamination was similar to that observed with GluR1-NR1 labeling (Fig 4-3b) and was stable from P14 to P28 (P14,  $n=14$  images from 2 animals; P21,  $n=12$  images from 4 animals; P28,  $n=11$  images from 3 animals;  $p > 0.05$ ; Figure 4-3b,c). As with GluR1-NR1 labeling, GluR4-NR1 clustering at the end of

sublamination was not significantly different from that before its onset ( $p>0.05$ ), although it did increase at P21 (Fig 2-3d). Interestingly, at later ages (P21 and P28), there were some neurons which expressed NR1 but had very to low to non-existent levels of the GluR1 subunit. In contrast, there were no neurons at any age that expressed NR1 but did not express GluR4, suggesting that GluR4 may be a more stable and ubiquitous AMPA receptor subunit in the ferret LGN, as previously described in monkeys<sup>130,131</sup>. These results indicate that the stable colocalization of AMPA and NMDA receptors during the period of sublamination is not a specific property of the GluR1 subunit, but is a general property of AMPA receptors that is shared with the GluR4 subunit.

As indicated above, one of the shortcomings of this immunostaining technique is that it does not differentiate between intracellular and extracellular receptors. In order to examine NR1, GluR1, and GluR4 colocalization associated with retinogeniculate input, CTB injections were made into the eyes, where it could be taken up by retinal ganglion cells and transported in the anterograde direction along their axons<sup>132</sup>. Subsequently, triple labeling experiments were performed where AMPA and NMDA receptor subunits were visualized in conjunction with CTB labeling of the retinogeniculate axon terminals. By restricting the analysis of GluR1 and NR1 subunit colocalization to the immediate vicinity of retinogeniculate terminals (see Methods), it was possible to virtually eliminate all somatic staining and focus on the putative

location of synaptic input. Further, this technique isolated the retinogeniculate input from the more extensive corticogeniculate<sup>138</sup> or modulatory brainstem input. Colocalization opposite CTB-stained retinogeniculate fibers revealed a pattern that was not significantly different from that seen with the more general double-labeling method (Figure 4-4). Both colocalization and clustering were no different after ON/OFF sublamination than before (P14, n=8 images from 1 animal; P28, n=5 images from 1 animal;  $p>0.05$ ). Triple-labeling of retinogeniculate terminals, GluR4, and NR1 (Figure 4-5) showed the same results as with GluR1; colocalization and clustering opposite retinogeniculate terminals were similar before and after ON/OFF sublamination (P14, n=3 images from 1 animal; P28, n=7 images from 1 animal;  $p>0.05$ ). These results suggest that, even when analysis is restricted to locations apposed to retinogeniculate terminals, AMPA and NMDA receptor colocalization is stable over the period of ON/OFF sublamination.

In separate experiments, labeling for synaptophysin, a presynaptic vesicle protein, was used to confirm that primarily synaptic boutons at retinal terminals, rather than fibers of passage, were labeled by the CTB injections. The vast majority of CTB label (98%) was colocalized with synaptophysin (Figure 4-5f), indicating that the periphery of CTB label was an appropriate constraint for examining presumptive postsynaptic locations for GluR1-NR1 (or GluR4-NR1) colocalization. Whereas there

was very little CTB label that was not colocalized with synaptophysin, there was, of course, synaptophysin labeling that was not colocalized with CTB (52% of the label in Figure 4-5f), reflecting extensive non-retinal input to the LGN (e.g. cortical and brainstem terminals).

### **Relative AMPA and NMDA receptor expression**

To examine the regulation of glutamatergic receptors during the period of ON/OFF sublamination, acute slices of thalamus were bathed in ACSF with various pharmacological agents to either stimulate or inhibit action potentials or synaptic activity. These slices were then fixed, cut into thin sections, and immunostained for AMPA and NMDA receptor expression. The baseline variability of AMPA and NMDA receptor expression was assessed with timed control experiments in which LGN slices from single animals were bathed in ACSF alone for 30, 60, or 120 minutes (Figure 4-6). Sample images from one experiment at P14 are shown in Figure 4-6a. Image settings were optimized for the 30 minute ACSF exposure condition and were collected with identical settings on the confocal microscope for all subsequent images. NR1 and GluR1 receptor subunit expression was stable over the two hour period for this experiment (30 min n=8 images; 60 min n=5 images; 120 min n=5 images;  $p>0.05$  for both NR1 and GluR1) as well as a second experiment at P21 (30 min n=6 images; 60 min n=6 images; 120 min n=4 images;  $p>0.05$  for both NR1 and GluR1). Since there was no significant

variation in GluR1 or NR1 expression, the AMPA to NMDA ratio (A/N ratio) was very close to 1 (no increase in one or the other receptor subunit). This indicates that, although there is a degree of variability in the expression of NR1 and GluR1, their relative expression is stable over several hours in the LGN.

Since the efficacy of a synapse can be affected by activity<sup>126</sup>, LGN slices were subjected to various forms of activity blockade or enhancement. Homeostatic mechanisms that adjust synaptic receptor expression based on the total amount of activity might be expected to upregulate glutamatergic receptor subunits following activity blockade and to down-regulate subunits following periods of overly high activity. Glutamatergic activity was manipulated by bathing LGN slices in ACSF with 30  $\mu$ M NMDA or 100  $\mu$ M AP5, the selective antagonist of the NMDA receptor (Figure 4-7a), while general excitatory and inhibitory activity was regulated by blocking action potentials with 1  $\mu$ M TTX or blocking GABAergic inhibition with 20  $\mu$ M BMI (Figure 4-7b). In 12 separate experiments (Figure 4-7c), there was significant variation in NR1 and GluR1 expression following treatment with AP5 (NR1: 32% reduction to 18% increase; GluR1: 35% reduction to 48% increase), NMDA (NR1: 34% reduction to 33% increase; GluR1: 48% reduction to 57% increase), TTX (NR1: 25-51% increase; GluR1: 36% reduction to 27% increase), and BMI (NR1: 14-48% increase; GluR1: 14-120% increase).

Age did not account for any of this variability, as experiments conducted at P21 (n=3) were as variable as those conducted at P28 (n=9).

In order to pool the effect of each activity manipulation across experiments, the relative level of NR1 and GluR1 were normalized to control values for each individual experiment. After pooling (Fig 2-7d), there was no significant effect of AP5 (n=146 images from 8 animals;  $p>0.05$  for both NR1 and GluR1) or NMDA (n=136 images from 9 animals;  $p>0.05$  for both NR1 and GluR1) on AMPA or NMDA receptor expression. However, action potential blockade with TTX significantly increased NR1 expression by 40% (n=40 images from 2 animals;  $p<0.001$ ) without altering GluR1 expression ( $p>0.05$ ). Counterintuitively, blockade of GABAergic inhibition with BMI also significantly increased NR1 expression by 26% (n=50 images from 2 animals;  $p<0.001$ ) as well as GluR1 expression by 52% ( $p<0.001$ ). Since TTX differentially affected AMPA and NMDA receptor expression by increasing NR1 expression, it also significantly reduced the A/N ratio ( $p<0.001$ ), while BMI, by increasing GluR1 expression more than NR1 expression, slightly increased the A/N ratio ( $p<0.005$ ). These results argue that general levels of excitation and inhibition are important for regulating AMPA and NMDA receptor expression and that simple homeostatic mechanisms cannot easily account for these effects.

As mentioned above, the immunostaining technique employed in these experiments does not differentiate between intracellular and extracellular receptors. However, in the case of AMPA and NMDA receptor expression, the amount of receptor which is being produced in the cell body may actually be a good measure of cell-wide processes that are up- or down-regulating subunit expression. Nevertheless, the amount of receptor at retinogeniculate contacts would be a good indicator of whether changes in expression profiles altered the complement of receptors at putatively synaptic locations. When NR1 and GluR1 expression were restricted to positions apposed to retinogeniculate terminals labeled in triple-labeling experiments, the data recapitulated the results of the double-labeling experiments (Figure 4-8). There was no significant effect of AP5 (n=44 images from 2 animals;  $p>0.05$  for both NR1 and GluR1) or NMDA (n=45 images from 3 animals;  $p>0.05$  for both NR1 and GluR1) on AMPA or NMDA receptor expression. TTX significantly increased NR1 expression by 34% (n=34 images from 2 animals;  $p<0.001$ ) without altering GluR1 expression ( $p>0.05$ ), thereby reducing the A/N ratio ( $p<0.001$ ). As above, BMI also significantly increased NR1 expression by 35% (n=40 images from 2 animals;  $p<0.001$ ) as well as GluR1 expression by 60% ( $p<0.001$ ) and, in doing so, significantly increased the A/N ratio ( $p<0.05$ ). This correlation between cell-wide expression and expression near retinogeniculate terminals suggests that processes which alter AMPA and NMDA receptor expression

throughout the cell are likely to influence the complement of receptors at synaptic locations.

The relationship between NR1 and GluR1 expression, for both double-labeling (circles) and triple-labeling (squares) experiments, is summarized for all experiments in Figure 4-9. For AP5 and NMDA treatments, nearly all points lie in a tight cluster about the line describing a one to one relationship between the expression level of the two subunits. Experiments with TTX treatment lie exclusively below this line, favoring an increase in NR1 expression at the expense of GluR1. On the other hand, experiments with BMI treatment appear to favor increased GluR1 expression at the expense of NR1, though several points lie directly on the one to one relationship line. The relationships shown in this figure highlight the previous results, emphasizing that AP5 and NMDA treatment had variable, though minimal effect on NR1 and GluR1 expression, while TTX treatment increased NR1 expression and BMI treatment increased GluR1 expression.

## **DISCUSSION**

The findings described here represent an attempt to correlate changes in the synaptic distribution of glutamatergic receptors with what is known about the activity-dependent remodeling of the LGN. The results, obtained with fluorescence immunohistochemistry, indicate that the colocalization of glutamate receptor subunits

is stable throughout the A and A1 layers of the LGN, particularly at locations opposite to retinogeniculate terminals. Further, brief treatments with either NMDA or AP5 fail to alter the relative levels of receptor expression, while both TTX and BMI treatments significantly change the AMPA to NMDA ratio.

### **Consideration of immunofluorescence imaging technique**

Each of the results presented here are predicated on the accuracy with which immunofluorescence can assess the spatial distribution of AMPA and NMDA receptors. Since the antibodies used in this study were targeted to intracellular epitopes, it might be possible to use antibodies for extracellular domains to specifically target membranous receptors. However, in practice, the specificity of such antibodies would be reduced by tissue permeabilization attributable to the process of tissue sectioning itself. Although the antibodies used in this study could label intracellular as well as extracellular receptors, several studies have suggested that synaptic receptor expression is well correlated with the amount of local intracellular receptor<sup>49-52</sup>. Also, overexpressed, exogenous AMPA receptor subunits, once driven into dendritic spines, could be detected with electrophysiological recordings<sup>22,37,53</sup>, suggesting that visualizing receptors in volumes which are approximately the size of spines (1-2  $\mu\text{m}$  long and 0.5  $\mu\text{m}$  wide and deep) might be sufficient to predict their synaptic expression.

Two further techniques were used in this study to examine and reduce the potential bias of non-synaptic receptors. The first technique calculated a clustering coefficient<sup>137</sup> to quantify the “closeness” of colocalized AMPA and NMDA receptor subunits. If receptors are synthesized in close proximity, then receptor expression should become very high in these regions and cause a spurious increase in colocalization which might mask events at synapses. The clustering coefficient for NR1-GluR1 and NR1-GluR4 was significantly elevated at P21, suggesting that large increases of receptor production may have occurred at this age. However, the degree of clustering was similar before and after sublamination, indicating that changes in receptor production did not overwhelm more subtle changes in colocalization at synapse at these ages.

The second technique to remove extra-synaptic bias was to perform triple-labeling experiments utilizing the anterograde axon tracing of CTB to label retinogeniculate terminals. In these experiments, restricting analysis to locations apposed to terminals quite obviously eliminated the majority of somatic staining (Figure 4-4a, 4-5a, 4-8) and had the additional advantage of isolating retinal input while discarding corticothalamic or modulatory brainstem synaptic terminals. The combination of each of these techniques with the caveats concerning correlated intracellular and extracellular receptor expression provide a reasonably strong metric

for assessing both the spatial distribution of AMPA and NMDA receptor subunits as well as their relative expression levels.

### **AMPA and NMDA receptor colocalization**

The finding that AMPA and NMDA receptor colocalization is stable during the period of sublamination suggests that these receptors already coexist at retinogeniculate synapses at the earliest time points examined. While it remains possible that AMPA receptors continue to be inserted into synapses during this period without being detected by the immunofluorescence assay, several points argue against this. The first point comes from careful studies of the properties of spontaneous EPSCs and miniature evoked EPSCs (recorded with extracellular strontium) which are principally generated by AMPA receptor currents (assessed by CNQX sensitivity) in the LGN<sup>128</sup>. Both of these EPSCs maintained stable properties and were largely unaffected by the ongoing anatomical reorganization during ON/OFF sublamination. Secondly, NMDA receptors also maintained stable properties throughout this period<sup>48,127</sup>. Finally, although silent synapses were detected before ON/OFF sublamination, an equivalent proportion were also detected after sublamination<sup>48</sup>. This finding leaves room for the conversion of silent into functional synapses, though this interpretation would also require a mechanism for generating a compensatory number of new silent synapses to replace the ones which had been lost. These points, combined with the anatomical finding that AMPA and

NMDA receptor colocalization remains constant throughout this developmental period, particularly near retinogeniculate terminals, give a strong indication that the functional properties of these synapses are not influenced by the changing properties of AMPA and NMDA receptors. It should be noted, however, that these results do not preclude a role for AMPA receptor insertion at silent synapses in an earlier period of retinogeniculate development.

### **Activity-dependent AMPA and NMDA receptor expression**

NMDA receptor activation is critical to the development of ON/OFF sublaminae, as *in vivo* blockade of NMDA receptors with AP5 between P14 and P21 disrupts the formation of sublaminae<sup>108,109</sup>. The same blockade also increases the number of dendritic branch points and the density of dendritic spines on LGN neurons, a process which occurs *in vitro* within hours of AP5 application<sup>139</sup>. These results suggest that the process of ON/OFF sublamination is particularly sensitive to modifications of NMDA receptor activity and that blockade of this receptor may have dramatic consequences for the rearrangement of anatomical connections and the regulation of spine and synapse number on LGN neurons.

Activation and blockade of the NMDA receptor, as well as regulation of excitatory and inhibitory activity, have previously been shown to alter the distribution and functional properties of both AMPA and NMDA receptors. In cultures of

hippocampal neurons, long-term NMDA receptor blockade led to an increase in either the size or number of NMDA receptor clusters<sup>50,140</sup>. Similarly, in hippocampal or spinal neuron cultures, chronic AMPA receptor blockade led to an increase in either the size or number of AMPA receptor clusters<sup>50,141</sup>. Additionally, AMPA and NMDA receptors have exhibited sensitivity to long-term changes in network activity such that chronic blockade of activity upregulated NMDA receptor expression<sup>140</sup>, upregulated AMPA receptor expression<sup>141</sup>, and increased the size of AMPA and NMDA receptor mEPSCs<sup>126,142</sup>, while enhanced activity had the opposite effect<sup>51,126,142,143</sup>. These findings suggest that AMPA and NMDA receptors may be regulated independently, although large scale changes in network activity are likely to alter both AMPA and NMDA receptors simultaneously. However, these conclusions rely exclusively on manipulating network activity over long periods of time (one to several days) in preparations of dissociated, cultured neurons.

The results presented here are distinguished from these prior experiments in that they utilized acute slices, which better preserve the intrinsic circuitry in the LGN, as well as brief drug treatments. Under these conditions, activation or blockade of NMDA receptors had no effect on AMPA and NMDA receptor expression throughout the thalamic tissue or at isolated retinogeniculate contacts. The NMDA receptor blockade in these experiments was shorter than that required to induce new spines<sup>139</sup> and any

structural processes that were initiated were insufficient to alter the relative expression levels of AMPA or NMDA receptors. However, brief modification of excitation and inhibition on these short time scales was capable of altering the AMPA to NMDA ratio; action potential blockade favored a relative increase in NR1 expression while blockade of inhibitory GABAergic transmission favored a relative increase in GluR1 expression. These results suggest that the developing LGN, while undergoing significant reorganization, is sensitive to activity-dependent modification and attempts to maintain a constant AMPA and NMDA spatial distribution and expression profile.

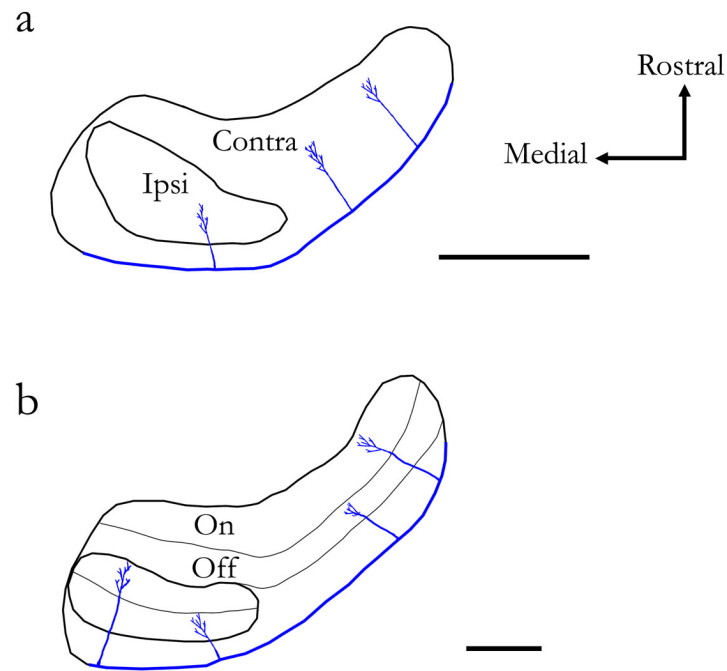


**Figure 4-1.** Eye-specific segregation is followed by ON/OFF sublamination in the developing ferret LGN. **a**, Retinal axons from the two eyes first segregate into the A (contralateral input) and A1 (ipsilateral input) layers of the LGN over the first two postnatal weeks. **b**, ON-center and OFF-center retinal axons then segregate into separate sublaminae. This sublamination is complete by the fourth postnatal week. Scale bars, 500  $\mu\text{m}$  at each age.

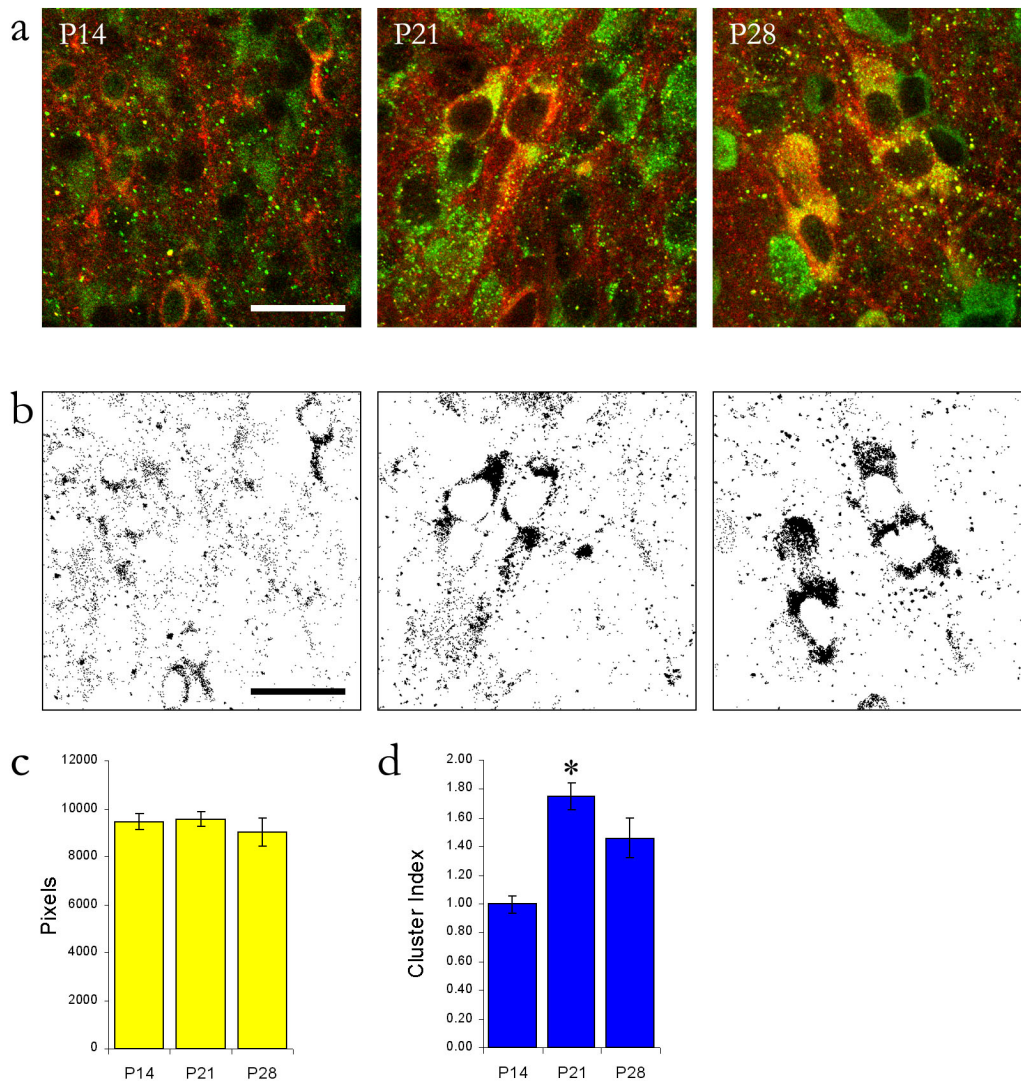


**Figure 4-2.** AMPA and NMDA receptor subunit colocalization is stable over ON/OFF sublamination. **a**, Example images of NR1 (NMDA) and GluR1 (AMPA) subunit expression from P14 to P28. **b**, NR1 and GluR1 colocalization, where each yellow pixel in the images in **a** is reproduced as a black pixel. **c**, NR1 and GluR1 colocalization remains constant from P14 to P28. **d**, The clustering of colocalized pixels is similar before and after sublamination, although it increases during the third postnatal week. Scale bar, 25  $\mu$ m.

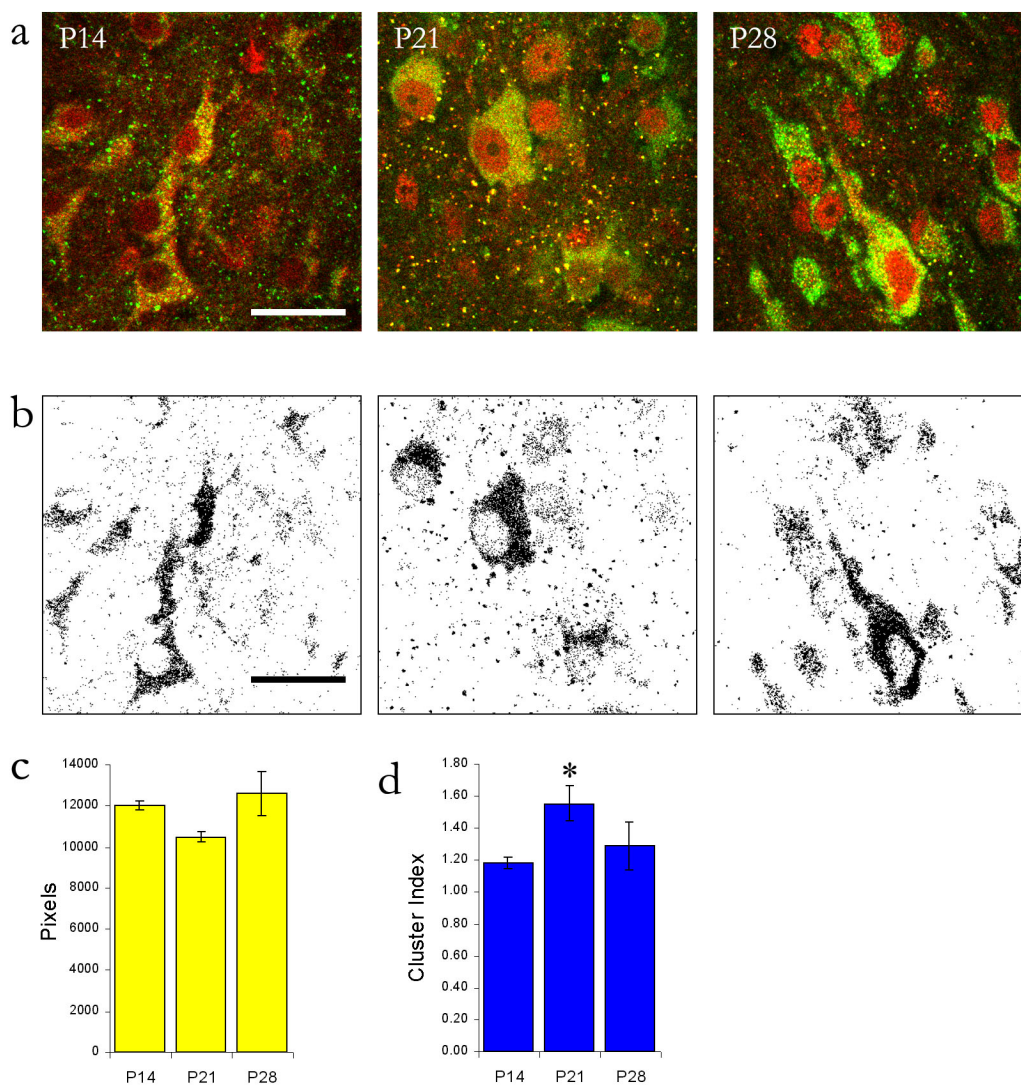


**Figure 4-3.** The pattern of AMPA-NMDA colocalization is not unique to GluR1. **a-d**, Same conventions as in Figure 2-2. GluR4-NR1 colocalization is stable across ON/OFF sublamination and clustering of colocalized pixels is similar before and after sublamination, although it increases during the third postnatal week. Scale bar, 25  $\mu$ m.

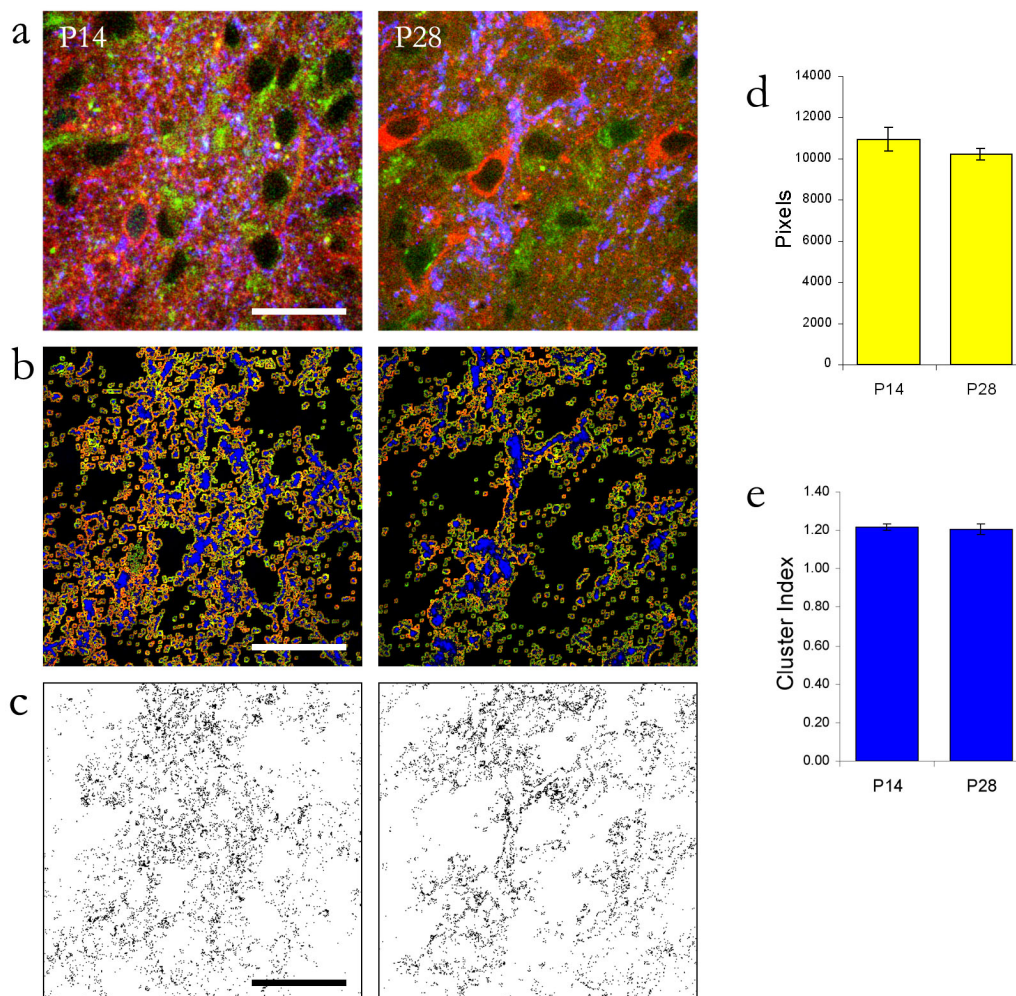


**Figure 4-4.** The pattern of AMPA-NMDA colocalization opposite retinogeniculate terminals is not different from the global pattern of colocalization in the LGN. **a**, Examples of triple-labeling with NR1 (green) and GluR1 (red) opposite CTB-labeled retinogeniculate terminals (blue). **b**, The same images as in **a**, but with only those red and green pixels that are adjacent to CTB labeling. **c**, NR1 and GluR1 colocalization restricted to retinogeniculate terminals. **d**, Colocalization at P28 is unchanged from P14. **e**, Likewise, the clustering of colocalized pixels is similar before and after sublamination. Scale bar, 25  $\mu\text{m}$ .

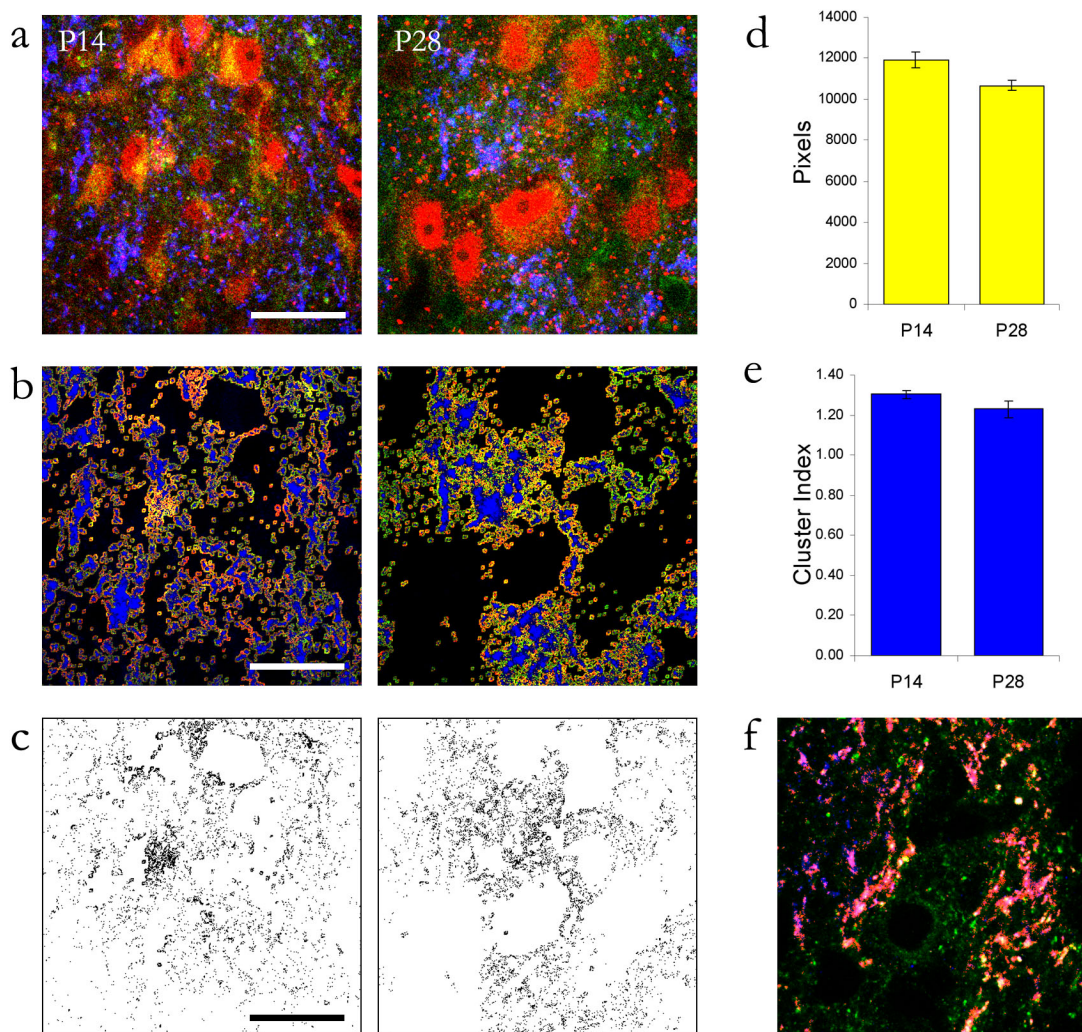


**Figure 4-5.** The pattern of AMPA-NMDA colocalization opposite retinogeniculate terminals is not unique to GluR1. **a-e**, Same conventions as in Figure 2-4. GluR4-NR1 colocalization at P28 is unchanged from P14 and clustering of colocalized pixels opposite retinogeniculate terminals is stable across ON/OFF sublamination. **f**, CTB label overwhelmingly represents synaptic boutons, marked by synaptophysin, rather than fibers of passage. The vast majority of CTB label (blue) is colocalized with synaptophysin (green); colocalized label is shown in pink. There is also a significant amount of synaptophysin labeling independent of CTB, reflecting the nonretinal innervation of the LGN. Scale bar, 25  $\mu$ m.

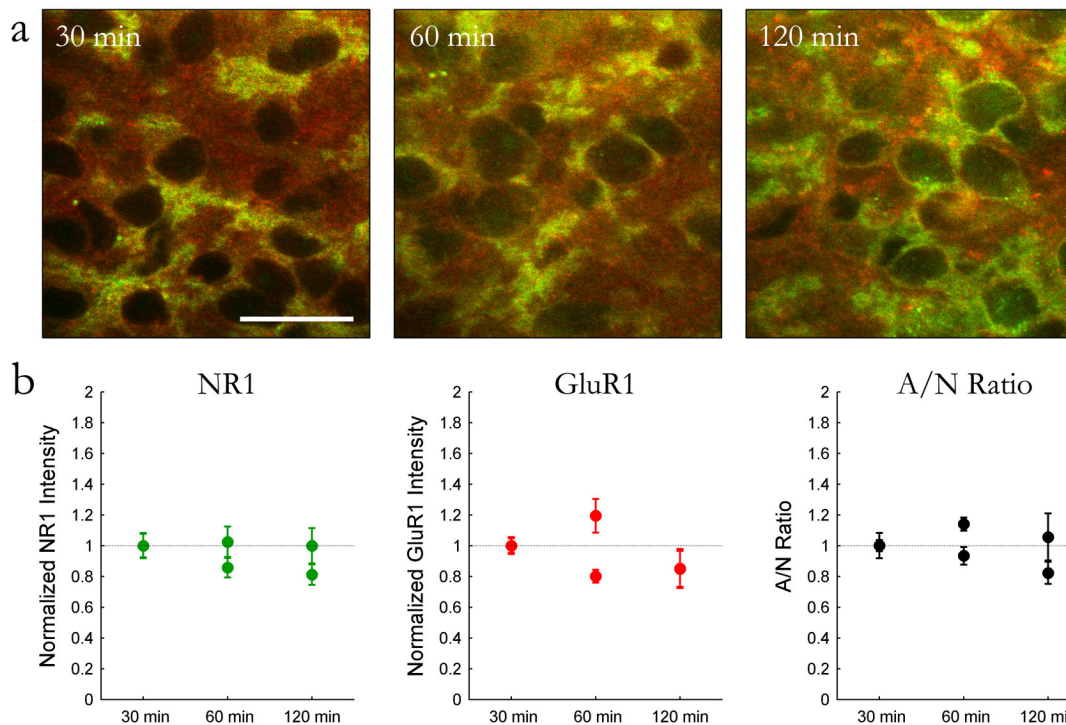


**Figure 4-6.** AMPA and NMDA receptor expression is stable over two hours in acute slices. **a**, Example images of NR1 (green) and GluR1 (red) immunofluorescence following 30, 60, and 120 minutes in normal ACSF. **b**, NR1 and GluR1 expression are stable over two hours. Relative expression is normalized to the 30 minute condition. Two experiments are shown, one conducted at P14 and a second at P21. The AMPA to NMDA ratio (A/N ratio) is also stable over two hours. Scale bar, 25  $\mu$ m.

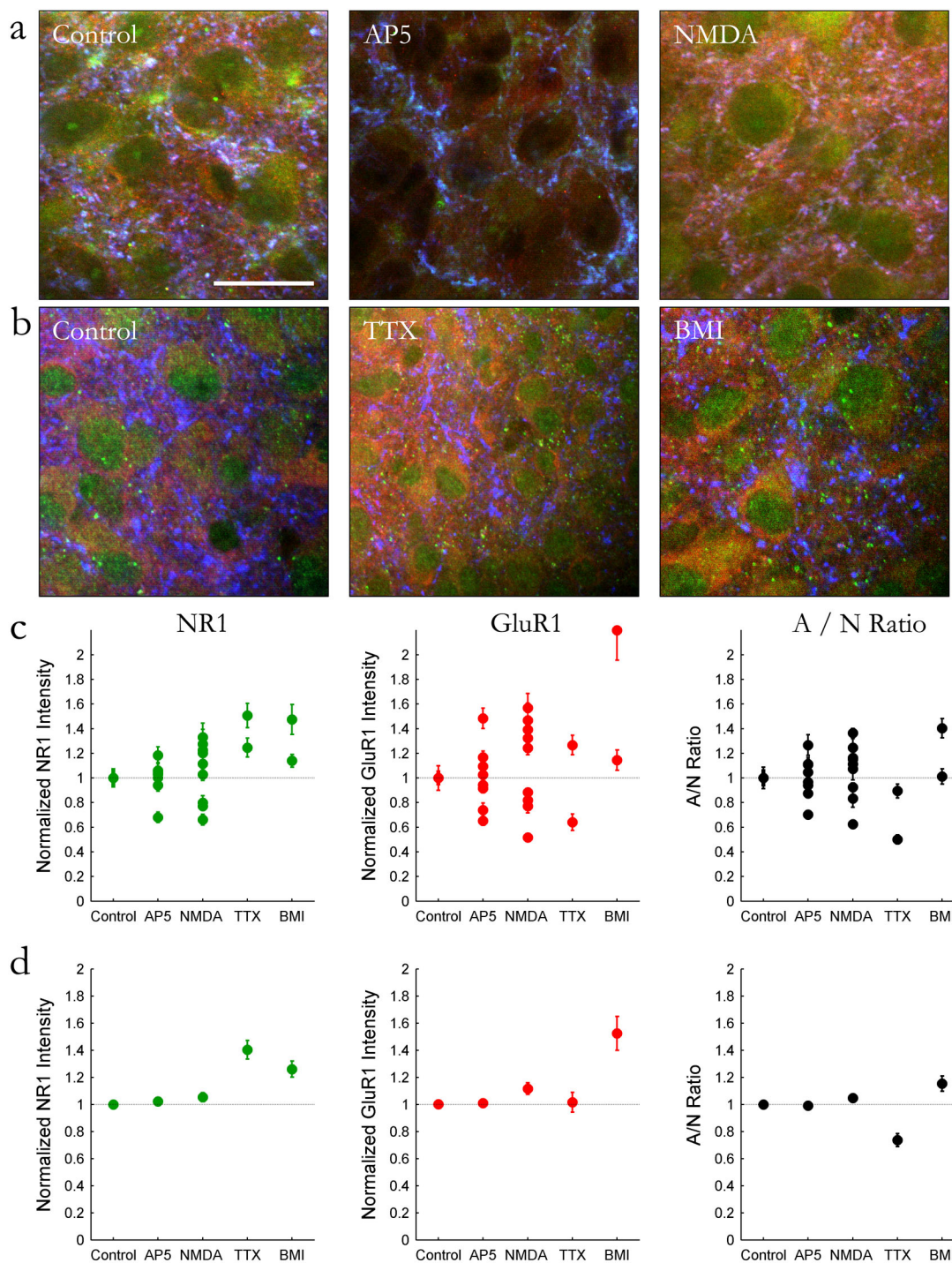


**Figure 4-7.** Variable AMPA and NMDA expression following pharmacological treatment. **a,b**, Example images showing NR1 (green) and GluR1 (red) immunofluorescence following treatment with normal ACSF, AP5, NMDA, TTX, or BMI. **c**, In 12 experiments, NR1 and GluR1 expression are strikingly variable in comparison to control. **d**, TTX and BMI alter both receptor expression and the A/N ratio while AP5 and NMDA do not. Scale bar, 25  $\mu$ m.

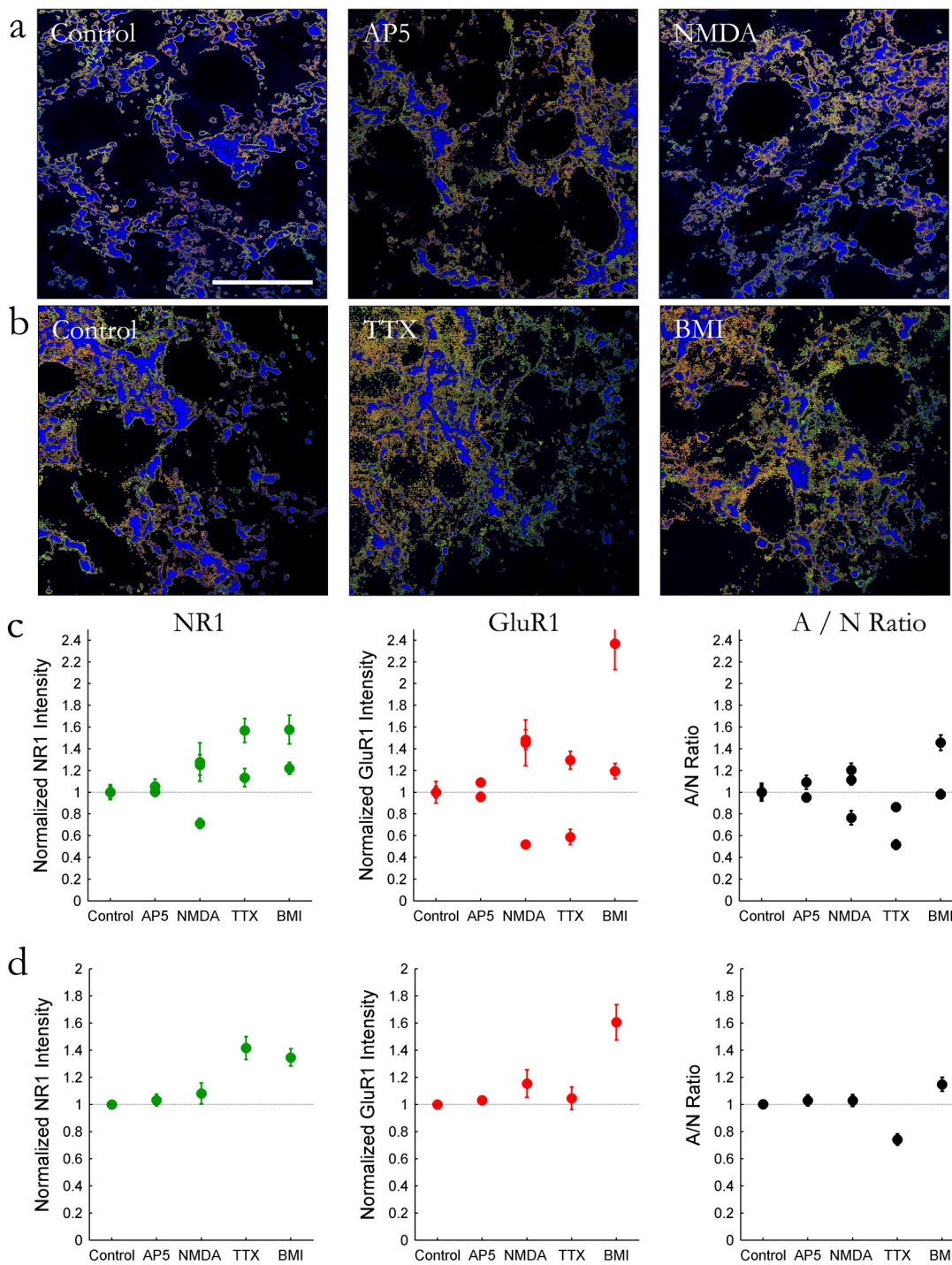


**Figure 4-8.** Variable AMPA and NMDA receptor expression at retinogeniculate terminals following pharmacological treatment. **a-d**, Same convention as Figure 2-7. In 6 experiments, TTX and BMI alter both receptor expression and the A/N ratio while AP5 and NMDA do not. Scale bar, 25  $\mu$ m.

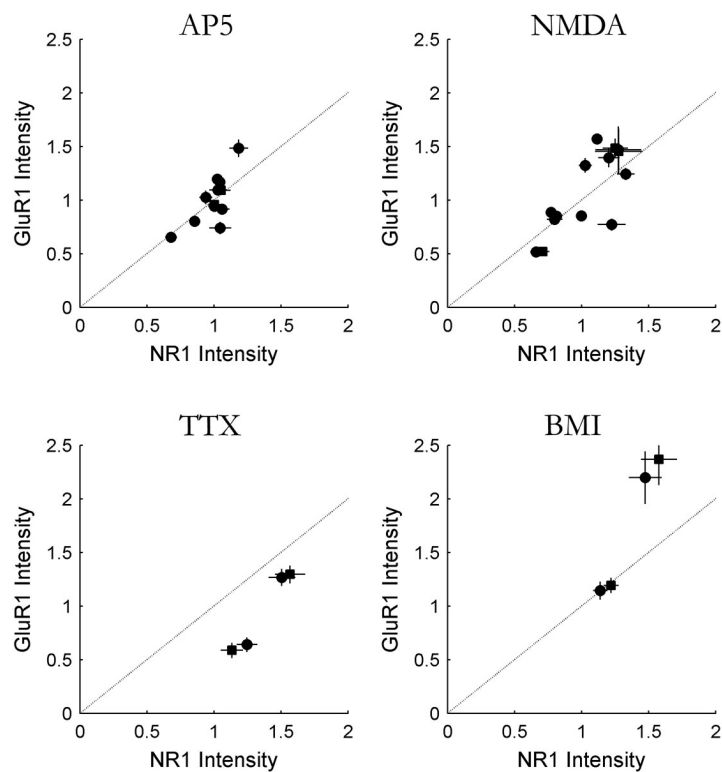


**Figure 4-9.** Relative changes in AMPA and NMDA receptor expression are summarized for all experiments. Double-labeling experiments (global NR1 and GluR1) are marked with circles and triple-labeling experiments (retinogeniculate NR1 and GluR1) are marked with squares. AP5 and NMDA treatment have a minimal effect on NR1 and GluR1 expression and all experimental data points are clustered around the line marking a one to one relationship between the expression of the two subunits. On the other hand, TTX experiments are biased towards higher NR1 expression, while some BMI experiments are biased toward higher GluR1 expression.

## CHAPTER 5

### Summary and Conclusions

In the first chapter, I emphasized the importance of examining and correlating structure and function in the nervous system. The purpose of this was to highlight the idea that morphology and structure play a role in determining function and, importantly, changes that alter functionality are likely to have an impact on structure. Indeed, the studies conducted for this thesis make it clear that function and structure, particularly at the level of dendritic spines and synapses are inter-related and potentially, inseparable.

In the second chapter, I examined the properties of dendritic spines on cortical layer V pyramidal neurons. Spines on these neurons possessed dynamic morphologies which were regulated both by development and glutamatergic activity. These results suggest that developing neurons, particularly those undergoing high levels of synaptogenesis may be experiencing a period of heightened cytoskeletal dynamics, consistent with cell growth and the creation and formation of many synapses, and that this program is likely to affect the relative stability of existing synaptic connections. Those synapses which receive appropriate glutamatergic input are likely to be

stabilized, and may be preferentially maintained, thereby avoiding synapse loss or spine withdrawal. To more closely examine the relationship between spine dynamics and glutamatergic activity, I attempted to correlate spine motility and glutamate receptor expression in individual spines. Although both spine dynamics and glutamate receptors are developmentally regulated in the cortex, the two were not correlated in individual spines. However, a specific subclass of dendritic protrusions, filopodia, bore an interesting profile of receptors suggestive of their role as functionally and structurally immature points of synaptic contact.

In the third chapter, I extended the work on dendritic spines to a later point in development (P28) which corresponds to the period of ocular dominance plasticity in the visual cortex. Integrating the data from the previous chapter, it appears that basal spine motility declined to an even lower level at this later age (Figure 5-1). This suggests that, although this period possesses a high potential for plasticity, this characteristic is not evident in basal spine dynamics. However, during this period, brief occlusion of an eye for two to three days was sufficient to induce an upregulation in spine dynamics both *in vivo* and *in vitro*. Interestingly, this upregulation was restricted to parts of the dendritic arbor in the superficial and deep cortical layers, which predominantly receive input from horizontal connections. Further, the change in spine dynamics could be mimicked by enzymatic degradation of the extracellular matrix and this mechanism

was also implicated *in vivo*. The chapter concluded with a model of functional and structural plasticity where rapid functional changes at synapses were consolidated by inducing structural plasticity in an environment made permissive by extracellular matrix degradation.

In the fourth chapter, I turned to a system which undergoes well-characterized anatomical rearrangements over the first four postnatal weeks. During the period of ON/OFF sublamination, which is particularly sensitive to action potential and NMDA receptor blockade, subunits of the AMPA and NMDA glutamatergic receptors were constantly expressed and their colocalization was stable. Combined with electrophysiological experiments that characterized the stable functional properties of AMPA and NMDA receptors, these findings provide a counterpoint to the idea that synaptic development necessarily occurs by regulating the insertion of AMPA receptors into immature synapses. In addition, manipulations of synaptic activity did not preferentially alter the expression of either AMPA or NMDA receptors. However, action potential blockade favored a relative increase in the number of NMDA receptors while enhanced neuronal excitability favored a relative increase in the number of AMPA receptors. These results imply suggest that the period of ON/OFF sublamination is not characterized by a simple increase in the proportion of AMPA receptors at retinogeniculate synapses. Rather, this period of development seems to

require glutamatergic synapses to transmit information regarding general levels of excitability which may then inform anatomical rearrangements.

## **Conclusions**

The work presented in this thesis explored the relationship between structure and function in three model systems: (1) the developing mouse cortex during the period of synaptogenesis, (2) the mouse primary visual cortex during the critical period for ocular dominance plasticity, and (3) the developing ferret lateral geniculate nucleus during the period of ON/OFF sublamination. Each system provided important insights into the interplay between structure and function. In the developing mouse cortex, structural stability was induced by synaptic activity, providing a potential means of selecting synaptic connections to be retained, while others, which did not receive appropriate input, could be removed. During the period of ocular dominance plasticity, reduced input from the deprived eye, leading to a loss of synaptic efficacy, could induce a series of events that created a permissive environment for effecting structural change. Finally, in the developing LGN, stable synaptic properties could be observed during a period of extended anatomical and structural rearrangement. In sum, the conclusions of this thesis provide a substantial contribution to the field of neuroscience and advance our understanding of the interaction between structure and function at subcellular levels of analysis.

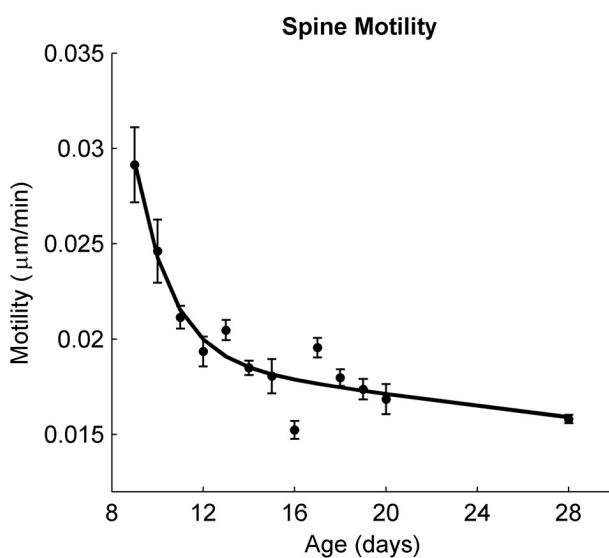


**Figure 5-1.** Double exponential decline of spine motility over development. Data from Chapter 2 was resampled to match the acquisition parameters from the series of experiments in Chapter 3. When considering the critical period data (P28), a double exponential fits the points better than the linear fit shown in Figure 2-3. Extrapolating along the curve, the increased spine motility following monocular deprivation corresponds approximately to developmental days P12 or P13.

## References

1. Gray, E. Electron microscopy of synaptic contacts on dendritic spines of the cerebral cortex. *Nature* **183**, 1592-1593 (1959).
2. Palay, S. Synapses in the central nervous system. *J Biophys Biochem Cytol* **2**, 193-201 (1956).
3. Yuste, R., Majewska, A. & Holthoff, K. From form to function: calcium compartmentalization in dendritic spines. *Nat Neurosci* **3**, 653-9 (2000).
4. Hering, H. & Sheng, M. Dendritic spines: structure, dynamics and regulation. *Nat Rev Neurosci* **2**, 880-8. (2001).
5. Bonhoeffer, T. & Yuste, R. Spine Motility: Phenomenology, Mechanisms, and Function. *Neuron* **35**, 1019-1027 (2002).
6. Dunaevsky, A., Tashiro, A., Majewska, A., Mason, C. & Yuste, R. Developmental regulation of spine motility in the mammalian central nervous system. *Proc Natl Acad Sci U S A* **96**, 13438-43 (1999).
7. Fischer, M., Kaech, S., Knutti, D. & Matus, A. Rapid actin-based plasticity in dendritic spines. *Neuron* **20**, 847-54 (1998).
8. Fischer, M., Kaech, S., Wagner, U., Brinkhaus, H. & Matus, A. Glutamate receptors regulate actin-based plasticity in dendritic spines. *Nat Neurosci* **3**, 887-94 (2000).
9. Korkotian, E. & Segal, M. Regulation of dendritic spine motility in cultured hippocampal neurons. *J Neurosci* **21**, 6115-24 (2001).
10. Korkotian, E. & Segal, M. Spike-associated fast contraction of dendritic spines in cultured hippocampal neurons. *Neuron* **30**, 751-8 (2001).

11. Lendvai, B., Stern, E. A., Chen, B. & Svoboda, K. Experience-dependent plasticity of dendritic spines in the developing rat barrel cortex in vivo. *Nature* **404**, 876-881 (2000).
12. Majewska, A. & Sur, M. Motility of dendritic spines in visual cortex in vivo: Changes during the critical period and effects of visual deprivation. *Proc Natl Acad Sci U S A* **100**, 16024-16029 (2003).
13. Majewska, A., Tashiro, A. & Yuste, R. Regulation of spine calcium dynamics by rapid spine motility. *J Neurosci* **20**, 8262-8. (2000).
14. Catalano, S. M., Chang, C. K. & Shatz, C. J. Activity-dependent regulation of NMDAR1 immunoreactivity in the developing visual cortex. *J Neurosci* **17**, 8376-90 (1997).
15. Carmignoto, G. & Vicini, S. Activity-dependent decrease in NMDA receptor responses during development of the visual cortex. *Science* **258**, 1007-11 (1992).
16. Flint, A. C., Maisch, U. S., Weishaupt, J. H., Kriegstein, A. R. & Monyer, H. NR2A subunit expression shortens NMDA receptor synaptic currents in developing neocortex. *J Neurosci* **17**, 2469-76 (1997).
17. Sheng, M., Cummings, J., Roldan, L. A., Jan, Y. N. & Jan, L. Y. Changing subunit composition of heteromeric NMDA receptors during development of rat cortex. *Nature* **368**, 144-7 (1994).
18. Kumar, S. S., Bacci, A., Kharazia, V. & Huguenard, J. R. A developmental switch of AMPA receptor subunits in neocortical pyramidal neurons. *J Neurosci* **22**, 3005-15 (2002).
19. Isaac, J. T. R., Nicoll, R. A. & Malenka, R. C. Evidence for silent synapses: Implications for the expression of LTP. *Neuron* **15**, 427-434 (1995).

20. Liao, D., Hessler, N. A. & Malinow, R. Activation of postsynaptically silent synapses during pairing-induced LTP in CA1 region of hippocampal slice. *Nature* **375**, 400-404 (1995).
21. Durand, G. M., Kovalchuk, Y. & Konnerth, A. Long-term potentiation and functional synapse induction in developing hippocampus. *Nature* **381**, 71-75 (1996).
22. Shi, S.-H. et al. Rapid spine delivery and redistribution of AMPA receptors after synaptic NMDA receptor activation. *Science* **284**, 1811-1816 (1999).
23. Feng, G. et al. Imaging neuronal subsets in transgenic mice expressing multiple spectral variants of GFP. *Neuron* **28**, 41-51. (2000).
24. Majewska, A., Yiu, G. & Yuste, R. A custom-made two-photon microscope and deconvolution system. *Pflugers Arch* **441**, 398-408. (2000).
25. Harris, K. M., Jensen, F. E. & Tsao, B. Three-dimensional structure of dendritic spines and synapses in rat hippocampus (CA1) at postnatal day 15 and adult ages: implications for the maturation of synaptic physiology and long-term potentiation. *J Neurosci* **12**, 2685-705 (1992).
26. De Felipe, J., Marco, P., Fairen, A. & Jones, E. G. Inhibitory synaptogenesis in mouse somatosensory cortex. *Cereb Cortex* **7**, 619-34 (1997).
27. Petit, T. L., LeBoutillier, J. C., Gregorio, A. & Libstug, H. The pattern of dendritic development in the cerebral cortex of the rat. *Brain Res* **469**, 209-19 (1988).
28. Wise, S. P., Fleshman, J. W., Jr. & Jones, E. G. Maturation of pyramidal cell form in relation to developing afferent and efferent connections of rat somatic sensory cortex. *Neuroscience* **4**, 1275-97 (1979).
29. Dailey, M. E. & Smith, S. J. The dynamics of dendritic structure in developing hippocampal slices. *J Neurosci* **16**, 2983-94 (1996).

30. Ziv, N. E. & Smith, S. J. Evidence for a role of dendritic filopodia in synaptogenesis and spine formation. *Neuron* **17**, 91-102 (1996).
31. Parnass, Z., Tashiro, A. & Yuste, R. Analysis of spine morphological plasticity in developing hippocampal pyramidal neurons. *Hippocampus* **10**, 561-8 (2000).
32. Matus, A., Ackermann, M., Pehling, G., Byers, H. R. & Fujiwara, K. High actin concentrations in brain dendritic spines and postsynaptic densities. *Proc Natl Acad Sci U S A* **79**, 7590-4 (1982).
33. Matus, A. Actin-based plasticity in dendritic spines. *Science* **290**, 754-8 (2000).
34. Star, E. N., Kwiatkowski, D. J. & Murthy, V. N. Rapid turnover of actin in dendritic spines and its regulation by activity. *Nat Neurosci* **5**, 239-46. (2002).
35. Rogers, S. W. et al. The characterization and localization of the glutamate receptor subunit GluR1 in the rat brain. *J. Neurosci.* **11**, 2713-2724 (1991).
36. Barria, A. & Malinow, R. Subunit-specific NMDA receptor trafficking to synapses. *Neuron* **35**, 345-53 (2002).
37. Hayashi, Y. et al. Driving AMPA receptors into synapses by LTP and CaMKII: requirement for GluR1 and PDZ domain interaction. *Science* **287**, 2262-7 (2000).
38. Shi, S.-H., Hayashi, Y., Esteban, J. A. & Malinow, R. Subunit-specific rules governing AMPA receptor trafficking to synapses in hippocampal pyramidal neurons. *Cell* **105**, 331-43 (2001).
39. Takumi, Y., Ramírez-León, V., 4, P. L., Rinvik, E. & Ottersen, O. P. Different modes of expression of AMPA and NMDA receptors in hippocampal synapses. *Nature Neuroscience* **2**, 618-624 (1999).
40. Matsuzaki, M. et al. Dendritic spine geometry is critical for AMPA receptor expression in hippocampal CA1 pyramidal neurons. *Nat Neurosci* **4**, 1086-92 (2001).

41. McKinney, R. A., Capogna, M., Dürr, R. & Gähwiler, B. H. Miniature synaptic events maintain dendritic spines via AMPA receptor activation. *Nature Neuroscience* **2**, 44-49 (1999).
42. Maletic-Savatic, M., Malinow, R. & Svoboda, K. Rapid dendritic morphogenesis in CA1 hippocampal dendrites induced by synaptic activity. *Science* **283**, 1923-7. (1999).
43. Engert, F. & Bonhoeffer, T. Dendritic spine changes associated with hippocampal long-term synaptic plasticity. *Nature* **399**, 66-70 (1999).
44. Trachtenberg, J. T. et al. Long-term in vivo imaging of experience-dependent synaptic plasticity in adult cortex. *Nature* **420**, 788-94 (2002).
45. Grutzendler, J., Kasthuri, N. & Gan, W. B. Long-term dendritic spine stability in the adult cortex. *Nature* **420**, 812-6 (2002).
46. Blue, M. E. & Parnavelas, J. G. The formation and maturation of synapses in the visual cortex of the rat. II. Quantitative analysis. *J Neurocytol* **12**, 697-712 (1983).
47. Juraska, J. M. The development of pyramidal neurons after eye opening in the visual cortex of hooded rats: a quantitative study. *J Comp Neurol* **212**, 208-13 (1982).
48. Hohnke, C. D., Oray, S. & Sur, M. Activity-dependent patterning of retinogeniculate axons proceeds with a constant contribution from AMPA and NMDA receptors. *Journal of Neuroscience* **20**, 8051-8060 (2000).
49. Mammen, A. L., Huganir, R. L. & O'Brien, R. J. Redistribution and stabilization of cell surface glutamate receptors during synapse formation. *J. Neurosci.* **17**, 7351-7358 (1997).
50. Liao, D., Zhang, X., O'Brien, R., Ehlers, M. D. & Huganir, R. L. Regulation of morphological postsynaptic silent synapses in developing hippocampal neurons. *Nat Neurosci* **2**, 37-43 (1999).

51. O'Brien, R. J. et al. Activity-dependent modulation of synaptic AMPA receptor accumulation. *Neuron* **21**, 1067-78 (1998).
52. Rubio, M. E. & Wenthold, R. J. Differential distribution of intracellular glutamate receptors in dendrites. *J. Neurosci.* **19**, 5549-5562 (1999).
53. Piccini, A. & Malinow, R. Critical postsynaptic density 95/disc large/zonula occludens-1 interactions by glutamate receptor 1 (GluR1) and GluR2 required at different subcellular sites. *J Neurosci* **22**, 5387-92 (2002).
54. Wiesel, T. N. & Hubel, D. H. Single-Cell Responses in Striate Cortex of Kittens Deprived of Vision in One Eye. *J Neurophysiol* **26**, 1003-17 (1963).
55. Hubel, D. H. & Wiesel, T. N. The period of susceptibility to the physiological effects of unilateral eye closure in kittens. *J Physiol* **206**, 419-36 (1970).
56. Olson, C. R. & Freeman, R. D. Progressive changes in kitten striate cortex during monocular vision. *J Neurophysiol* **38**, 26-32 (1975).
57. Gordon, J. A. & Stryker, M. P. Experience-dependent plasticity of binocular responses in the primary visual cortex of the mouse. *Journal of Neuroscience* **16**, 3274-3286 (1996).
58. Hensch, T. K. et al. Local GABA circuit control of experience-dependent plasticity in developing visual cortex. *Science* **282**, 1504-1508 (1998).
59. Huang, Z. J. et al. BDNF regulates the maturation of inhibition and the critical period of plasticity in mouse visual cortex. *Cell* **98**, 739-55 (1999).
60. Fagiolini, M. & Hensch, T. K. Inhibitory threshold for critical-period activation in primary visual cortex. *Nature* **404**, 183-6 (2000).
61. Fagiolini, M. et al. Specific GABAA circuits for visual cortical plasticity. *Science* **303**, 1681-3 (2004).
62. Movshon, J. A. & Dursteler, M. R. Effects of brief periods of unilateral eye closure on the kitten's visual system. *J Neurophysiol* **40**, 1255-65 (1977).

63. Mioche, L. & Singer, W. Chronic recordings from single sites of kitten striate cortex during experience-dependent modifications of receptive-field properties. *J Neurophysiol* **62**, 185-97 (1989).
64. Trachtenberg, J. T., Trepel, C. & Stryker, M. P. Rapid extragranular plasticity in the absence of thalamocortical plasticity in the developing primary visual cortex. *Science* **287**, 2029-32. (2000).
65. Kirkwood, A., Dudek, S. M., Gold, J. T., Aizenman, C. D. & Bear, M. F. Common forms of synaptic plasticity in the hippocampus and neocortex in vitro. *Science* **260**, 1518-21 (1993).
66. Kirkwood, A. & Bear, M. F. Homosynaptic long-term depression in the visual cortex. *J Neurosci* **14**, 3404-12 (1994).
67. Heynen, A. J. et al. Molecular mechanism for loss of visual cortical responsiveness following brief monocular deprivation. *Nat Neurosci* **6**, 854-62 (2003).
68. Shatz, C. J. & Stryker, M. P. Ocular dominance in layer IV of the cat's visual cortex and the effects of monocular deprivation. *J Physiol* **281**, 267-83 (1978).
69. Antonini, A. & Stryker, M. P. Rapid remodeling of axonal arbors in the visual cortex. *Science* **260**, 1819-21 (1993).
70. Antonini, A., Fagiolini, M. & Stryker, M. P. Anatomical correlates of functional plasticity in mouse visual cortex. *Journal of Neuroscience* **19**, 4388-4406 (1999).
71. Trachtenberg, J. T. & Stryker, M. P. Rapid anatomical plasticity of horizontal connections in the developing visual cortex. *J Neurosci* **21**, 3476-82 (2001).
72. Yuste, R. & Denk, W. Dendritic spines as basic functional units of neuronal integration. *Nature* **375**, 682-4 (1995).
73. Koester, H. J. & Sakmann, B. Calcium dynamics in single spines during coincident pre- and postsynaptic activity depend on relative timing of back-

- propagating action potentials and subthreshold excitatory postsynaptic potentials. *Proc. Natl. Acad. Sci. USA* **95**, 9596-9601 (1998).
74. Emptage, N., Bliss, T. V. & Fine, A. Single synaptic events evoke NMDA receptor-mediated release of calcium from internal stores in hippocampal dendritic spines. *Neuron* **22**, 115-24 (1999).
  75. Helmchen, F., Svoboda, K., Denk, W. & Tank, D. W. In vivo dendritic calcium dynamics in deep-layer cortical pyramidal neurons. *Nature Neuroscience* **2**, 989-996 (1999).
  76. Yuste, R., Majewska, A., Cash, S. S. & Denk, W. Mechanisms of calcium influx into hippocampal spines: heterogeneity among spines, coincidence detection by NMDA receptors, and optical quantal analysis. *J Neurosci* **19**, 1976-87. (1999).
  77. Majewska, A., Brown, E., Ross, J. & Yuste, R. Mechanisms of calcium decay kinetics in hippocampal spines: role of spine calcium pumps and calcium diffusion through the spine neck in biochemical compartmentalization. *J Neurosci* **20**, 1722-34 (2000).
  78. Holthoff, K., Tsay, D. & Yuste, R. Calcium dynamics of spines depend on their dendritic location. *Neuron* **33**, 425-37 (2002).
  79. Sabatini, B. L., Oertner, T. G. & Svoboda, K. The life cycle of Ca<sup>2+</sup> ions in dendritic spines. *Neuron* **33**, 439-52 (2002).
  80. Müller, C. M. & Griesinger, C. B. Tissue plasminogen activator mediates reverse occlusion plasticity in visual cortex. *Nat Neurosci* **1**, 47-53 (1998).
  81. Mataga, N., Nagai, N. & Hensch, T. K. Permissive proteolytic activity for visual cortical plasticity. *Proc Natl Acad Sci U S A* **99**, 7717-21 (2002).
  82. Croisier, E., Leamey, C. A., Tonegawa, S. & Sur, M. Novel gene transcripts expressed in developing sensory neocortex in the mouse. *2002 Abstract Viewer and Itinerary Planner Online*, Program No. 131.11 (2002).

83. Leamey, C. A., Wang, K. H., Tonegawa, S. & Sur, M. Differential gene expression by specific sets of neocortical neurons during development in the mouse. 2002 *Abstract Viewer and Itinerary Planner Online*, Program No. 131.12 (2002).
84. Leamey, C. A. et al. Ten-m3 is expressed in the developing visual pathway. 2003 *Abstract Viewer and Itinerary Planner Online*, Program No. 567.19 (2003).
85. Lyckman, A. W., Ellsworth, C., Horng, S., Leamey, C. A. & Sur, M. Gene expression during the critical period for ocular dominance plasticity in mouse V1. 2003 *Abstract Viewer and Itinerary Planner Online*, Program No. 7.11 (2003).
86. Wahle, P. & Beckh, S. A method of in situ hybridization combined with immunocytochemistry, histochemistry, and tract tracing to characterize the mRNA expressing cell types in heterogeneous neuronal populations. *J Neurosci Methods* **41**, 153-66 (1992).
87. Salles, F. J. & Strickland, S. Localization and regulation of the tissue plasminogen activator-plasmin system in the hippocampus. *J Neurosci* **22**, 2125-34 (2002).
88. Pawlak, R., Magarinos, A. M., Melchor, J., McEwen, B. & Strickland, S. Tissue plasminogen activator in the amygdala is critical for stress-induced anxiety-like behavior. *Nat Neurosci* **6**, 168-74 (2003).
89. Duchossoy, Y., Horvat, J. C. & Stettler, O. MMP-related gelatinase activity is strongly induced in scar tissue of injured adult spinal cord and forms pathways for ingrowing neurites. *Mol Cell Neurosci* **17**, 945-56 (2001).
90. Mataga, N., Mizuguchi, Y. & Hensch, T. K. Experience-dependent pruning of dendritic spines by tPA-plasmin in visual cortex. (co-submission).
91. Sawtell, N. B. et al. NMDA Receptor-Dependent Ocular Dominance Plasticity in Adult Visual Cortex. *Neuron* **38**, 977-85 (2003).
92. Pizzorusso, T. et al. Reactivation of ocular dominance plasticity in the adult visual cortex. *Science* **298**, 1248-51 (2002).

93. Dityatev, A. & Schachner, M. Extracellular matrix molecules and synaptic plasticity. *Nat Rev Neurosci* **4**, 456-68. (2003).
94. Siconolfi, L. B. & Seeds, N. W. Induction of the plasminogen activator system accompanies peripheral nerve regeneration after sciatic nerve crush. *J Neurosci* **21**, 4336-47 (2001).
95. Baranes, D. et al. Tissue plasminogen activator contributes to the late phase of LTP and to synaptic growth in the hippocampal mossy fiber pathway. *Neuron* **21**, 813-25 (1998).
96. Krystosek, A. & Seeds, N. W. Plasminogen activator release at the neuronal growth cone. *Science* **213**, 1532-4 (1981).
97. Qian, Z., Gilbert, M. E., Colicos, M. A., Kandel, E. R. & Kuhl, D. Tissue-plasminogen activator is induced as an immediate-early gene during seizure, kindling and long-term potentiation. *Nature* **361**, 453-7 (1993).
98. Gualandris, A., Jones, T. E., Strickland, S. & Tsirka, S. E. Membrane depolarization induces calcium-dependent secretion of tissue plasminogen activator. *J Neurosci* **16**, 2220-5 (1996).
99. Fiumelli, H., Jabaudon, D., Magistretti, P. J. & Martin, J. L. BDNF stimulates expression, activity and release of tissue-type plasminogen activator in mouse cortical neurons. *Eur J Neurosci* **11**, 1639-46 (1999).
100. Seeds, N. W., Basham, M. E. & Ferguson, J. E. Absence of tissue plasminogen activator gene or activity impairs mouse cerebellar motor learning. *J Neurosci* **23**, 7368-75 (2003).
101. Sappino, A. P. et al. Extracellular proteolysis in the adult murine brain. *J Clin Invest* **92**, 679-85 (1993).
102. Werb, Z. ECM and cell surface proteolysis: regulating cellular ecology. *Cell* **91**, 439-42 (1997).

103. Fukazawa, Y. et al. Hippocampal LTP Is Accompanied by Enhanced F-Actin Content within the Dendritic Spine that Is Essential for Late LTP Maintenance In Vivo. *Neuron* **38**, 447-60 (2003).
104. Hall, A. Rho GTPases and the actin cytoskeleton. *Science* **279**, 509-14 (1998).
105. Katz, L. C. & Shatz, C. J. Synaptic activity and the construction of cortical circuits. *Science* **274**, 1133-1138 (1996).
106. Cramer, K. S., Angelucci, A., Hahm, J.-O., Bogdanov, M. B. & Sur, M. A role for nitric oxide in the development of the ferret retinogeniculate projection. *J. Neurosci.* **16**, 7995-8004 (1996).
107. Sur, M. & Leamey, C. A. Development and plasticity of cortical areas and networks. *Nature Reviews Neuroscience* **2**, 251-262 (2001).
108. Hahm, J.-O., Langdon, R. B. & Sur, M. Disruption of retinogeniculate afferent segregation by antagonists to NMDA receptors. *Nature* **351**, 568-570 (1991).
109. Hahm, J.-O., Cramer, K. S. & Sur, M. Pattern formation by retinal afferents in the ferret lateral geniculate nucleus: Developmental segregation and the role of N-Methyl-D-Aspartate receptors. *J. Comp. Neurol.* **411**, 327-345 (1999).
110. Meister, M., Wong, R. O. L., Baylor, D. A. & Shatz, C. J. Synchronous bursts of action potentials in ganglion cells of the developing mammalian retina. *Science* **252**, 939-943 (1991).
111. Wong, R. O. L. & Oakley, D. M. Changing patterns of spontaneous bursting activity of On and Off retinal ganglion cells during development. *Neuron* **16**, 1087-1095 (1996).
112. Mooney, R., Penn, A. A., Gallego, R. & Shatz, C. J. Thalamic relay of spontaneous retinal activity prior to vision. *Neuron* **17**, 979-990 (1996).

113. Penn, A. A., Riquelme, P. A., Feller, M. B. & Shatz, C. J. Competition in retinogeniculate patterning driven by spontaneous activity. *Science* **279**, 2108-12 (1998).
114. Wong, R. O. L. Retinal waves and visual system development. *Annu Rev Neurosci* **22**, 29-47 (1999).
115. Cramer, K. S. & Sur, M. Blockade of afferent impulse activity disrupts on / off sublamination in the ferret lateral geniculate nucleus. *Developmental Brain Research* **98**, 287-290 (1997).
116. Brown, T. H., Chapman, P. F., Kairiss, E. W. & Keenan, C. L. Long-term synaptic potentiation. *Science* **242**, 724-728 (1988).
117. Bliss, T. V. P. & Collingridge, G. L. A synaptic model of memory: Long-term potentiation in the hippocampus. *Nature* **361**, 31-39 (1993).
118. Mooney, R., Madison, D. V. & Shatz, C. J. Enhancement of transmission at the developing retinogeniculate synapse. *Neuron* **10**, 815-825 (1993).
119. Petralia, R. S. et al. Selective acquisition of AMPA receptors over postnatal development suggests a molecular basis for silent synapses. *Nature Neuroscience* **2**, 31-36 (1999).
120. Takahashi, T., Svoboda, K. & Malinow, R. Experience strengthening transmission by driving AMPA receptors into synapses. *Science* **299**, 1585-8 (2003).
121. Lee, H. K., Kameyama, K., Huganir, R. L. & Bear, M. F. NMDA induces long-term synaptic depression and dephosphorylation of the GluR1 subunit of AMPA receptors in hippocampus. *Neuron* **21**, 1151-62 (1998).
122. Lee, H. K., Barbarosie, M., Kameyama, K., Bear, M. F. & Huganir, R. L. Regulation of distinct AMPA receptor phosphorylation sites during bidirectional synaptic plasticity. *Nature* **405**, 955-9 (2000).

123. Liu, G., Choi, S. & Tsien, R. W. Variability of neurotransmitter concentration and nonsaturation of postsynaptic AMPA receptors at synapses in hippocampal cultures and slices. *Neuron* **22**, 395-409 (1999).
124. Renger, J. J., Egles, C. & Liu, G. A developmental switch in neurotransmitter flux enhances synaptic efficacy by affecting AMPA receptor activation. *Neuron* **29**, 469-84 (2001).
125. Xiao, M. Y., Wasling, P., Hanse, E. & Gustafsson, B. Creation of AMPA-silent synapses in the neonatal hippocampus. *Nat Neurosci* **7**, 236-243 (2004).
126. Watt, A. J., Rossum, M. C. W. v., MacLeod, K. M., Nelson, S. B. & Turrigiano, G. G. Activity coregulates quantal AMPA and NMDA currents at neocortical synapses. *Neuron* **26**, 659-670 (2000).
127. Ramoa, A. S. & McCormick, D. A. Enhanced activation of NMDA receptor responses at the immature retinogeniculate synapse. *Journal of Neuroscience* **14**, 2098-2105 (1994).
128. Hohnke, C. D. & Sur, M. Stable properties of spontaneous EPSCs and miniature retinal EPSCs during the development of ON/OFF sublamination in the ferret lateral geniculate nucleus. *J. Neuroscience* **19**, 236-347 (1999).
129. Carder, R. K. Immunocytochemical characterization of AMPA-selective glutamate receptor subunits: Laminar and compartmental distribution in Macaque striate cortex. *Journal of Neuroscience* **17**, 3352-3363 (1997).
130. Jones, E. G., Tighilet, B., Tran, B.-v. & Huntsman, M. M. Nucleus- and cell-specific expression of NMDA and non-NMDA receptor subunits in monkey thalamus. *J. Comp. Neurol.* **397**, 371-393 (1998).
131. Tighilet, B. et al. Cell-specific expression of type II Calcium/Calmodulin-dependent protein kinase isoforms and glutamate receptors in normal and

- visually deprived lateral geniculate nucleus of monkeys. *J. Comp. Neurol.* **390**, 278-296 (1998).
132. Angelucci, A., Clascá, F. & Sur, M. Anterograde axonal tracing with the subunit B of cholera toxin: A highly sensitive immunohistochemical protocol for revealing fine axonal morphology in adult and neonatal brains. *Journal of Neuroscience Methods* **65**, 101-112 (1996).
133. Voigt, T., De Lima, A. D. & Beckmann, M. Synaptophysin immunohistochemistry reveals inside-out pattern of early synaptogenesis in ferret cerebral cortex. *J Comp Neurol* **330**, 48-64 (1993).
134. Stelzer, E. H. K. in *Handbook of biological confocal microscopy* (ed. Pawley, J.) 139-154 (Plenum, New York, 1995).
135. Wilson, J. R., Friedlander, M. J. & Sherman, S. M. Fine structural morphology of identified X- and Y-cells in the cat's lateral geniculate nucleus. *Proc. R. Soc. Lond. B* **221**, 411-436 (1984).
136. Hamos, J. E., Horn, S. C. V., Raczkowski, D. & Sherman, S. M. Synaptic circuits involving an individual retinogeniculate axon in the cat. *Journal of Comparative Neurology* **259**, 165-192 (1987).
137. Ruthazer, E. S. & Stryker, M. P. The role of activity in the development of long-range horizontal connections in area 17 of the ferret. *J Neurosci* **16**, 7253-69 (1996).
138. Sherman, S. M. & Koch, C. in *The Synaptic Organization of the Brain* (ed. Shepherd, G.) 289-328 (Oxford University Press, 1998).
139. Rocha, M. & Sur, M. Rapid acquisition of dendritic spines by visual thalamic neurons after blockade of N-methyl-D-aspartate receptors. *Proc, Natl. Acad. of Sci. USA* **92**, 8026-8030 (1995).
140. Rao, A. & Craig, A. M. Activity regulates the synaptic localization of the NMDA receptor in hippocampal neurons. *Neuron* **19**, 801-12 (1997).

141. O'Brien, R. J. et al. The development of excitatory synapses in cultured spinal neurons. *J. Neurosci.* **17**, 7339-7350 (1997).
142. Turrigiano, G. G., Leslie, K. R., Desai, N. S., Rutherford, L. C. & Nelson, S. B. Activity-dependent scaling of quantal amplitude in neocortical neurons. *Nature* **391**, 892-6 (1998).
143. Lissin, D. V. et al. Activity differentially regulates the surface expression of synaptic AMPA and NMDA glutamate receptors. *Proc Natl Acad Sci U S A* **95**, 7097-102 (1998).